9-1-2020

GEOMECHANICAL STATE OF ROCKS WITH DEPLETION IN UNCONVENTIONAL COALBED METHANE RESERVOIRS

Suman Saurabh
Southern Illinois University Carbondale, sumanan047@gmail.com

GEOMECHANICAL STATE OF ROCKS WITH DEPLETION IN UNCONVENTIONAL COALBED METHANE RESERVOIRS

by

Suman Saurabh

B.S., Indian Institute of Technology (ISM Dhanbad), India, 2013

A Dissertation
Submitted in Partial Fulfillment of the Requirements for the
Doctor of Philosophy Degree

Department of Mining and Mineral Resources Engineering
in the Graduate School
Southern Illinois University Carbondale
August 2020

DISSERTATION APPROVAL

GEOMECHANICAL STATE OF ROCKS WITH DEPLETION IN UNCONVENTIONAL COALBED METHANE RESERVOIRS

by

Suman Saurabh

A Dissertation Submitted in Partial

Fulfillment of the Requirements

for the Degree of

Doctor of Philosophy

in the field of Engineering Science

Approved by:

Dr. Satya Harpalani, Chair

Dr. Rasit Koc

Dr. Steven P. Esling

Dr. Bruce DeVantier

Dr. Nicolas Espinoza

Dr. Kanchan Mondal

Graduate School
Southern Illinois University Carbondale
November 8, 2019

AN ABSTRACT OF THE DISSERTATION OF

Suman Saurabh, for the Doctor of Philosophy degree in Engineering Science, presented on August 30, 2019, at Southern Illinois University Carbondale.

TITLE: GEOMECHANICAL STATE OF ROCKS WITH DEPLETION IN UNCONVENTIONAL COALBED METHANE RESERVOIRS

MAJOR PROFESSOR: Dr. Satya Harpalani

One of the major reservoir types in the class of unconventional reservoirs is coalbed methane. Researchers have treated these reservoirs as isotropic when modeling stress and permeability, that is, mechanical properties in all directions are same. Furthermore, coal is a highly sorptive and stress- sensitive rock. The focus of this dissertation is to characterize the geomechanical aspects of these reservoirs, strain, stresses, effective stress and, using the information, establish the dynamic flow/permeability behavior with continued depletion. Several aspects of the study presented in this dissertation can be easily extended to shale gas reservoirs.

The study started with mechanical characterization and measurement of anisotropy using experimental and modeling work, and evaluation of how the sorptive nature of coal can affect the anisotropy. An attempt was also made to characterize the variation in anisotropy with depletion. The results revealed that the coals tested were orthotropic in nature, but could be approximated as transversely isotropic, that is, the mechanical properties were isotropic in the horizontal plane, but significantly different in vertical direction.

Mechanical characterization of coal was followed by flow modeling. Stress data was used to characterize the changes in permeability with depletion. This was achieved by plotting stress path followed by coal during depletion. The model developed was used to successfully predict the permeability variation in coal with depletion for elastic deformations. As expected, the developed model failed to predict the permeability variation resulting from inelastic deformation

given that it was based on elastic constitutive equations. Hence, the next logical step was to develop a generalized permeability model, which would be valid for both elastic and inelastic deformations. Investigation of the causes of coal failure due to anisotropic stress redistribution during depletion was also carried out as a part of this study. It was found that highly sorptive rocks experience severe loss in horizontal stresses with depletion and, if their mechanical strength is not adequate to support the anisotropic stress redistribution, rock failure can result.

In order to develop a generalized permeability model based on stress data, stress paths for three different coal types were established and the corresponding changes in permeability were studied. Stress path plotted in an octahedral mean stress versus octahedral shear stress plane provided a signal for changes in the permeability for both elastic as well as inelastic deformations. This signal was used to develop a mechanistic model for permeability modeling, based on stress redistribution in rocks during depletion. The model was able to successfully predict the permeability variation for all three coal types. Finally, since coal is highly stress-sensitive, changes in effective stresses were found to be the dictating factor for deformations, changes in permeability and possible failure with depletion. Hence, the next step was to develop an effective stress law for sorptive and transversely isotropic rocks.

For development of an effective stress law for stress sensitive, transversely isotropic rocks, previously established constitutive equations were used to formulate a new analytical model. The model was then used to study changes in the variation of Biot's coefficient of these rocks. It was found that Biot's coefficient, typically less than one, can take values larger than one for these rocks, and their values also change with depletion. The study provides a methodology which can be used to estimate the Biot's coefficient of any rock.

As a final step, preliminary work was carried out on the problem of under-performing

coal reservoirs in the San Juan basin, where coal is extremely tight with very low permeability. An extension of the work presented in this dissertation is to use the geomechanical characterization techniques to unlock these reservoirs and improve their performance. The experimental data collected during this preliminary study is included in the last chapter of the dissertation.

ACKNOWLEDGMENTS

I have had the opportunity to work in major industries and research institutions before I opted for graduate education. I found that research experience gives me the most fulfillment. Hence, when the opportunity came to work under Dr. Satya Harpalani, I grabbed it.

First and foremost, I thank my academic advisor, Dr. Harpalani, who all his graduate students affectionately call “Dr. H”. I would thank him for not only giving me the opportunity to work with him, but to be a part of his very successful research group. Dr. Harpalani is a great mentor and I will always be grateful to him for helping me grow, both as a researcher and as a person. Finally, I would always be grateful for his savvy researcher outlook as well as for his company during various sorts of conversations over the last four years.

Second, I thank my committee members, Dr. Steven P. Esling, Dr. Rasit Koc, Dr. Nicolas Espinoza, Dr. Bruce A. DeVantier and Dr. Kanchan Mondal. Three courses taken from Dr. Esling served as a solid foundation during the exercise of my modeling work.

I would like to thank my co-workers, lab-mates and friends. I will always admire your profound knowledge and positive attitude towards life.

Last, but certainly not the least, my deepest appreciation goes to my family for their belief in me, and for all their love and support.

This dissertation has been financially supported in part by BP America and a Doctoral Fellowship from Southern Illinois University. I would also like to thank BP and SIU for the support.

PREFACE

This dissertation is submitted for the degree of Doctor of Philosophy in Engineering Science at the Southern Illinois University Carbondale. The research described herein was carried out under the supervision of Dr. Satya Harpalani in the College of Engineering, Southern Illinois University Carbondale, between August 2015 and August 2019.

This study is, to the best of my knowledge, original except where references are made to previous work. Neither this, nor any substantially similar dissertation has been or is being submitted for any other degree, diploma or other qualification at any other university.

The main body of the dissertation consists of Chapters 2, 3, 4 and 5. Chapter 1 introduces the dissertation. Chapter 2, 3, 4 and 5 are four published journal papers respectively. Finally, Chapter 6 summarizes the work completed and presents the preliminary data and plan for future studies. In the order of chapter appearance, these papers are:

1. Saurabh, S. & Harpalani, S. Anisotropy of coal at various scales and its variation with sorption. *International Journal of Coal Geology*, Volume 201, 2019, pp 14-25.
2. Saurabh S, Harpalani S, Singh V. Implications of stress re-distribution and rock failure with continued gas depletion in coalbed methane reservoirs. *International Journal of Coal Geology*, Volume 162, 2016, pp 183-192.
3. Saurabh S and Harpalani S. Stress path with depletion in coalbed methane reservoirs and stress based permeability modeling, *International Journal of Coal Geology*, Volume 185, 2018, pp 12-22, ISSN 0166-5162.
4. Saurabh S and Harpalani S. The effective stress law for stress-sensitive transversely isotropic rocks, *International Journal of Rock Mechanics and Mining Sciences*, Volume 101, 2018, pp 69-77, ISSN 1365-1609.

My role as first author in the above listed papers implies my principal role in conducting experiments, data analysis and developing mathematical models, except in places where data has been taken from cited works.

Chapter 2, 3, 4 and 5 are Elsevier journal papers published and are in public domain. Elsevier provides the authors of journal papers complete right to share the work as it is or modified form for personal use and other conditions that can be confirmed on the Elsevier website. The link for copyright policy for authors can be found at the following link: https://www.elsevier.com/about/policies/copyright#Author-rights.

TABLE OF CONTENTS

CHAPTER PAGE

ABSTRACT i

AKNOWLEDGMENTS iv

PREFACE v

LIST OF TABLES x

LIST OF FIGURES xi

CHAPTERS

CHAPTER 1 INTRODUCTION 1

1.1 Overview 1

1.2 Motivation 2

1.3 Outline of the Dissertation 2

CHAPTER 2 PRELIMINARY INVESTIGATION ON TRANSVERSE ISOTROPY 8

2.1 Introduction 9

2.2 Experiment: Sample Preparation and Procedure 14

2.3 Results and Analysis 18

2.4 Discussion 34

2.5 Conclusions 37

CHAPTER 3 PERMEABILITY MODELING AND INVESTIGATION OF FAILURE WITH DEPLETION 40

3.1 Introduction 41

3.2 Sample Charecterization 42

3.3 Experimental Works and Results 43

3.4 Analysis.....47
3.5 Conclusions and Recommendations for Future Work 69
CHAPTER 4 GENERALIZED STRESS-DEPENDENT PERMEABILITY MODELING 72
4.1 Introduction.....73
4.2 Experimental Work and Results 75
4.3 Analysis and Discussion 79
4.4 Permeability Modeling77.....90
4.5 Octahedral Effective Shear Stress Compressibility 97
4.6 Conclusions 101
CHAPTER 5 EFECTIVE STRESS LAW FOR TRNSVERSELY ISOTROPIC, STRESS-SENSITIVE ROCKS.....104
5.1 Introduction.....105
5.2 Overview.....106
5.3 Experimental Work.....112
5.4 Analysis.....120
5.5 Discussion.....127
5.6 Conclusions.....130
CHAPTER 6 SUMMARY AND FUTURE RESEARCH.....133
6.1 Summary of Work.....133
6.2 Potential Future Research and Preliminary Results.....134
REFERENCES 136
APPENDICES

APPENDIX A - DETERMINATION OF BIOT'S-LIKE COEFFICIENT FOR CHAPTER 2 149

APPENDIX B - DETERMINATION OF MATRIX SHRINKAGE COMPRESSIBILITY (C_M) FOR CH. 3 151

VITA 152

LIST OF TABLES

TABLE PAGE

Table 2.1 Specifications for unconstrained flooding experiment 17

Table 2.2 Unconfined compressive strength test laboratory results 18

Table 2.3 Values of coal elastic moduli estimated at matrix scale – obtained by solving Eq. 3 using data in Figure 4a and assuming a value of v_1 28

Table 2.4 Gas composition and pressure for simulation 30

Table 2.5 Coal mechanical parameters obtained at bulk scale 35

Table 3.1 Relevant statistics for pressure-dependent-permeability experiment 46

Table 3.2 Triaxial strength test results 47

Table 3.3 Elastic moduli used for the calculations 48

Table 4.1 Sample location and rank of coals tested 77

Table 4.2 Proximate analysis results for coals tested 77

Table 4.3 Values of C_s used for permeability modeling 96

Table 5.1 Sample location and rank of coals tested 113

Table 5.2 Proximate analysis results for coals tested 113

Table 5.3 Relevant data for pressure-dependent-permeability experiments 118

Table 5.4 Estimated moduli of coal at matrix scale. (*assumed values) 124

Table 5.5 Estimated moduli of coal at bulk scale 124

Table 5.6 Estimated Biot's coefficient for coal types at bulk scale 125

LIST OF FIGURES

FIGURE PAGE

Figure 2.1 Geometrical model (representative elemental volume) used for Anisotropy ratio (A_n) modeling....10

Figure 2.2 Sample preparation flow and schematic for experiments....15

Figure 2.3 Coal sample and experimental setup used for the study....15

Figure 2.4 Strain with helium, methane and CO_2 injection....19

Figure 2.5 Comparative strain with helium, methane and CO_2 injection....20

Figure 2.6 Anisotropy ratio with helium, methane and CO_2....26

Figure 2.7 Variation of Anisotropy ratio (A_n) with methane pressure. 29

Figure 2.8 Anisotropy ratio variation of coal matrix with variable composition 31

Figure 2.9 Variation of Anisotropy ratio of coal at bulk scale 34

Figure 3.1 Measured strain with changes in pressure (unconstrained (unjacketed), helium)....44

Figure 3.2 Measured strain with changes in pressure (unconstrained (unjacketed), methane) ...45

Figure 3.3 Changes in horizontal stress with helium and methane depletion. (Uniaxial strain conditions)....46

Figure 3.4 Variation of adsorption coupling in vertical and horizontal directions with depletion....50

Figure 3.5 Biot's-like coefficient in vertical and horizontal directions....51

Figure 3.6 Variation of effective stresses with pressure for methane and helium depletion. (Uniaxial strain conditions)....53

Figure 3.7 Stress invariant path with gas depletion in coal sample along with failure envelope. 56

Figure 3.8 Variation in octahedral stresses with pressure with methane and helium depletion ..58

Figure 3.9 Calculated rate of change of horizontal stress with pressure depletion.....60

Figure 3.10 Experimental rate of change of horizontal stress with pressure depletion 61

Figure 3.11 Integrated value of horizontal stress with pressure from Equation 3.14 and Figure 3.10 62

Figure 3.12 Schematic of coal matrix (with small pores) and cleat - longitudinal section of relative elemental volume used for permeability modelling.....65

Figure 3.13 Permeability variation using proposed model compared and experimental data (Singh, 2014). (Bimodal variation for two pressure ranges) 67

Figure 3.14 Exponential fit for the proposed Biot's-like coefficient in vertical and horizontal directions.....68

Figure 4.1 Pictures of coal cores showing the cleated structure of San Juan coal (SJM/SJSJ, left) and Indonesian coal (SS, right).....77

Figure 4.2 Variation of total stresses with methane depletion.....78

Figure 4.3 Variation in permeability with methane depletion 79

Figure 4.4 Strain data analysis for SJM coal with helium and methane depletion.....82

Figure 4.5 Stress path of various coal types with depletions.....87

Figure 4.6 Schematic presentation of assumptions for permeability changes 92

Figure 4.7(a-c) Experimental and modeled permeability for various coal types 95

Figure 4.8 Ultrasonic P-wave velocity with methane depletion (SJM).....100

Figure 4.9 $(d(V_p)^m)/\left((V_p)^m\right)_0$ vs effective octahedral shear stress 101

Figure 4.10 Comparison of calculated and values used in the permeability modeling for SJM coal.....101

Figure 5.1 Adsorption isotherms for coal types.....114

Figure 5.2 Unconstrained matrix experiment for coal types using helium
(a) SJ coal, (b) SS coal 115
Figure 5.3 Unconstrained matrix experiment for coal types using methane
(a) SJ coal, (b) SS coal 117
Figure 5.4 Horizontal stress variation with helium depletion 119
Figure 5.5 Vertical strain with helium depletion 119
Figure 5.6 Horizontal stress variation with methane depletion 120
Figure 5.7 Vertical strain with methane depletion 120
Figure 5.8 Biot-like coefficient in vertical and horizontal direction for SJ coal 123
Figure 5.9 Biot-like coefficient in vertical and horizontal directions for SS coal 123
Figure 5.10 Effective stress coefficient with methane depletion for SS coal 127
Figure 5.11 Effective stress coefficient with methane depletion for SJM coal 127
Figure 6.1 Sorption behavior of outside fairway area San Juan coal 134
Figure 6.2 Pressure dependent permeability experimental result with helium and
methane for San Juan coal, south of fairway 134

CHAPTER 1

INTRODUCTION

1.1 Overview

This dissertation focuses on characterizing the geomechanical state of unconventional reservoirs with depletion. The dissertation presents a combination of experimental and modeling studies. The experiments conducted were mostly measurement of stress, strain and permeability of rocks with depletion of gas at various scales, like small quadrants to larger rock core samples of two to four inches in diameter. Various models are proposed in this study to characterize the geomechanical state of reservoirs with depletion, like the one that can quantify anisotropy of rocks and measure its variation with depletion. Another model presented is for stress-dependent permeability, which includes the anisotropic nature of formation rocks. The last and final model presented in this dissertation is that of effective stress law for transversely isotropic rock given that unconventional reservoir rocks are believed to be very stress sensitive. Hence, an updated effective stress law, validated by experimental results, was much needed in the current literature.

The primary contributions of the dissertation are summarized as follows:

1. Experimental determination of various mechanical states of rocks with depletion, that is, variation in total stress, strain, anisotropy, mechanical moduli with depletion.
2. Development of permeability model based on three-dimensional stress state for characterization of permeability variation due to variation in the stress state with depletion.
3. Model to characterize anisotropy of rock and its variation with depletion.
4. Formulation of an effective stress law validated using experimental results on unconventional rocks.

1.2 Motivation

Unconventional natural gas reservoirs are a major source of energy while we are in transition from coal and oil-based energy to greener and cleaner energies like solar, wind and nuclear, among others. Hence, it is very important to develop an understanding of the unconventional natural gas reservoirs, like coalbed methane and shale gas, for their efficient and effective exploitation. These reservoirs are known to be transversely isotropic, sorptive and very stress sensitive. Hence, the focus of this dissertation is to characterize the geomechanical aspects, like strain, stresses, effective stress, and using this information to characterize the flow/permeability in these reservoirs with depletion, that is, production over time. Based on the understanding of variation of these geomechanical parameters in the reservoir, effective strategies and technologies can be developed for production of natural gas from these reservoirs. Achieving such a feat will not only help with greener and smaller carbon footprint of energy industry until we transition to more reliable and cheaper solar, wind and other greener sources of energy, but also help reduce carbon dioxide emission when extracting energy from coal.

1.3 Outline of Dissertation

Each chapter in this dissertation is a complete study in its own. Hence, an elaborate general introduction is not provided here but is available in each chapter. The four different problems that were investigated as a part of this study are described below to provide an overview of the subsequent four chapters:

1. Chapter 2: Preliminary Investigation on Transverse Isotropy. The first problem addressed is development of an experimental method to characterize and measure anisotropy of rocks in a laboratory environment. The next associated problem is to investigate any changes in anisotropy of these rocks with depletion. This problem is

addressed in Chapter 2, where a model is presented, based on experimental results, to investigate the problem. For most flow modeling work, coal is considered transversely isotropic, factors responsible for the anisotropy being fabric, pore structure at different scales and stress, among others. This study characterizes anisotropy of coal at two scales, matrix, and bulk. Matrix anisotropy was estimated under varying conditions of hydrostatic pressure, measuring strains in the three principal directions. Using the results, Anisotropy ratio (A_n), defined as the ratio of derivative of strains in the horizontal and vertical directions with respect to pressure, and its variation were estimated for helium, methane and carbon dioxide. Next, Anisotropy ratio was estimated for bulk scale and its evolution presented for hydrostatic reservoir condition with methane depletion.

The Anisotropy ratio was found to be constant for helium, but less than one, suggesting a definite anisotropy to begin with. For the two sorbing gases, methane and CO_2, the ratio was the same at very low pressure but varied differently with changes in pressure, its value being higher at high pressure. Hence, sorption phenomenon decreases the anisotropy of coal with increase in pressure. Since the variation of coal matrix as well as bulk anisotropy varied for methane and carbon dioxide pressure differently, the variation under in situ conditions would depend on both gas composition and pressure. The implication of a variable Anisotropy ratio is that it results in underestimation of dynamic stresses in the reservoir or, overestimation of in situ strength

2. Chapter 3: Permeability Modeling and Investigation of Failure with Depletion. The second problem addressed is development of a permeability model for anisotropic rocks with information of stress variation during depletion. Investigation of how anisotropic structure

affects the stress redistribution and, therefore, permeability variation with depletion was also carried out as a part of this problem. This problem is addressed in Chapter 3, where analytical model for anisotropic permeability of coal was developed for elastic zone and the model was validated for San Juan coal. Significant increases in permeability of coal with continued production of coalbed methane (CBM) is a well-accepted phenomenon, particularly in the San Juan basin in the US and Surat basin in Australia. Modeling this increase is either based on the resulting increase in fracture porosity of coal or the associated changes in stresses resulting from the sorption-induced strain. This study combines the experimental results of the sorption-induced coal matrix volumetric strain with depletion and a model proposed to estimate the associated changes in stress. The overall changes in stress resulting from the combined effect of the poro-mechanical behavior and sorption-induced strain were estimated by introducing a Biot-like coefficient. Plotting the stress path followed during depletion along with the failure envelope for the coal-type clearly showed that shear failure of coal is possible due to anisotropic loading resulting from a large reduction in the horizontal stresses. This would explain the large increases in permeability, typically observed in San Juan CBM operations. Finally, a permeability model was developed using the Biot-like coefficient, and assuming transversely isotropic behavior of coal. A comparison of the experimental and modeled permeability results showed that the model works well as long as coal does not fail. However, it clearly demonstrated that a permeability model incorporating failure of coal is warranted for reliable prediction of permeability variation.

3. Chapter 4: Generalized Stress-Dependent Permeability Modeling. The third problem presented involves development of a generalized permeability model, which is applicable to elastic as well as inelastic regime of coal deformation. This chapter investigates the changes in mean and shear stress and the corresponding changes in permeability of rocks. A comparative

study of stress variation in three coal types was carried out and the corresponding permeability variation was measured. The variation of stress and permeability were used to develop the generalized stress dependent permeability model for coal. That permeability is a critical parameter dictating the performance of naturally fractured reservoirs, like coalbed methane (CBM), is evident from the available field, experimental and permeability modeling information in the literature. Although modeling is often achieved at the expense of several input parameters, the exercise is unable to match sudden increases in coal permeability, typically encountered in deep coals after significant depletion. This paper is aimed at coupling stress and permeability in order to reduce the number of parameters required for modeling the permeability variation. Stresses in the reservoir are translated to invariants and stress path of coal is established in octahedral effective stress plane. Based on a detailed analysis of the stress path of three different coal types, a permeability model is presented in terms of stresses alone, that is, applicable for elastic as well as inelastic deformations of coal. The model is validated using pressure-dependent-permeability experimental data for thee coal types along with the geomechanical testing data used to develop the failure envelope.

The primary implication of the study is improved capability to predict permeability of deep coal deposits, given that they are likely to undergo inelastic deformation or shear failure with continued depletion, using a single parameter. Finally, realistic constraints on the values of the parameter are provided to enable operators with the necessary tools to use the model for field applications, particularly in the new and upcoming fields.

4. Chapter 5. Effective Stress Law for Transversely Isotropic, Stress-Sensitive Rocks. Finally, the last problem is to develop the fundamental effective stress law for transversely isotropic, sorptive rock. Investigation of variation in Biot’s coefficient of rock in different

directions, and with depletion, was carried out as a part of this study. This problem is addressed in Chapter 5, where analytical modeling was used to develop the effective stress law for transversely isotropic, sorptive rock and variation of Biot's coefficient was established using the developed model and experimental results. This study first presents a review of the development of the concept of effective stress, followed by major experimental and theoretical studies carried out to estimate the Biot's coefficient. It then uses the constitutive equations for vertically transverse isotropic (VTI) reservoirs, like coal, derived using the principles of thermodynamics for estimation of the Biot's coefficients in the vertical and horizontal directions. Laboratory data for tests conducted on two coal types, taken from different geologic settings and geographical locations, was used to carry out the modeling and validation exercise. Evidence is presented that values of Biot's coefficient can be greater than one, proposed by Biot to be the limiting value, for sorptive rocks. To address this, the term Biot's coefficient is replaced with "effective stress coefficient". Finally, this study discusses the pressure- and stress- dependent behavior of the Biot's coefficient. The results of the study show that the estimated values of Biot's coefficients in both vertical and horizontal directions are different, varying with pressure for methane depletion, but remaining constant for helium depletion. Simultaneously, the nature of Biot's coefficient, re-termed effective stress coefficient, was found to be greater than unity for methane depletion. As a last step, a conceptual physical model is proposed to explain the pressure-dependent variation of effective stress/Biot's coefficients in terms of the contact area between grains. Based on the findings that the effective stress coefficient decreases with pressure, it is concluded that the effective vertical stress would increase significantly with depletion which, in turn, would result in shear failure and increased permeability.

5. Chapter 6: Summary and Future Research. This chapter includes preliminary

experimental results of a study aimed at sorption and permeability behavior of another coal type in the San Juan basin, from an area currently under development. The chapter highlights the results, which explain the poor production performance of wells in the region. These results are included to identify future research in exploring the various factors that result in low production and technologies to unlock the potential of the area.

CHAPTER 2

PRELIMINARY INVESTIGATION ON TRANSVERSE ISOTROPY

This Chapter is an exact copy (except for format change) of the journal paper entitled "Anisotropy of coal at various scales and its variation with sorption", published in *International Journal of Coal Geology*, 2019. DOI: 10.1016/j.coal.2018.11.008. Elsevier holds the copyright for this paper. This material may be downloaded for personal use only. Any other use requires prior permission of Elsevier.

Authors:

Suman Saurabh and Satya Harpalani

Abstract

For most flow modeling work, coal is considered transversely isotropic, factors responsible for the anisotropy being fabric, pore structure at different scales and stress, among others. This study characterizes anisotropy of coal at two scales, matrix, and bulk. Matrix anisotropy was estimated under varying conditions of hydrostatic pressure, measuring strains in the three principal directions. Using the results, Anisotropy ratio (An), defined as the ratio of derivative of strains in horizontal and vertical directions with respect to pressure, and its variation were estimated for helium, methane and carbon dioxide. Next, Anisotropy ratio was estimated for bulk scale and its evolution was discussed for hydrostatic reservoir condition with methane depletion.

The Anisotropy ratio was found to be constant for helium, but less than one, suggesting a definite anisotropy, to begin with. For the two sorbing gases, methane and CO_2, the ratio was the same at very low pressure but varied differently with changes in pressure, its value is higher at high pressure. Hence, sorption phenomenon decreases the anisotropy of coal with an increase

in pressure. Since the variation of coal matrix, as well as bulk anisotropy, varied for methane and carbon dioxide pressure differently, the variation under in situ conditions would depend on both gas composition and pressure. The implication of a variable Anisotropy ratio is that it results in an underestimation of dynamic stresses in the reservoir or, overestimation of in situ strength.

Keywords: Coal; Matrix; Variable anisotropy; Sorptive and non-sorptive gases.

2.1 Introduction

2.1.1. Background

Coal is a dual porosity medium, with macropores in the form of cleats and micro- and meso- pores in the matrix (Liu et al., 2012; Moore et al., 2014; Pan and Connell, 2011; Saurabh et al., 2016). The matrix is responsible for methane storage by the phenomenon of sorption on coal surface and macropores, whereas the natural fractures are responsible for the flow of gas. One of the best geometrical representation of coal is the bundle of matchstick model (Liu et al., 2016; Palmer et al., 2007; Pan and Connell, 2011) (Figure 2.1). The spaces between the matchsticks are natural fractures/cleats and the matchsticks represent the coal matrix blocks. Coal shows a remarkable property of matrix swelling when exposed to methane/CO_2 or, any sorptive gas. Several experimental and modeling studies on coal swelling have been reported in the literature. The role of water, methane and carbon dioxide in swelling of different coal ranks, changes in permeability, strength and other important aspects of coal have been widely studied (Balan and Gumrah, 2009; Day et al., 2008; Espinoza et al., 2014; Hol and Spiers, 2012; Liu et al., 2016; Liu et al.,2010; Mazumder et al., 2006; Mazumder and Wolf, 2008; Pan and Connell, 2012; Seidle and Huitt, 1995; van Bergen et al., 2011). Flow in coal occurs in mostly orthogonal, natural fracture network, known as cleats. There is a more prominent set of natural fractures known as face cleats and another less prominent set, terminating on face cleats, called the butt

cleats.

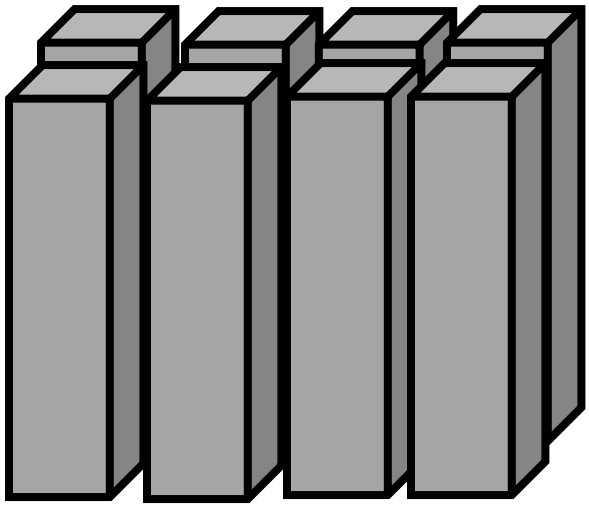

Figure 2.1 Geometrical model (representative elemental volume) used for Anisotropy ratio (An) modeling.

In addition, given that coal is a sedimentary rock, it has bedding planes perpendicular to natural fractures. All of this imparts a complete anisotropic nature to coal at bulk scale. However, for purposes of flow modeling, coal is considered a transversely isotropic medium (Espinoza et al., 2013; Moore et al., 2014; Pan and Connell, 2011; Saurabh et al., 2016; Saurabh and Harpalani, 2018), characterized by isotropy in the horizontal plane while properties in the vertical direction are different. Anisotropy in rocks is associated with several factors, such as fabric anisotropy (Sayers, 1994; Thomsen, 1986), pore structure anisotropy (Hudson, 1981) and stress-induced anisotropy. Fabric anisotropy of coal results from diagenesis and is a property of the skeleton. Pore structure anisotropy is related to the aligned microcracks and faults/fractures, depending on the scale of the analysis. Both pore structure and fabric anisotropies can be related to bulk scale anisotropy in an engineering sense by a strain-based relationship given as:

$$\varepsilon_b = \phi\varepsilon_p + (1-\phi)\varepsilon_s \quad (2.1)$$

where, $\varepsilon_b, \varepsilon_p, \varepsilon_s and\ \phi$ are the bulk strain, pore strain, solid fabric strain and porosity respectively. Hence, if the above relationship is resolved in both horizontal and vertical directions, their strain ratio would be indicative of anisotropy in each component of the rock structure, bulk, pore or fabric. Stress-induced anisotropy is related to the anisotropic behavior of rock under differential stress condition. Coal mine methane (CMM) was considered a serious hazard in underground coal mining operations, leading to major disasters, such as, gas outbursts and explosions. However, once coalbed methane (CBM) was introduced and shown to be a commercially viable source of energy in the early eighties, the CMM liability turned into a resource, substantially increasing the natural gas reserve base in the United States. Additionally, enhanced coalbed methane (ECBM) by injection of a second gas, nitrogen or CO_2, as well as CO_2 sequestration in deep coal seams became attractive options economically as well as environmentally speaking. However, from a practical perspective, CBM exploitation by pressure depletion, its enhanced recovery by injection and/or CO_2 sequestration largely depend on coal permeability and its evolution with changes in pressure.

2.1.2. Objectives

The paper, based on a laboratory study, is aimed at characterizing the fabric and pore structure anisotropy of coal at matrix scale. Hence, in this study, we measure the changes in anisotropic strain in the coal matrix under hydrostatic pressure of gases (helium, methane and CO_2), assuming that they completely fill the accessible (connected) pores, and estimate the coal matrix anisotropy, to eliminate the stress-induced anisotropy component in strain measured. It is important to mention that true fabric and pore structure anisotropy of coal at matrix scale are properties of solid grain/skeleton and external forces, and changes with gas pressure. Also, true

fabric anisotropy is almost impossible to estimate in the laboratory because of the presence of closed pores. The experimental work presented in this paper was conducted to characterize matrix scale anisotropy under hydrostatic condition to eliminate the effect of stress-induced anisotropy. To conduct such an experiment, a free-standing sample, sealed in an air-tight vessel was flooded with gas. An important assumption associated with this experimental setting is that, when gas is introduced, it enters all the pores in the sample. This assumption is based on the fact that the kinetic diameters of helium, methane and, CO_2 are 260, 380 and, 232 pm respectively, ensuring that, when flooded, gas entered all connected pores larger than the diameter of the injected gas. Hence, with increasing/decreasing pressure, there was different strain caused in the coal matrix, depending on the gas injected. Since the pressure inside and outside the pores is same under such a setting, the pore volume would remain almost constant, enabling evaluation of only the matrix or, in this case, the fabric anisotropy alone (Harpalani and Chen, 1997). Although it has been reported that coal matrix consists of unconnected/isolated pores (Bae et al., 2009; He et al., 2012; Melnichenko et al., 2012; Zhang et al., 2015), their effects were not evaluated in this study. However, the effect of unconnected pores would be the same for all three gases and would, therefore, not introduce any bias for a specific gas. Previous researchers have also reported that gas accessibility of methane and CO_2 to micropores is different (He et al., 2012; Melnichenko et al., 2012; Zhang et al., 2015). This happens because the kinetic diameter of CO_2 is smaller than that of methane and helium. This can be a significant factor impacting the strain behavior caused by different gases, particularly in terms of anisotropic accessibility to the pores. Under these conditions, when the pressure/stress (because of unconstrained conditions) acting across the cleats of coal is same (hydrostatic), the measured strains are for coal matrix alone. In our experiment, strains were measured in vertical (z-) as well as horizontal (x- and y-)

directions.

Coming back to the mathematical justification for the assumption associated with the experiment, let us see what happens to Equation (2.1) under our experimental setting and the underlying assumption. Since we assume the pore strain as well as the porosity of coal to be very small, the first term in Equation (2.1) becomes negligible and the equation can be rewritten as:

$$\varepsilon_b \approx (1-\phi)\varepsilon_s \tag{2.2}$$

Further simplification by approximating the term $(1-\phi)$ as 1 gives:

$$\varepsilon_b \approx \varepsilon_s \tag{2.3}$$

Hence, under this experimental setting, we can estimate the fabric anisotropy, which in engineering sense is a measure of the bulk anisotropy of coal matrix.

As stated earlier in this paper, we aim to estimate anisotropy of rock by measuring strain in different directions and taking their ratio. However, since coal is a sorptive rock, strain is the result of two phenomena, mechanical stress and sorption. Hence, the definition of Anisotropy ratio should be expanded further to take the pressure dependence of strain into account. Including the pressure-dependence of strain in the definition of anisotropy ratio, we can define the Anisotropy ratio to be the ratio of the derivative of strain in the horizontal and vertical directions with respect to pressure.

In addition to experimentally determining the Anisotropy ratio and defining it, a mechanistic model for Anisotropy ratio is derived from constitutive equations suitable for a microporous, transversely isotropic, dual porosity, sorptive media, like coal. A second empirical model, based on the theory of Langmuir sorption, is also presented for the variation of Anisotropy ratio with changes in pressure. Finally, a comparison of the two models is presented.

As the last step, the Anisotropy ratio of coal was simulated for bulk scale given that the

experiments were conducted at matrix scale only. Bulk Anisotropy ratio of coal was then estimated for constant triaxial stress condition for methane and multi-component methane/CO_2 mixture.

2.1.3. Practical Application of Study

The anisotropy parameter has practical application in coalbed methane (CBM) reservoirs, CO_2 sequestration in deep coals and geotechnical problems encountered in coal mining. In CBM reservoirs, the Anisotropy ratio variation is an outcome of the sorption characteristics and the concept can be used to simplify the permeability models, for example, by Moore et al., (2014). For carbon sequestration, injection of CO_2 alters the Anisotropy ratio, with significant effects on the stress path with continued injection, resulting in changes in coal permeability. Similarly, anisotropy as a result of methane seepage in coal mines can cause stress buildup and eventual failure of coal.

2.2 Experiment: Sample Preparation and Procedure

The samples used were of sub-bituminous coal rank, taken from the San Juan basin. Two experiments were conducted as a part of this study. First, unconstrained flooding of small pieces of coal in airtight vessels was carried out to measure the strain in the coal matrix skeleton with increasing gas pressure (helium, methane and carbon dioxide). The second experiment involved compressive strength testing, using five-centimeter diameter and seven-and-a-half-centimeter length coal core, to determine the mechanical moduli in horizontal and vertical directions.

Sample preparation consisted of drilling two long runs of core from a coal block and chopping the ends of one of the core, as shown in Figure 2.2.

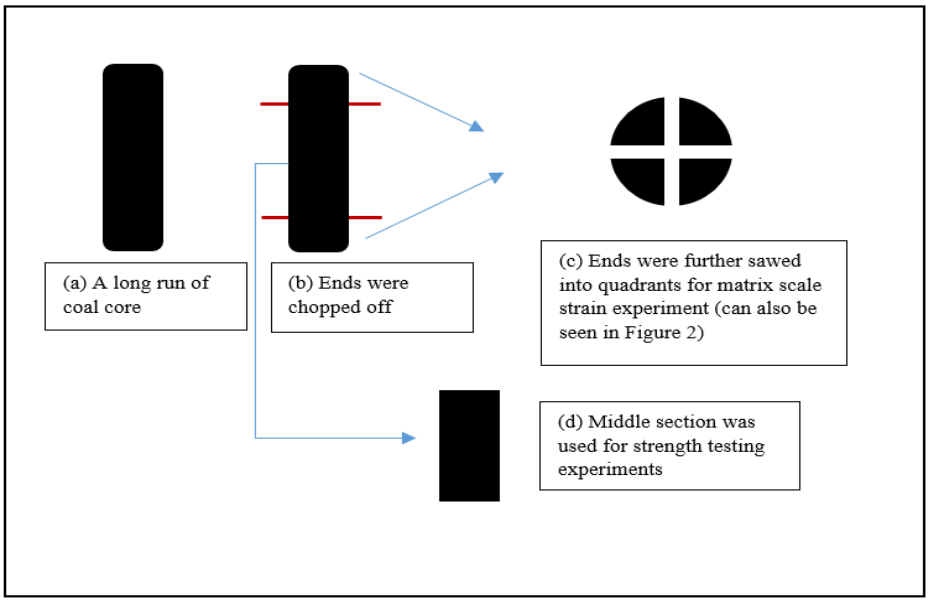

Figure 2.2 Sample preparation flow and schematic for experiments.

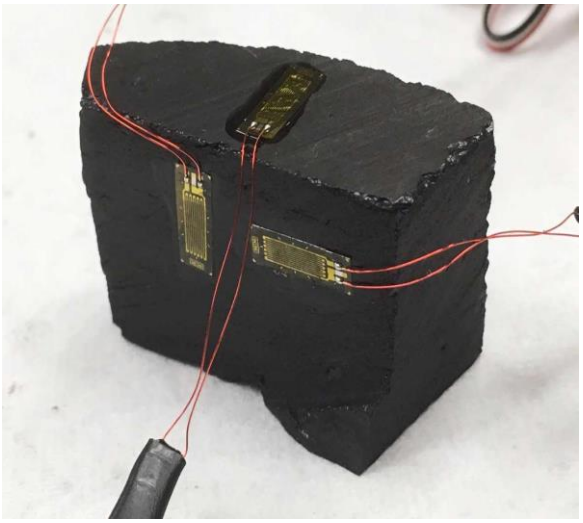

Figure 2.3a Coal sample with strain gauges to measure the three linear strains.

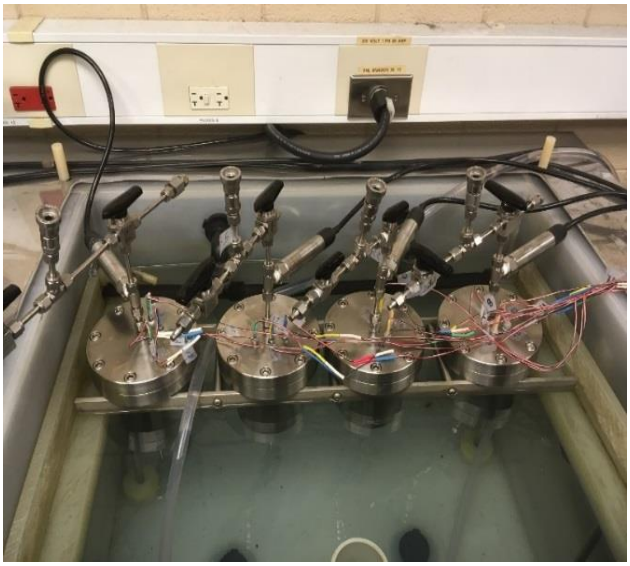

Figure 2.3b Setup for flooding experiments.

Figure 2.3 Coal sample and experimental setup used for the study.

The middle section of the core was used later for strength testing and the chopped ends were further sawed into quadrants (Figure 2.3) for matrix scale strain measurement, or the

unconstrained, drained flooding experiment. A set of two unconfined compressive strength tests were carried out using the two cores. Samples were stored in a moisture-equilibrated state for each experiment. The sample used for unconstrained flooding was cut off as a core quadrant from a five-centimeter diameter core, obtained from the San Juan basin in the United States. The coal was of sub-bituminous rank and the depth of the seam was approximately 1000 m. Strain gauges were affixed to the three perpendicular faces of each quadrant (Figure 2.3a). Coal samples were then placed in high-pressure vessels (Figure 2.3b) and pressurized gradually with helium, methane, and CO_2 (carbon dioxide) respectively. The pressure in the containers was increased to a maximum of 10 MPa in case of helium/methane and 6 MPa for CO_2 (to stay below the critical point for CO_2). The pressure was then decreased in a step-wise manner in steps of approximately 1 MPa, allowing adequate time for coal to attain strain equilibrium at each step (usually ~ 24-36 hours). When the change in strain was less than 0.1 % over a twenty-four-hour period, the strain was recorded. Detailed information about the coal and testing procedure is given in Singh (2014). The temperature throughout the experiment was kept constant at 95^0 F, ensuring isothermal condition. A brief summary of experimental condition and sample specification is presented in Table 2.1. The experimental technique used in this study is similar to that used by previous researchers to determine the strain at matrix scale (Harpalani and Chen, 1997; Liu and Harpalani, 2013; Singh, 2014).

Table 2.1 Specifications for unconstrained flooding experiment.

Sample specifications	
Parameter	Values
Depth (m)	~ 1000
Quadrant prepared form a core of Diameter (cm)	5
Rank of coal sample	Sub-Bituminous
Experimental Specifications	
Isothermal condition temperature (F)	~ 95^0
Step size of pressure change (MPa)	~ 1
Equilibrium time (Hours)	~ (24 to 36)

The compressive strength testing on the coal type was carried out by application of axial load and recording the axial stress, strain and diametrical strain until failure. The moduli were estimated in the horizontal and vertical directions using assumed values of Poisson's ratio in both directions, this was necessary because we had data only for axial loading, the values so obtained are just approximate values to be used for modeling purposes in the paper. The sample diameter was 5 cm and the length to diameter ratio was 1.5, which is smaller than that recommended in the ISRM standards. Given the friable nature of coal, it was difficult to prepare intact core, 10 cm long (L: D = 2, which is ideal. Hence, the compressive strength of coal reported in the paper can be assumed to be a little higher than acceptable values. Also, it is important to mention that the values obtained for the compressive strength of coal from the experiment, even with some error,

were used as one input parameter in the presented model and did not affect the underlying science presented. A table containing the specifications of unconfined compressive strength testing are presented in Table 2.2

Table 2.2 Unconfined compressive strength test laboratory results.

	UCS (MPa)	Young's Modulus (MPa)	Poisson's Ratio (-)
Sample 1	7.6	1.1	0.29
Sample 2	6.9	1.3	0.30

2.3 Results and Analysis

2.3.1. Matrix Scale Anisotropy

The measured strains in the coal matrix with continued pressure variation of helium, methane and carbon dioxide are presented in Figures 2.4(a-c). The strain results for helium were fit using a linear relationship because of the pressure-strain behavior, as evident from the graph (Figure 2.4a). The strain-pressure relationship in Figures 2.4b and 2.4c for methane and CO_2 has been presented using a Langmuir-like model. The values of Langmuir pressure-***like*** constants for methane are 6.2 and 13.8 MPa in vertical and horizontal directions respectively.

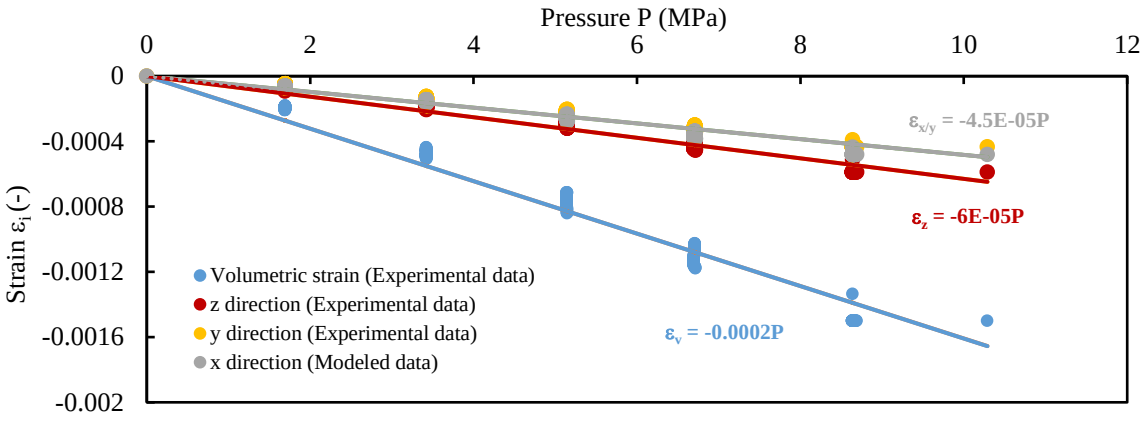

Figure 2.4a Strain with helium injection.

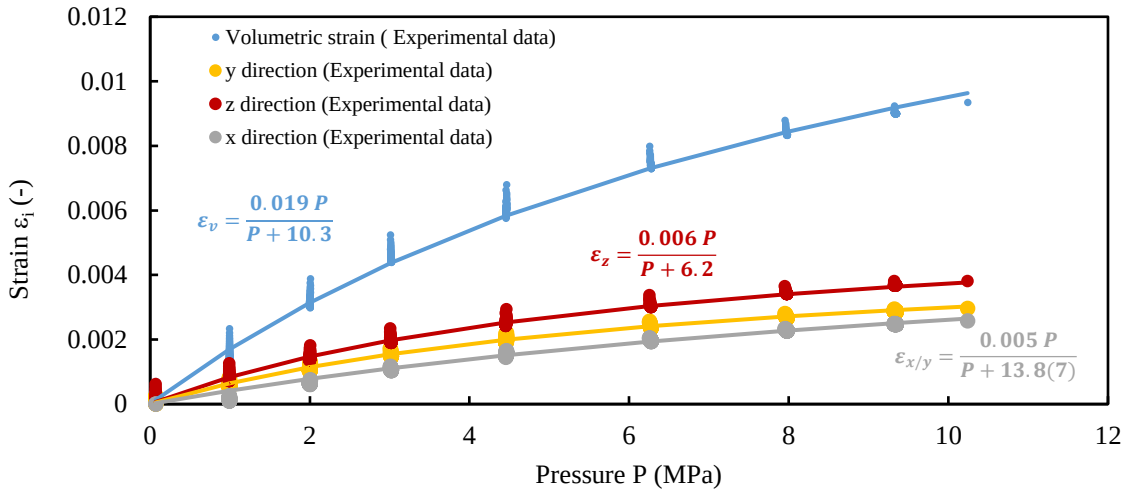

Figure 2.4b Strain with methane injection.

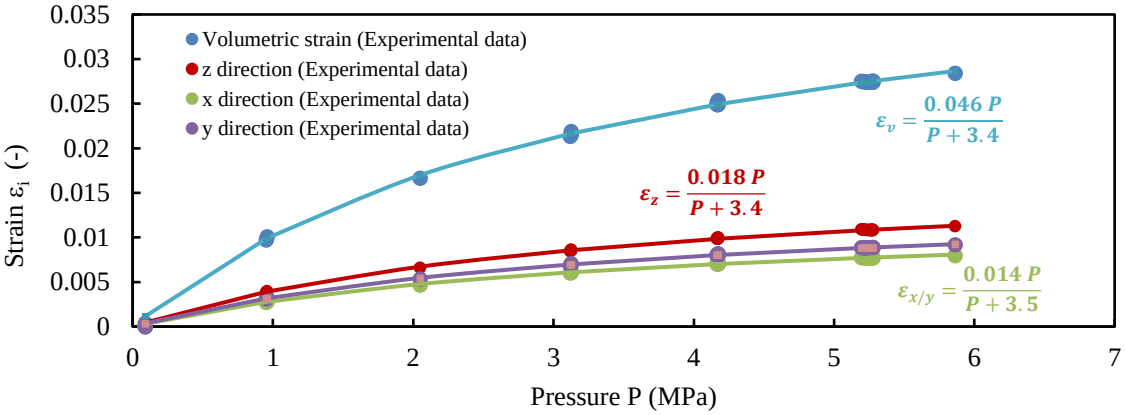

Figure 2.4c Strain with CO_2 injection.

Figure 2.4 Strain with helium, methane and CO_2 injection.

The value of Langmuir volume-***like*** constants are 0.006 and 0.005 in the vertical and horizontal directions respectively. Similarly, the values for CO_2 are 3.4/3.5 MPa in the vertical and horizontal directions and 0.018/0.014 in the two directions respectively. The combined results for the three gases, as shown in Figure 2.5, highlight the different behavior exhibited when coal is exposed to different gases.

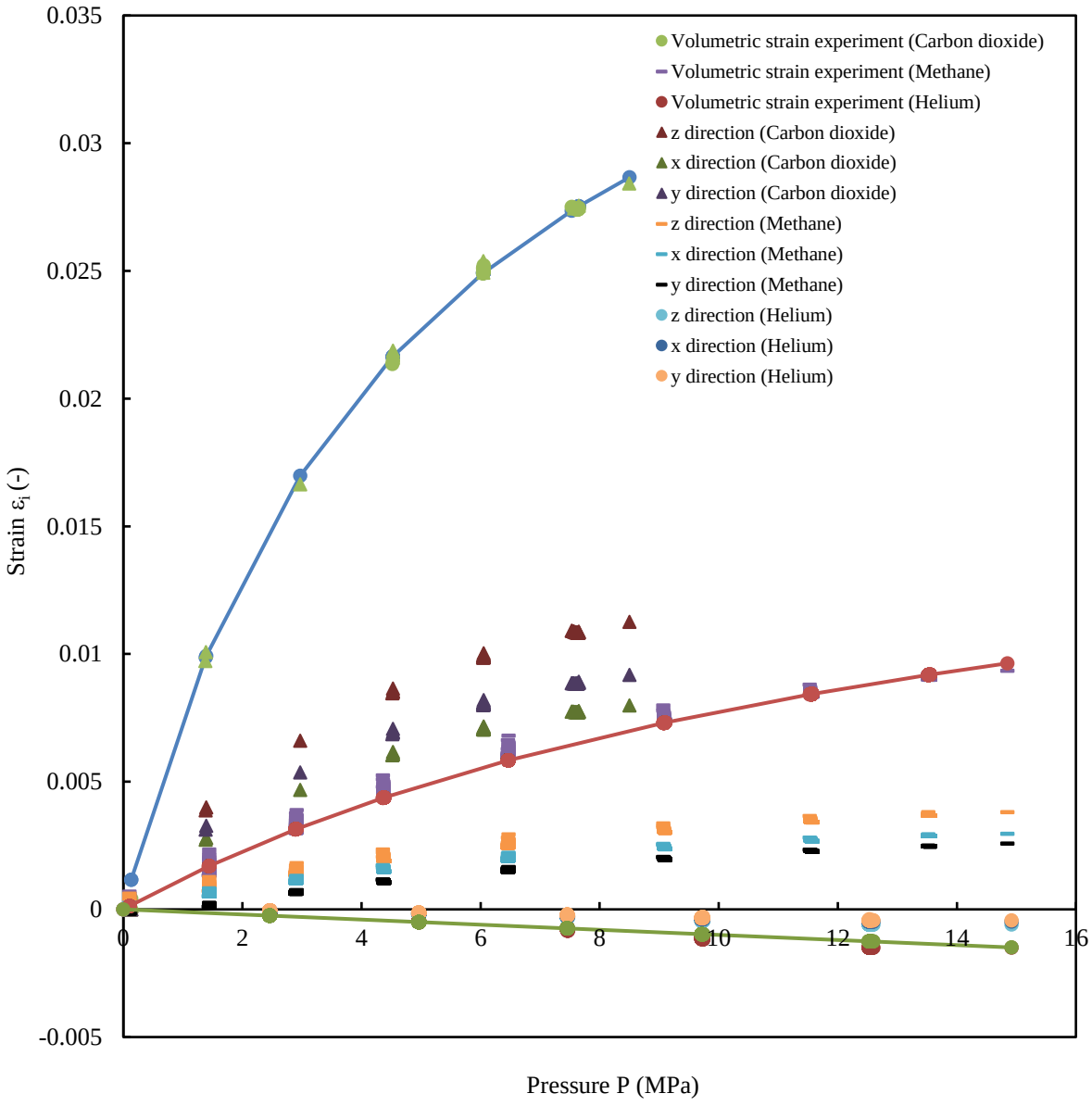

Figure 2.5 Comparative strain with helium, methane and CO_2 injection.

There is a reduction in the grain size due to mechanical compression with continued helium (non-sorbing) injection, compression being shown as negative strain. However, there is a dominant swelling effect with increased pressure of sorbing gases (methane and CO_2), shown as positive strain. It is important to note that the positive strain in this case is the combined effect of mechanical compression due to increased gas pressure and swelling due to sorption of gases. The results of injection and depletion of gas on coal have been reported to be similar (Harpalani and Chen, 1997). Figures 2.4(a-c) show that strains in the three directions (x-, y- and z-) are different for the three gases, suggesting that, even under hydrostatic condition, coal matrix exhibits distinct anisotropy. Given the difference between strains in the vertical (z-) and horizontal (x-, y-) directions, as shown in Figure 2.4(a-c), the anisotropic behavior can be approximated as *transverse isotropy* (more evident in Figure 2.5). In Figure 2.4a, strains in x- and y- directions differ from strains in the z- direction by an order of magnitude. Hence the assumption of transversely isotropic behavior of coal is justified for helium. For sorptive gases, like methane and CO_2, we need to analyze the corresponding Langmuir volume-***like*** strain constant for each direction. First, we analyze the methane results presented in Figure 2.4b. The difference between the values of Langmuir volume-***like*** strain constants in the strain-pressure plot for x- and y-directions with respect to the value in the y-direction, that is, $\frac{\varepsilon_y^L-\varepsilon_x^L}{\varepsilon_y^L}$ is 0.16, where, ε_i^L is Langmuir volume-***like*** strain constant in ith direction. Similarly, the difference between the values of Langmuir volume-***like*** constants in the strain-pressure plot (Figure 2.4b) between x- and z- directions with respect to the value in the z-direction, i.e. $\frac{\varepsilon_z^L-\varepsilon_x^L}{\varepsilon_z^L}$ is 0.74. For carbon dioxide,$\frac{\varepsilon_y^L-\varepsilon_x^L}{\varepsilon_y^L}$ and $\frac{\varepsilon_z^L-\varepsilon_x^L}{\varepsilon_z^L}$ are 0.22 and .70 respectively (Figure 2.4c). This is a clear indication that coal can be approximated as transversely isotropic medium for sorptive gases as well.

Furthermore, to analyze the results in a mechanistic way, we first establish the constitutive equations applicable for a transversely isotropic material, like coal, in the following sub-section.

2.3.1.1. Constitutive Equation

The following constitutive equation, used in the analysis, was introduced by Espinoza et al. (2014) for sorptive anisotropic microporous solids:

$$\sigma_{11} = C_{11}\varepsilon_{11} + C_{12}\varepsilon_{22} + C_{13}\varepsilon_{33} - b_1 p_c - (1 - b_1)s_m^{a1}(p) \quad (2.4a)$$

$$\sigma_{22} = C_{12}\varepsilon_{11} + C_{11}\varepsilon_{22} + C_{13}\varepsilon_{33} - b_1 p_c - (1 - b_1)s_m^{a1}(p) \quad (2.4b)$$

$$\sigma_{33} = C_{13}\varepsilon_{11} + C_{13}\varepsilon_{22} + C_{33}\varepsilon_{33} - b_3 p_c - (1 - b_3)s_m^{a3}(p) \quad (2.4c)$$

$$\sigma_{23} = 2C_{44}\varepsilon_{23} \quad (2.4d)$$

$$\sigma_{31} = 2C_{44}\varepsilon_{31} \quad (2.4e)$$

$$\sigma_{12} = 2\frac{(C_{11} - C_{12})}{2}\varepsilon_{12} \quad (2.4f)$$

where, σ_{ij} is the total stress along i-j direction, C_{ij} is the i-jth component of compliance matrix, ε_{ij} is the strain in i-jth direction, b_i is the Biot's coefficient in the ith direction, p_c is the pore pressure in the cleat system, and $s_m^{ai}(p)$ is the pressure-dependent sorption based stress. The subscript m denotes that the parameter is for matrix scale. The subscript convention in this paper is 1/2- for horizontal directions and 3 for vertical direction; hence subscripts to stress and strain have been inter-changeably used as 11 or x/h for horizontal direction and 33 or z/v for vertical direction. Since, the experiment was unconstrained; there is no Biot's coefficient term in Equations (2.4a-2.4c). Also, under hydrostatic gas pressure, Equations (2.4d-2.4f) are meaningless because there is no shear stress. Hence, Equations (2.4a-2.4c) were simplified as follows (all parameters in these equations are at matrix scale) and used to analyze the matrix anisotropy:

$$\sigma_{11} = \sigma_{22} = -p = (C_{11} + C_{12})\varepsilon_{11} + C_{13}\varepsilon_{33} - s_1^a(p) \quad (2.5a)$$

$$\sigma_{33} = -p = 2(C_{13}\varepsilon_{11}) + C_{33}\varepsilon_{33} - s_3^a(p) \quad (2.5b)$$

The above equations assume horizontal isotropy, that is, subscript 1 and 2 are written as 1, representing the horizontal direction and 3 represents parameters in the vertical direction.

2.3.1.2. Anisotropy of Coal at Matrix Scale (Non-sorbing Gas - Helium)

For helium, there is no sorption term and the equations (Equation 2.5a and Equation 2.5b) are further simplified as:

$$\begin{bmatrix}\varepsilon_{11}\\ \varepsilon_{33}\end{bmatrix} = \begin{bmatrix}\frac{1-\nu_1}{E_1} & \frac{-\nu_3}{E3}\\ \frac{-2\nu_3}{E_3} & \frac{1}{E_3}\end{bmatrix}\begin{bmatrix}-p\\ -p\end{bmatrix} \quad (2.6)$$

where, ε_{11} and ε_{33} are strains in horizontal and vertical directions, E_1, E_3, $\nu_1$and ν_3 are Young's modulus in horizontal direction, Young's modulus in vertical direction, Poisson's ratio in horizontal direction and in vertical direction respectively. Taking the derivative of Equation (2.6) gives the coal matrix compressibility in the horizontal and vertical directions. To the best of our knowledge, currently available literature does not provide an expression for estimating the anisotropic compressibility of coal at matrix scale in different directions, given as:

$$\begin{bmatrix}\frac{d\varepsilon_{11}}{dp}\\ \frac{d\varepsilon_{33}}{dp}\end{bmatrix} = \begin{bmatrix}\frac{1-\nu_1}{E_1} & \frac{-\nu_3}{E3}\\ \frac{-2\nu_3}{E_3} & \frac{1}{E_3}\end{bmatrix}\begin{bmatrix}-1\\ -1\end{bmatrix} \quad (2.7)$$

The results of strain at different pressure, presented in Figure 2.4, were used to satisfy Equation (2.6) and Equation (2.8). Since there were four unknowns E_1, E_2, $\nu_1$and ν_3 and only three equations, the value of $\nu_1$was assumed to be 0.19.

$$\frac{\nu_1}{\nu_3} = \frac{E_1}{E_3} \quad (2.8)$$

Using the results presented in Figure 2.3, the assumed value of 0.19 for ν_1, and solving

for other mechanical constants in Equation (2.7), we estimated the full stiffness matrix presented in the equation at matrix scale. In addition, Equations (2.9) and (2.10) can be written for the pressure derivative of strains in the horizontal and vertical directions using the results presented in Figure 2.4a.

$$\frac{d\varepsilon_{x/y}}{dP} = S_{x/y} = -4.5E-05 \text{ MPa}^{-1} \quad (2.9)$$

$$\frac{d\varepsilon_{z}}{dP} = S_{z} = -6E-05 \text{ MPa}^{-1} \quad (2.10)$$

where, S_i is a symbol used to indicate the slope of the strain with respect to pressure in the i^{th} direction and $\varepsilon_{x/y}$ and ε_z are strains in horizontal and vertical direction used interchangeably for ε_{11} and ε_{33}. To analyze the results, we first define Anisotropy ratio (A_n) as the ratio of the derivative of strains in the horizontal and vertical directions with respect to pressure, mathematically given as:

$$A_n = \frac{S_{x/y}}{S_z} = 0.75 \quad (2.11)$$

It can be seen that the value of A_n remained constant at 0.75 with changes in helium pressure. Hence, coal exhibits a constant transverse anisotropy throughout the experiment for helium.

At this point, we would like to introduce a mechanistic analysis of the Anisotropy ratio (A_n). Anisotropy ratio (A_n), as presented in Equation (2.11), is simply the ratio of elastic moduli of coal at matrix scale using Equation (2.7), which can be presented as follows:

$$A_n = \frac{S_{x/y}}{S_z} = 0.75 = \frac{\frac{d\varepsilon_{11}}{dp}}{\frac{d\varepsilon_{33}}{dp}} = \frac{-\left(\frac{1-\nu_1}{E_1}\right)+\frac{\nu_3}{E_3}}{\frac{2\nu_3}{E_3}-\frac{1}{E_3}} \quad (2.12)$$

Since helium is non-sorptive, elastic moduli of coal are not impacted by the sorption phenomenon, and the Anisotropy ratio remains constant with changes in pressure. The value of Anisotropy ratio is 0.75, which is less than one, where unity denotes isotropic rock.

2.3.1.3. Anisotropy of Coal at Matrix Scale (Sorbing Gas – Methane/Carbon Dioxide)

Figure 2.4 shows that the magnitude of strain with CO_2 is larger than that for methane which, in turn, is larger than that for helium. The relationship of helium strain vs pressure is linear, whereas those for methane and CO_2 are fitted using the Langmuir-type model (Harpalani and Chen, 1997; Levine, 1996; Liu and Harpalani, 2014), shown as:

$$\varepsilon_i = \frac{\varepsilon_\infty P}{P_\varepsilon + P} \tag{2.13}$$

where, ε_i is strain in coal at pressure p, ε_∞ is strain in coal at infinite pressure or Langmuir volume-like constant and P_ε is the Langmuir pressure-like constant. The horizontal strain is taken as the average of the strains in the x- and y- directions, an approximation valid for transversely isotropic behavior given that the values in the directions were close. Since the slopes for methane and CO_2 plots are pressure-dependent, Equations (2.9-2.11) are re-written for sorptive gases as:

$$\frac{d\varepsilon_{x/y}}{dP} = S_{x/y} = \left\{\frac{\varepsilon_\infty P_\varepsilon}{(P_\varepsilon + P)^2}\right\}_{x/y} \tag{2.14}$$

$$\frac{d\varepsilon_z}{dP} = S_z = \left\{\frac{\varepsilon_\infty P_\varepsilon}{(P_\varepsilon + P)^2}\right\}_z \tag{2.15}$$

$$A_n = \frac{\left\{\frac{\varepsilon_\infty P_\varepsilon}{(P_\varepsilon + P)^2}\right\}_{x/y}}{\left\{\frac{\varepsilon_\infty P_\varepsilon}{(P_\varepsilon + P)^2}\right\}_z} \tag{2.16}$$

Using the above equations and results shown in Figures 2.4(b-c), A_n was estimated and the results are shown in Figures 2.6a and 2.6b. The change in Anisotropy ratio with continued injection (Figure 2.5a) appears to be insignificant when considering the variation on a scale of 0 to 1. A change of 0.04, from 0.74 being the value at lowest pressure (~0.3 MPa) to 0.79 at the highest pressure (10 MPa for methane and ~ 6 MPa for CO_2). However, it is more significant

when considered on a different scale, to only focus on changes in Anisotropy ratio for each gas from its initial value of 0.74, and this is highlighted in Figure 2.5b.

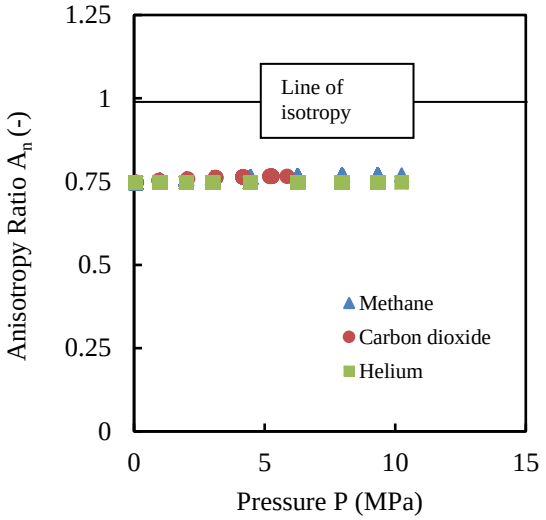

Figure 2.6a Anisotropy ratio with helium, methane, CO_2 injection on a scale of (0 to 1), where 1 refers to isotropy.

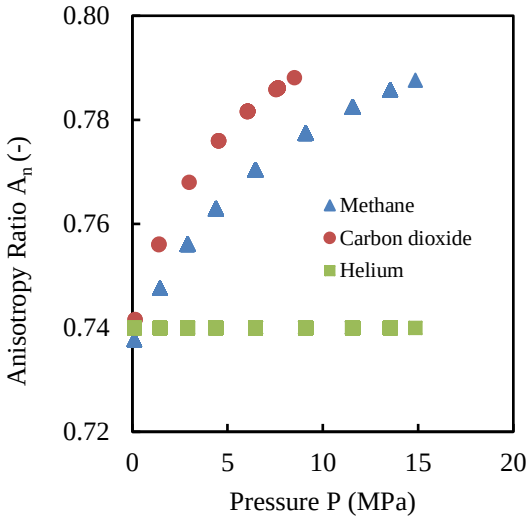

Figure 2.6b Anisotropy ratio with helium, methane, CO_2 injection (scaled from 0.72 to o.80).

Figure 2.6 Anisotropy ratio with helium, methane and CO_2.

It is important to mention that anisotropy variations are rarely reported as a large number, even under non-hydrostatic conditions (Nur and Simmons, 1969). It is interesting to note that the initial value of A_n is similar for all gases, suggesting that, at low pressure (~ 0.3 MPa), anisotropy is not affected by sorption and the values are the same for helium, methane and carbon dioxide. This is counterintuitive to the findings of previous researchers that different gases access different proportion of micropores in the coal matrix (Melnichenko et al., 2012; Zhang et al., 2015) and, this should affect the Anisotropy ratio. Also, it was found that the increase in the ratio for sorptive gases at higher pressure, approaching a constant value of 0.79, that is, higher isotropy, than at low pressure. Hence, the sorption phenomenon reduces the anisotropic behavior of coal under hydrostatic conditions. It is worthwhile pointing out that the behavior of anisotropy variation in Figure 2.6a was affected by the differential accessibility of methane and carbon

dioxide to micropores in the matrix. Carbon dioxide is more sorptive than methane, its affinity being three to ten times higher than that for methane (Busch et al., 2004; Krooss et al., 2002; van Bergen et al., 2011; Weniger et al., 2010). Another interesting feature about the variation of Anisotropy ratio is its resemblance with the Langmuir plot. Analysis was carried out using two approaches to model the variation of the Anisotropy ratio, first using the mechanistic concept of Biot's-like coefficient introduced by Espinoza et al., (2013), followed by another using the Langmuir-like fit.

A. Using Biot's Like Coefficient: Espinoza et al., (2013) introduced the concept of Biot's-like coefficient, which coupled the mechanical and sorptive behavior of microporous media, like coal. The concept is used here to model the variation of Anisotropy ratio (An) with variation in gas pressure. To develop such a mechanistic model of variation of Anisotropy ratio (An), we start with the constitutive equations, represented in Equations 2.5(a-b) in matrix form as:

$$\begin{bmatrix}\varepsilon_{11}\\ \varepsilon_{33}\end{bmatrix}=\begin{bmatrix}\frac{1-\nu_1}{E_1} & \frac{-\nu_3}{E3}\\ \frac{-2\nu_3}{E_3} & \frac{1}{E_3}\end{bmatrix}\begin{bmatrix}-p+\ s_1^a(p)\\ -p+\ s_3^a(p)\end{bmatrix} \tag{2.17}$$

Differentiating the above equation with respect to pressure gives the following:

$$\begin{bmatrix}\frac{d\varepsilon_{11}}{dp}\\ \frac{d\varepsilon_{33}}{dp}\end{bmatrix}=-\begin{bmatrix}\frac{1-\nu_1}{E_1} & \frac{-\nu_3}{E3}\\ \frac{-2\nu_3}{E_3} & \frac{1}{E_3}\end{bmatrix}\begin{bmatrix}\frac{ds_1^a(p)}{dp}-1\\ \frac{ds_3^a(p)}{dp}-1\end{bmatrix} \tag{2.18}$$

Anisotropy ratio (A_n) for coal matrix with sorptive gas pressure can then be estimated as:

$$A_n=\frac{\frac{d\varepsilon_{11}}{dp}}{\frac{d\varepsilon_{33}}{dp}}=\frac{\left\{\left(\frac{1-\nu_1}{E_1}\right)\left(\frac{ds_1^a(p)}{dp}-1\right)+\left(\frac{-\nu_3}{E3}\right)\left(\frac{ds_3^a(p)}{dp}-1\right)\right\}}{\left\{\left(\frac{-2\nu_3}{E_3}\right)\left(\frac{ds_1^a(p)}{dp}-1\right)+\left(\frac{1}{E_3}\right)\left(\frac{ds_3^a(p)}{dp}-1\right)\right\}} \tag{2.19}$$

Using Equation (2.19), changes in Anisotropy ratio (A_n) of coal matrix can be predicted after estimating the derivative of sorption stresses with pressure, also termed the Biot's-like

coefficient, and using shrinkage/swelling data for carbon dioxide and methane (Figure 2.4b and Figure 2.4c), along with the elastic constants of coal at matrix scale (Table 2.3). A discussion of the methodology of determining Biot's-like coefficient is included in Appendix I for the sake of completeness. However, a full treatment can be found in Espinoza et al. (2013).

Table 2.3 Values of coal elastic moduli estimated at matrix scale – obtained by solving Equation 3 using data in Figure 4a and assuming a value of v_1.

	E_1 (GPa)	E_3 (GPa)	v_1	v_3
Values	8.5	7	0.19	0.16

The results of the Anisotropy ratio modeling using Biot's-like coefficient modeling compared to experimentally obtained results are presented in Figure 2.7a.

B. Langmuir Like Fit: Another approach used in this study to quantify the Anisotropy ratio variation is curve fitting of experimentally derived data using a Langmuir-like fit given that the Anisotropy ratio (An) variation exhibited a similar trend (Figure 2.5b). However, at zero pressure, unlike the Langmuir fit, the value does not go to zero. Hence, the fit was modified to accommodate the non-zero value at zero pressure, mathematically given as:

$$A_n = (A_n)_{He} + \frac{(A_n)_L P}{P + P_{(A_n)_L}} \tag{2.20}$$

Where, $(A_n)_{He}$ is 0.75 for this coal type (determined from helium unconstrained experiment), $(A_n)_L$ is the Langmuir volume-like constant and $P_{(A_n)_L}$ is the Langmuir pressure-like constant. The value of $(A_n)_L$ was estimated to be 0.075 for methane and 0.077 for carbon dioxide. Similarly, the values of $P_{(A_n)_L}$ were 6 and 4 MPa for the two gases respectively. The results of the Anisotropy ratio modeling using Langmuir-like fit compared to experimentally

obtained results are presented in Figure 7b.

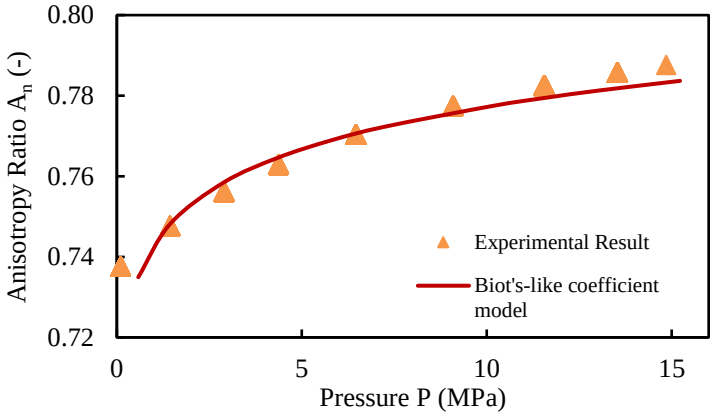

Figure 2.7a Variation of Anisotropy ratio (A_n) with methane pressure determined using Biot's like coefficient modeling

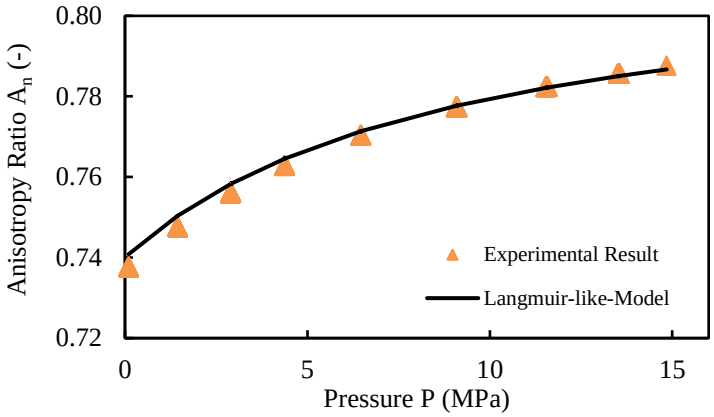

Figure 2.7b Variation of Anisotropy ratio (A_n) with methane pressure using Langmuir modeling.

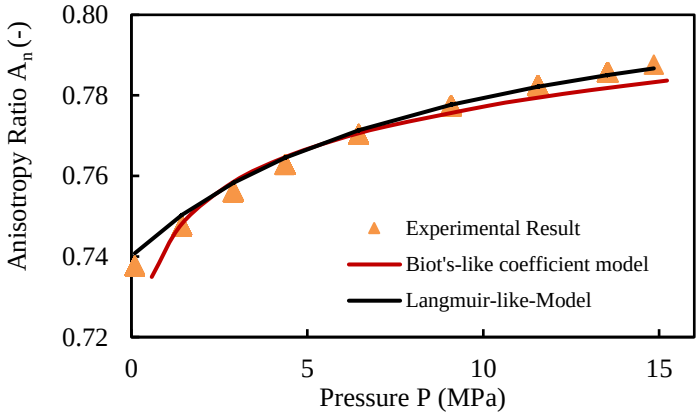

Figure 2.7c Comparison of variation of Anisotropy ratio (A_n) with methane pressure using both models

Figure 2.7 Variation of Anisotropy ratio (A_n) with methane pressure.

The correlation coefficient (R^2) between the experimental values of Anisotropy ratio and that predicted by Biot's-like coefficient-based model was 65%. Similarly, correlation coefficient between the experimental values of Anisotropy ratio and that predicted by Langmuir based model was 81%. The higher correlation coefficient for Langmuir based model suggests that it is more suitable for predicting the Anisotropy ratio for coal. However, we believe that the Biot's-like coefficient-based model is more appropriate since it gives a mechanistic view of the Anisotropy ratio, rather than an empirical prediction.

Since this technique works to model the Anisotropy ratio (A_n) variation of coal at matrix scale, we extended it to estimate the Anisotropy ratio of coal at bulk scale.

Finally, with CO_2/methane depletion, say in the San Juan basin, where CO_2 component in the produced gas is significant in several locations, the Anisotropy ratio would change in a Langmuir isotherm-*like* manner (Figure 2.7b). The anisotropy variation in a CBM reservoir would then depend on the gas composition in the reservoir (Bae et al., 2009; Zhang et al., 2015). At this point, we would like to present a comparative study between hypothetical depletion of a mixture of methane and carbon dioxide from coal matrix, with composition varying with pressure, as presented in Table 2.4.

Table 2.4 Gas composition and pressure for simulation.

Pressure (MPa)	Methane Concentration (%)	Carbon dioxide Concentration (%)
10	99	1
7	95	5
3	85	15
1	75	25

We used the concept of extended Langmuir-like model for simulation of the variation of Anisotropy ratio of coal with depletion of a multi-component methane/CO_2 mixture, as shown below:

$$(A_n)_i = (A_n)_{Li}\left\{\frac{\left(\frac{1}{P_{(A_n)_L}}\right)_i * p_i}{1+\Sigma\left(\frac{1}{P_{(A_n)_L}}\right)_i * p_i}\right\} \quad (2.21)$$

where, p_i is the partial pressure of the gas species, $(A_n)_{Li}$ is the Langmuir volume-like constant for coal and $\left(\frac{1}{P_{(A_n)_L}}\right)_i$ is Langmuir pressure-like constant for the gas species (methane or carbon dioxide). Also, this study can be conducted at bulk scale using the technique presented in the paper under hydrostatic conditions. The simulation result is presented in Figure 2.8, showing that the Anisotropy ratio of coal is affected by gas composition.

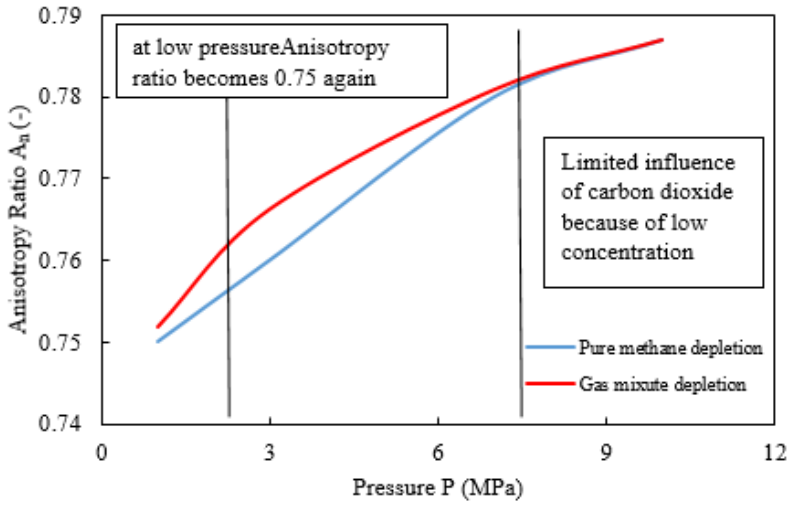

Figure 2.8 Anisotropy ratio variation of coal matrix with variable composition.

It can be seen that the of CO_2 in the composite gas is minimum at high pressure because of high methane concentration, but there is a significant difference in the middle portion of the plot, a difference of 0.2 or, 66 % of the total change during depletion. Again, with depletion, both plots start to converge to the value of 0.75, which is the value of Anisotropy ratio for

helium, that is, without any sorption effect.

2.3.2. Bulk Scale Anisotropy of Coal

To evaluate the anisotropy of coal under constrained bulk condition, we made the following basic assumptions:

A. Coal under *in situ* condition (bulk) can be geometrically represented as a bundle of matchsticks.

B. Under constant hydrostatic stress and constrained flow conditions, the ratio of strain in vertical and horizontal directions in bulk coal is due to both anisotropic nature of coal and stress-induced anisotropy.

Again, we start with the constitutive equations presented as Equations 2.4(a-f) and mathematical representation of the assumptions made, that is, hydrostatic condition. We assume horizontal isotropy, that is, x- and y- directions representing the horizontal plane are the same. These simplifications reduce Equations 2.4(a – c) to the following:

$$\sigma_h = (C_{11} + C_{12})\varepsilon_h + C_{13}\varepsilon_v - b_h p_c - (1 - b_h)s_m^{ah}(p) \quad (2.22a)$$

$$\sigma_v = 2C_{13}\varepsilon_h + C_{33}\varepsilon_v - b_v p_c - (1 - b_v)s_m^{av}(p) \quad (2.22b)$$

Furthermore, the assumption of constant triaxial hydrostatic stress condition gives the following relationship:

$$\sigma_h = \sigma_v = \sigma \quad (2.23)$$

Representing Equations 2.22(a-b) in matrix form, we have:

$$\begin{bmatrix}\sigma \\ \sigma\end{bmatrix} = \begin{bmatrix}C_{11} + C_{12} & C_{13} \\ 2C_{13} & C_{33}\end{bmatrix}\begin{bmatrix}\varepsilon_h \\ \varepsilon_v\end{bmatrix} - p_c\begin{bmatrix}b_h \\ b_v\end{bmatrix} - \begin{bmatrix}s_m^{ah}(p) & 0 \\ 0 & s_m^{av}(p)\end{bmatrix}\begin{bmatrix}1 - b_h \\ 1 - b_v\end{bmatrix} \quad (2.24)$$

Taking the derivative of the equation above gives the following:

$$\begin{bmatrix} \frac{d\varepsilon_h}{dp} \\ \frac{d\varepsilon_h}{dp} \end{bmatrix} = \left(\begin{bmatrix} C_{11} + C_{12} & C_{13} \\ 2C_{13} & C_{33} \end{bmatrix}^{-1} \right) \left\{ \begin{bmatrix} \frac{d\sigma}{dp} + b_h \\ \frac{d\sigma}{dp} + b_v \end{bmatrix} + \begin{bmatrix} \frac{ds_m^{ah}(p)}{dp} & 0 \\ 0 & \frac{ds_m^{av}(p)}{dp} \end{bmatrix} \begin{bmatrix} 1 - b_h \\ 1 - b_v \end{bmatrix} \right\} \quad (2.25)$$

$$\begin{bmatrix} \frac{d\varepsilon_h}{dp} \\ \frac{d\varepsilon_h}{dp} \end{bmatrix} = \begin{bmatrix} \frac{1-\nu_1}{E_1} & \frac{-\nu_3}{E_3} \\ \frac{-2\nu_3}{E_3} & \frac{1}{E_3} \end{bmatrix} \left\{ \begin{bmatrix} \frac{d\sigma}{dp} + b_h \\ \frac{d\sigma}{dp} + b_v \end{bmatrix} + \begin{bmatrix} \frac{ds_m^{ah}(p)}{dp} & 0 \\ 0 & \frac{ds_m^{av}(p)}{dp} \end{bmatrix} \begin{bmatrix} 1 - b_h \\ 1 - b_v \end{bmatrix} \right\} \quad (2.26)$$

Using Equation 2.26, the Anisotropy ratio (A_n) of coal at bulk scale can be determined. The elastic constants were determined at bulk scale using the compressive strength tests (reported in Table 2.2); a value of 0.95 and 0.78 for Biot's coefficient in horizontal and vertical directions, as determined for the same coal sample in a prior study (Saurabh et al., 2016), was used. Also, the values of Biot's-like coefficient used for modeling are the same as determined in sub-section 2.3.1.3. A comparison of Anisotropy ratio (A_n) at bulk and matrix scale is presented in Figure 2.9a. The variation is more apparent in Figure 2.9b, where the axis has been scaled to better demonstrate the variation. It can be seen in Figure 2.9b that, if sorption phenomenon is not considered, the Anisotropy ratio is 0.30 for coal at bulk scale prior to depletion and, at the end of depletion, the corresponding value is 0.23. The value of Anisotropy ratio at bulk scale was lower than at matrix scale, varying from a minimum value of 0.23 at ~0.5 MPa to 0.30 at ~10.5 MPa, whereas the value of Anisotropy ratio at matrix scale was 0.74 and 0.79. The probable reason behind this can be stronger anisotropic nature of coal at bulk scale due to the fracture network and bedding planes, which is manifested in the model in terms of the elastic moduli values used in the modeling process.

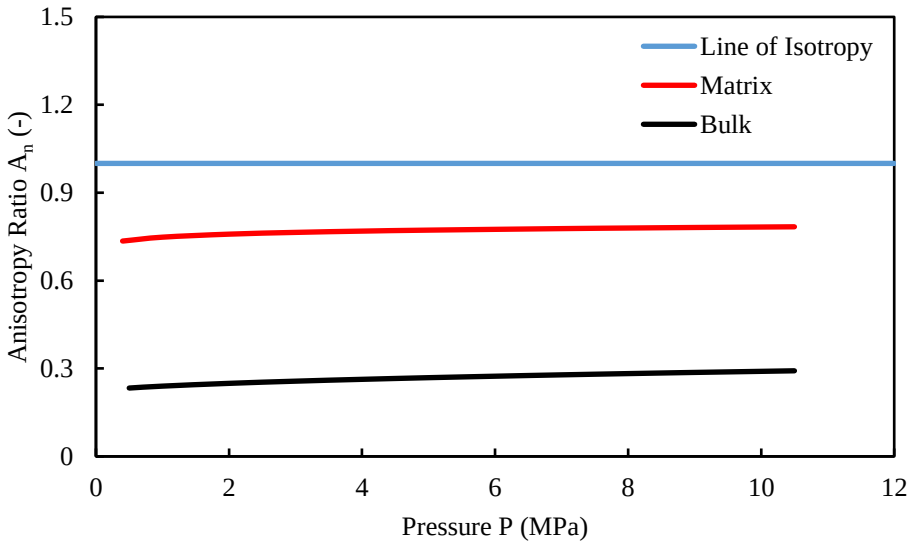

Figure 2.9a Variation of Anisotropy ratio of coal at matrix and bulk scales with methane pressure.

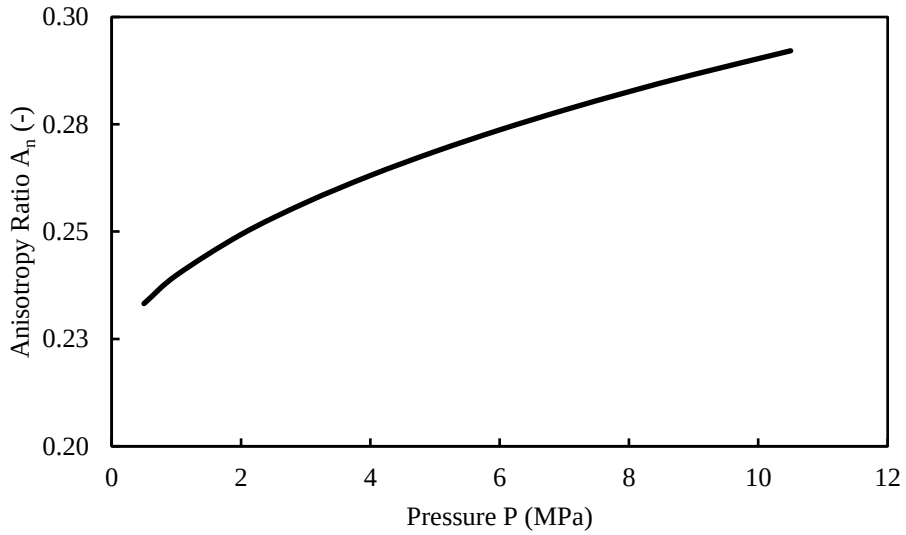

Figure 2.9b Variation of Anisotropy ratio of coal at bulk scale (scaled axis).

Figure 2.9 Variation of Anisotropy ratio of coal at bulk scale.

2.4 Discussion

The value of A_n is constant for helium and variable for sorptive gases. Hence, the matrix anisotropy of coal is a variable throughout depletion in CBM reservoirs, or a coal mine with

methane emissions, although changes in anisotropy do not appear to be significant (Figure 2.4a). However, in this section we establish the implications of the variation in Anisotropy ratio, which is an indicator of change in the rock anisotropy. On an absolute scale, the maximum that the Anisotropy ratio can increase is from 0.75 to 1, a total increase of 0.25. Of this, an increase of 0.04 was recorded at 10 MPa and an increase of 0.08 is possible using the theoretical limit at infinitely high pressure (Equation 20), which is 16% and 32 % of the maximum possible increase. Hence, the changes are not trivial as their absolute magnitude may suggest.

Change in Anisotropy ratio is not a primary phenomenon and is caused by sorption of methane on coal. Again, if sorption phenomenon is not considered, the Anisotropy ratio is 0.30 for coal at bulk scale prior to depletion and, at the end of depletion, the corresponding value is 0.23 (Figure 2.7). If minimal change in the Poisson's ratio is assumed, and using (Equation 2.9), the value of elastic moduli in vertical and horizontal directions at the end of depletion would be 1.5 and 0.85 GPa in the horizontal and vertical directions respectively. Comparing with the values presented in Table 2.5 suggests a change of ~0.2 GPa in the moduli values in each direction for the coal tested.

Table 2.5 Coal mechanical parameters obtained at bulk scale.

	E_1 (GPa)	E_3 (GPa)	v_1 (-)	v_3 (-)
Values	1.7	1.1	0.4	0.2

Assuming only elastic strain in the reservoir and Biot's coefficient to be 1 in all directions, we can simplify Equation 2.22a as:

$$\sigma_h = (C_{11} + C_{12})\varepsilon_h + C_{13}\varepsilon_v - p_c \quad (2.27)$$

This can be further simplified using the values of moduli presented in Table 2.5, and since pore-pressure is compressive in nature, as:

$$\sigma_h = (350)\varepsilon_h + (-180)\varepsilon_v + p_c \quad (2.28)$$

Taking the derivative of Equation 2.28 with respect to pressure, we can write the following:

$$\frac{d\sigma_h}{dP} = (350)\frac{d\varepsilon_h}{dP} + (-180)\frac{d\varepsilon_v}{dP} + 1 \quad (2.29)$$

We can write the above equation for three different cases now and analyze them one by one.

Case I: Hydrostatic stress condition and isotropic rock condition: Under hydrostatic stress and isotropic rock condition, $\frac{d\varepsilon_h}{dP}$ and $\frac{d\varepsilon_v}{dP}$ would be equal. Under such condition, for a depletion of 1 MPa in pore pressure, we can write the following after simplification:

$$\Delta\sigma_h = \Delta\varepsilon_v\,(170) + 1 \quad (2.30)$$

Assuming a strain of magnitude 0.001-0.01 in vertical direction, the predicted change in horizontal stress can vary between 2.7 and 1.17 MPa.

Case II: Hydrostatic stress condition and anisotropic rock condition, at 10.5 MPa (Figure 9b): Under such condition, the estimated Anisotropy ratio is 0.30 ($\left.\frac{d\varepsilon_h}{dP}\right/\frac{d\varepsilon_v}{dP}$) and we then can simplify Equation 2.29 and write the following for a depletion of 1 MPa in pore pressure:

$$\Delta\sigma_h = \Delta\varepsilon_v\,(-75) + 1 \quad (2.31)$$

Again, assuming a strain of 0.001-0.01, like in previous case, the predicted change in horizontal stress would be between 0.93 and 0.25 MPa.

Case III: Hydrostatic stress condition and anisotropic rock condition, at 0.5 MPa (Figure 9b): Under such condition, the estimated Anisotropy ratio is 0.23($\left.\frac{d\varepsilon_h}{dP}\right/\frac{d\varepsilon_v}{dP}$) and we can simplify Equation 2.29 and write the following for a depletion of 1 MPa in pore pressure:

$$\Delta\sigma_h = \Delta\varepsilon_v\,(-100) + 1 \quad (2.32)$$

Again, assuming a strain magnitude of 0.001-0.01, like in previous case, the predicted change in horizontal stress would be between 0.9 and 0 MPa.

Comparing the results of all three cases, we can say that there is over-estimation of stress variation under the assumption of isotropy by at least 1 MPa in our hypothetical case. Also, the variable anisotropy, Cases II and III, show that it affects the stress variation in the reservoir in the range of 0.3 and 0.03 MPa. The implication of variable anisotropy based prediction of stress variation can be significant if the deformation is larger. This translates to under-estimation of the mean stress, one of the primary factors controlling compaction/permeability in CBM reservoirs, leading to over-prediction of permeability under the assumption of isotropy or constant anisotropy. Hence, changes in anisotropy can be a major factor in stress variation and, hence, reservoir permeability.

When discussing the results of pressure and composition dependence of coal anisotropy (Figure 2.9), the effect can barely be seen at higher pressures because of high methane concentration. However, it is significant in the middle portion of the plot. Also, with depletion, the effect of composition diminishes and the nature of variation of Anisotropy ratio with compositional variation in a typical CBM reservoir can be expected to be parabolic in nature with a maximum somewhere in the mid-pressure range of depletion.

2.5 Conclusions

This paper presents a novel approach to coal anisotropy, quantifying it in a mechanistic way. In the past, this is typically treated as the ratio of two elastic moduli. Here, we have presented two modeling techniques to estimate the transverse isotropy and track it with depletion or injection of gases, and both gave excellent results. The overall approach is a significant

improvement over the traditional techniques.

The conclusions made based on the analysis and modeling carried out in this paper are as follows:

- Coal's behavior can be approximated to be transversely isotropic under non-sorptive gases (helium) or sorptive gases (methane or carbon dioxide). However, the important detail here is that this anisotropy is pressure-dependent for sorptive gases. Furthermore, it decreases at high pressures of sorptive gases. Hence, the anisotropy would increase with continued depletion of CBM reservoirs.
- Anisotropy ratio of coal varies differently for methane and carbon dioxide for the matrix, primarily due to their different sorptive affinities for coal. Interestingly, the variation for both resembles the classic Langmuir isotherm and this characteristic can be used to model the variation in the Anisotropy ratio.
- Coal Anisotropy ratio values at bulk scale was found to be lower than that at matrix scale (much lower than 1). However, the trend was similar to that of Anisotropy ratio variation at matrix level. The variation is attributed to sorptive behavior of coal and the higher scale of anisotropy (that is, lower value of Anisotropic ratio) is attributed to higher anisotropy of coal at bulk scale due to bedding planes and fracture networks involved at bulk scale, manifested in the model in terms of the elastic moduli values used for modeling purposes of Anisotropy ratio in the study.
- Lastly, the implication of the study presented is that coal anisotropy, under reservoir conditions, would depend on pressure as well as gas composition. At higher reservoir pressure and higher carbon dioxide concertation, the reservoir behavior would be more isotropic. The implication of such behavior can be seen most for carbon sequestration

projects, where carbon dioxide would decrease the anisotropy of the reservoir, as predicted by our model.

When simulating for a composite gas mixture of methane and carbon dioxide, the effect of carbon dioxide was only seen at lower pressures, probably because carbon dioxide concentration is high at low pressure.

CHAPTER 3

PERMEABILITY MODELING AND INVESTIGATION OF FAILURE WITH DEPLETION

This Chapter is an exact copy (except for format change) of the journal paper entitled "Implications of stress re-distribution and rock failure with continued gas depletion in coalbed methane reservoirs", published in *International Journal of Coal Geology*, 2016. DOI: 10.1016/j.coal.2016.06.006.

Authors:

Suman Saurabh, Satya Harpalani & Vivek Singh

Abstract

Significant increases in permeability of coal with continued production of coalbed methane (CBM) is a well-accepted phenomenon, particularly in the San Juan basin in the US and Surat basin in Australia. Modeling this increase is either based on the resulting increase in fracture porosity of coal or the associated changes in stresses as a result of the sorption-induced strain. This paper combines the experimental results of a study that measured sorption-induced coal matrix volumetric strain with depletion and a model proposed to estimate the associated changes in stress. The overall changes in stress, resulting from the combined effect of the poro-mechanical behavior and sorption-induced strain, were estimated by introducing a Biot-like coefficient. Plotting the stress path followed during depletion along with the failure envelope for the coal-type clearly showed that shear failure of coal is possible due to anisotropic loading resulting from a large reduction in the horizontal stresses. This would explain the large increases in permeability, typically observed in CBM operations. Finally, a permeability model was

developed using the Biot-like coefficient, and assuming transversely isotropic behavior of coal. A comparison of the experimental and modeled permeability results showed that the model works well as long as coal does not fail. However, it demonstrates that a permeability model, incorporating failure of coal, is warranted for reliable prediction of permeability variation.

Keywords: Coalbed Methane; Stress Redistribution; Permeability; Shrinkage Compressibility.

3.1 Introduction

US coalbed methane (CBM) production was 1.4 trillion cubic feet (TCF) in 2014 and proven reserves at the time were estimated to be 15.7 TCF (EIA, 2015). Leading in production in the US were the states of Colorado, Wyoming, New Mexico, Virginia, Utah and Oklahoma. Although production has dipped from the all-time high of 1.9 TCF in 2010, CBM continues to be an important source of energy in the US.

The controlling mechanism when producing CBM is accepted to be coal permeability, typically believed to decrease with increasing depth (Unconventional Oil & Gas Production, 2010). However, coal exhibits a unique behavior, termed “matrix shrinkage”, associated with desorption of gas, resulting in increased permeability (Harpalani and Chen, 1997; Levine, 1996; Mitra et al., 2012; Singh, 2014). The outcome is a negative declining production trend when producing CBM. With continued production, there is an associated drawdown in gas pressure, which eventually changes the stress environment in the reservoir. The horizontal stress in CBM reservoirs has been reported to decrease with pressure drawdown (Mitra et al., 2012; Liu and Harpalani, 2013; Singh, 2014), the rate of decrease being 50% higher than the corresponding drop in pore pressure. This is significantly higher than the response reported for conventional reservoirs (Hillis, 2001; Teufel et al., 1991). Theoretically, based purely on conventional poro-elasticity, this ratio cannot be higher than unity (Zoback, 2007). Such a large decrease in

horizontal stress, together with the well accepted uniaxial strain conditions in reservoirs, results in anisotropic loading conditions of coal and ultimately failure (Singh, 2014; Espinoza et al., 2015).

This paper attempts to model the experimental data acquired recently (Singh, 2014) in order to explain the sorption-induced reduction in the horizontal stress with depletion of gas using a model proposed by Espinoza et al. (2015). The model is based on shear failure of coal with depletion in CBM reservoirs. Although primary effort is aimed at validating this model, validation of an intermittent model relating sorption strain and stress (Espinoza et al., 2013), which included a Biot-like coefficient, became inevitable and this is included. As a final step, a permeability model using the Biot-like coefficient and transversely isotropic nature of coal was developed. This model is shown to work well for coal as long as there is no failure. However, the permeability model needs to be extended for conditions leading to coal failure. Such modeling would present a complete picture of permeability variation with pressure, especially for deeper coals, such as, the Greater Green River basin, where CBM production is practically non-existent due to the burial depth and the associated stress conditions prevalent *in situ*.

3.2 Sample Characterization

The coal tested in this study was retrieved from southwestern part of the San Juan basin. The rank of coal was sub-bituminous. The ash and moisture content was 5.1 % and 7.9 % respectively. For sorption experiments, powdered sample (0.0425–0.0149 cm) was used. For matrix shrinkage experiments, coal quadrants were prepared by trimming off the ends of the coal core. Each sample was, therefore, approximately 0.75 inches thick and one inch in radius. The remaining portion of the coal core, of diameter two inches and three inches long, was used for the pressure-dependent-permeability (PdK) experiment. The bulk density of the coal core was

1.34 g/cm^3.

3.3 Experimental Works and Results

3.3.1. Experimental Work

Experimental data for the analysis presented in this paper was obtained from a laboratory-based study aimed primarily at establishing the pressure-dependent-permeability (PdK) of CBM reservoirs in the San Juan basin (Singh, 2014).

Three different experiments were carried out as a part of the overall study. First, sorption characteristics for methane were established. Using the sorption data, the Langmuir Constants, P_L and V_L, were estimated. Second, quadrants of end pieces of the coal core used for flow tests were utilized to measure the volumetric shrinkage/swelling strains under incremental hydrostatic pressure for unconstrained condition (unjacketed). This was first carried out for a non-sorbing gas (helium) and then repeated for a sorptive gas (methane). Third, a flow experiment was carried out replicating the *in situ* reservoir stress and uniaxial strain condition during drawdown. As a part of this experiment, stresses, volumetric strains and flowrates were measured for a step-wise decrease in pore pressure for each step of depletion, for both sorptive and non-sorptive gases independently. As a final step, triaxial strength of the coal type was estimated under incremental confining stress to establish the failure envelope for the coal type. Details of all experimental setups used and testing procedures are presented in Singh (2014).

3.3.2. Experimental Results

The matrix shrinkage experiments included measurement of strains in the three principal directions for unconstrained coal using helium and methane. Helium results provided the change in matrix volume due to de-compression of solid coal associated with depletion (pressure decrease), while methane results provided the overall strain resulting from the combined effects

of solid de-compression and volumetric strain associated with matrix shrinkage. The two results are shown in Figures 3.1 and 3.2. With helium depletion, the volume of solid coal increased as the pressure decreased from ~10 MPa (1500 psi) to atmospheric. For methane, on the other hand, the volume of solid coal decreased with depletion due to the dominant effect of sorption-induced matrix shrinkage.

For permeability experiments, the coal sample was initially stressed to *in situ* condition of the reservoir (total vertical stress: 20 MPa (2900 psi); initial total horizontal stress prior to depletion: 12.8 MPa (1850 psi); and, pore pressure: ~10 MPa (1500 psi)).

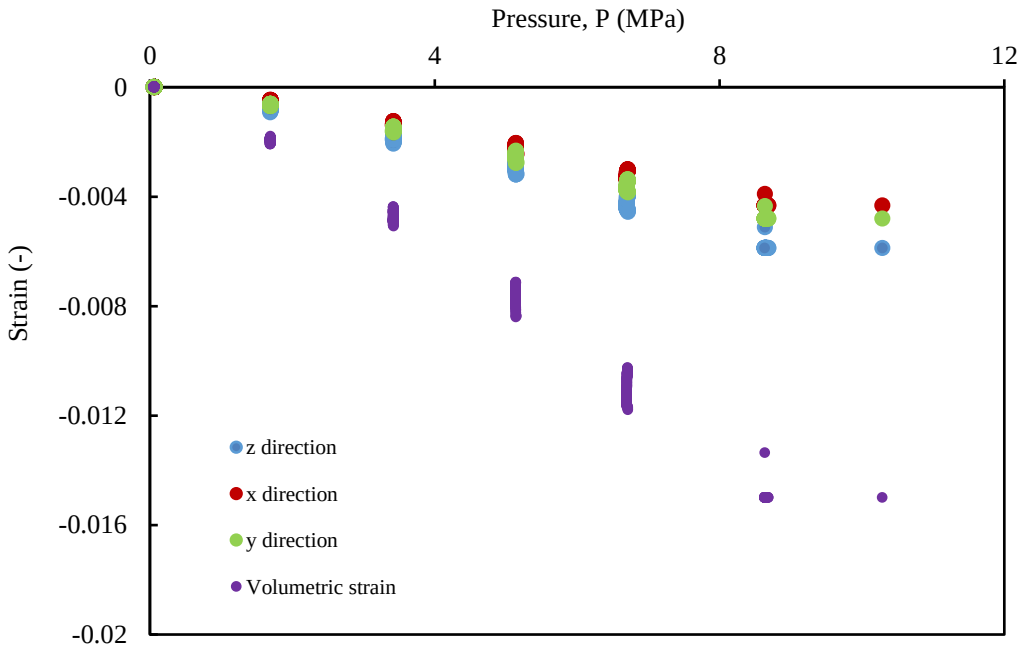

Figure 3.1 Measured strain with changes in pressure (unconstrained (unjacketed), helium).

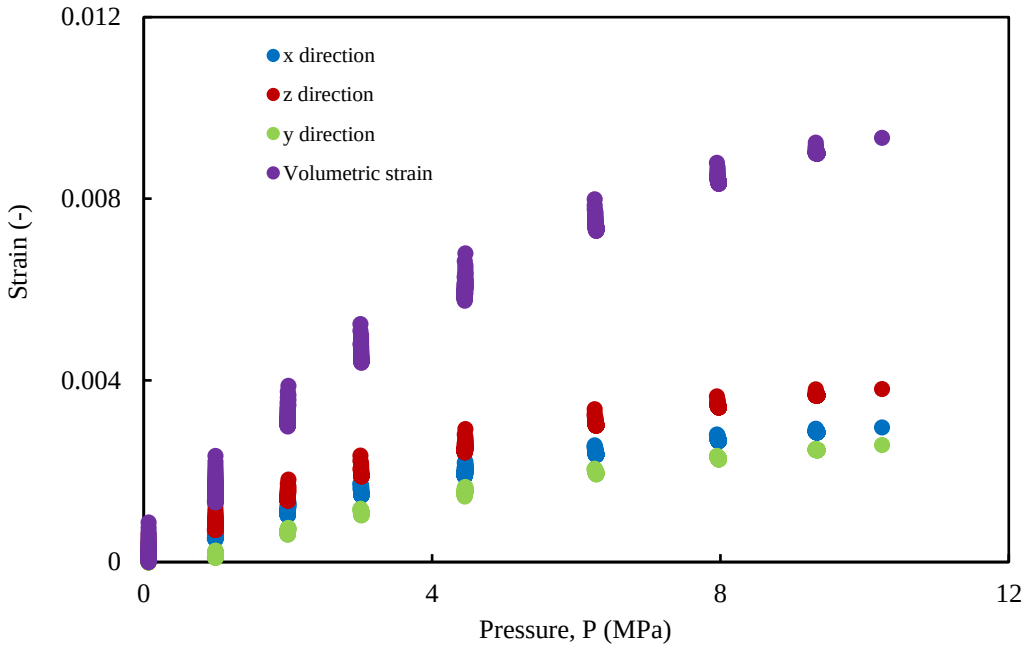

Figure 3.2 Measured strain with changes in pressure (unconstrained (unjacketed), methane).

Gas was then depleted in a stepwise manner for declining pressure, recording the strain and stresses continuously, and measuring the flowrate for each step under equilibrium conditions. Using the flowrate, permeability was calculated for each step, thus establishing the pressure-dependent-permeability trend for depletion. Throughout the experiment, uniaxial strain condition was maintained, that is, the horizontal strain was maintained zero and vertical stress was maintained constant. In order to compensate for the horizontal strain associated with matrix shrinkage, the horizontal stress was adjusted throughout the experiment. The results showing the change in horizontal stress for the two experiments are shown in Figure 3.3.

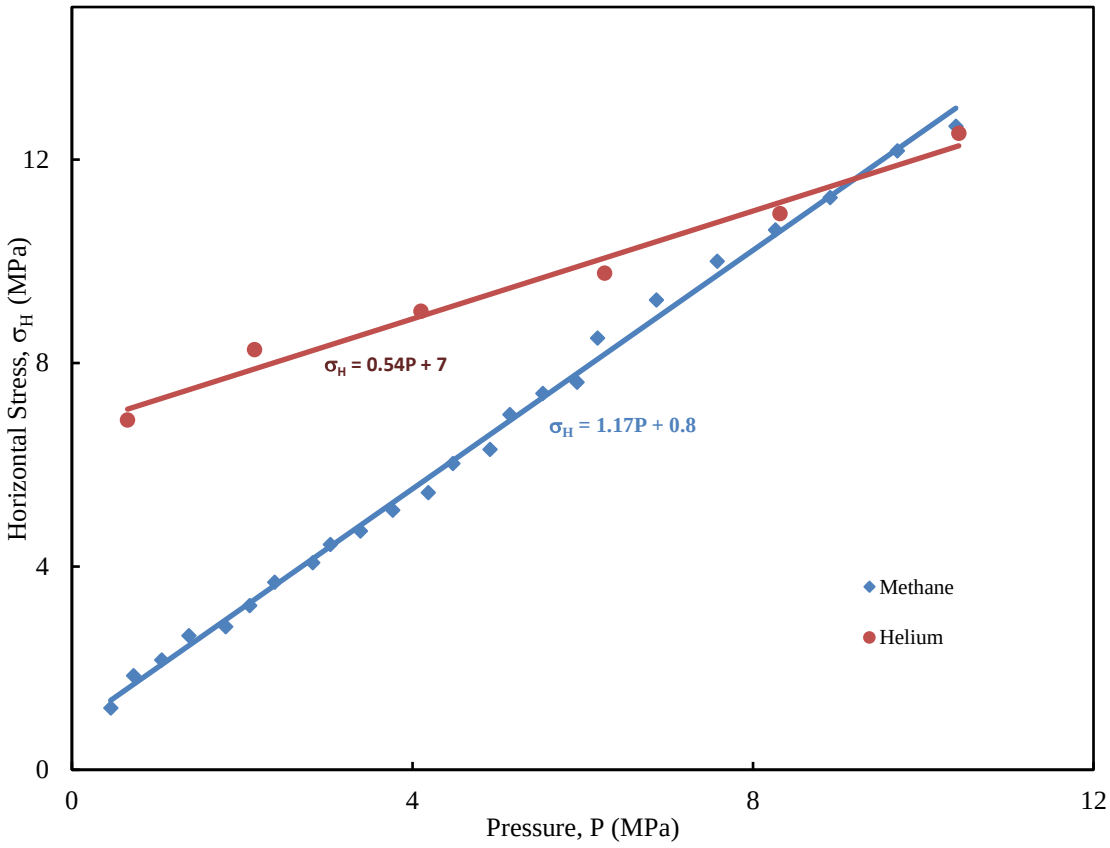

Figure 3.3 Changes in horizontal stress with helium and methane depletion. (Uniaxial strain conditions)

Relevant experimental statistics for the pressure- dependent-permeability experiment is presented in Table 3.1.

Table 3.1 Relevant statistics for pressure-dependent-permeability experiment.

Parameter	Range
Pressure (psi)	1505 – 66 Steps Size: 1500 – 900 (100 psi) 900 – 66 (50 psi)
Vertical Stress (psi)	2840- 2890
Horizontal Stress (psi)	1835- 176
Permeability, md	0.003- 1.213
k/k_0	1- 421

In addition to the flow and matrix shrinkage experiments, sorption isotherms for the coal type were established. The values of V_L and P_L were estimated to be 1.407 moles/l (749 scft) and 2.69 MPa (391 psi). Finally, triaxial strength testing was carried out on coal samples to establish the failure envelope for the coal type. The results are summarized in Table 3.2.

Table 3.2 Triaxial strength test results.

No.	Confining Pressure (MPa)	Axial Stress at Failure (MPa)
1	0	7.2 (UCS)
2	1.2	13.3
3	2.2	23.6
4	4.3	32.6

3.4 Analysis

3.4.1. Coal Transverse Isotropy

The results obtained from shrinkage/swelling experiment using helium, shown in Figure 3.1, suggest that coal behaves like an orthotropic rock. However, it can be approximated to be transversely anisotropic since the behavior in x- and y- directions is similar. This is not anomalous behavior for rock of sedimentary origin and has been suggested by Moore et al. (2014). Other experimental studies have also reported similar behavior (Evans and Pomeroy, 1966). The constitutive equations for a simplified transversely isotropic medium are as follows:

$$\begin{bmatrix} \sigma_x \\ \sigma_y \\ \sigma_z \\ \sigma_{xy} \\ \sigma_{yz} \\ \sigma_{xz} \end{bmatrix} = \begin{bmatrix} C_{11} & C_{11}-2C_{66} & C_{13} & 0 & 0 & 0 \\ C_{11}-2C_{66} & C_{11} & C_{13} & 0 & 0 & 0 \\ C_{13} & C_{13} & C_{13} & 0 & 0 & 0 \\ 0 & 0 & 0 & C_{44} & 0 & 0 \\ 0 & 0 & 0 & 0 & C_{44} & 0 \\ 0 & 0 & 0 & 0 & 0 & C_{66} \end{bmatrix} \begin{bmatrix} \varepsilon_x \\ \varepsilon_y \\ \varepsilon_z \\ \varepsilon_{xy} \\ \varepsilon_{yz} \\ \varepsilon_{xz} \end{bmatrix} \quad (3.1)$$

Where, the first matrix on the right is the stiffness matrix, which is the inverse of compliance matrix. In order to estimate the elastic constants, Equation 3.1 was first simplified

for pressure in all directions being equal, $\varepsilon_x = \varepsilon_y$, and no shear strain, as follows:

$$-p = (C_{11} + C_{12})\varepsilon_x + C_{13}\varepsilon_z \quad (3.2)$$

$$-p = (2C_{13}\varepsilon_x + C_{33}\varepsilon_z) \quad (3.3)$$

The above equations do not include the Biot's coefficient term. It is for a drained test where no part of the total stress is being taken by the fluid. The pore pressure is equal to the external stress and the mechanical strain in coal is only due to the external stress. The effective stress, external stress and pore pressure are, therefore, in equilibrium. Using reasonable values of Poisson's ratio in the two directions, taken from data in open literature (Evans and Pomeroy, 1966), the values of Young's moduli were calculated for each axis using shrinkage/swelling data for helium. The results are presented in Table 3.3. Hence, the value for the complete compliance matrix for Equation 3.1 became known. Since the values of Young's modulus were obtained using the coal quadrant instead of full core, these values may be slightly higher. However, they are well within the range reported in prior similar studies (Hol and Spiers, 2012).

Table 3.3 Elastic moduli used for the calculations.

Elastic moduli used for calculations		
	Horizontal (x-/y-) Direction	Vertical (z) Direction
Young's Modulus (GPa)	7.3	4.8
Poisson's ratio	0.21	0.41

3.4.2. Adsorption Stresses in Coal

In order to evaluate the implication of adsorption phenomenon on the stress path followed by coal with reservoir depletion, a thermodynamically rigorous and adsorption coupled poro-mechanical model for stresses, proposed by Espinoza et al. (2013) was used. The

experimental data for methane was utilized in the analysis. Based on the model, combining adsorption stresses with linear elastic constitutive equation (Equation 3.1), resulted in a new constitutive equation as:

$$\left.\begin{aligned}
\sigma_{xx} &= C_{11}\varepsilon_x + C_{12}\varepsilon_y + C_{13}\varepsilon_z - s_x^a(p)\\
\sigma_{yy} &= C_{12}\varepsilon_x + C_{11}\varepsilon_{22} + C_{13}\varepsilon_z - s_y^a(p)\\
\sigma_{zz} &= C_{13}\varepsilon_x + C_{13}\varepsilon_x + C_{13}\varepsilon_z - s_z^a(p)\\
\sigma_{yz} &= 2C_{44}\varepsilon_{yz}\\
\sigma_{zx} &= 2C_{44}\varepsilon_{zx}\\
\sigma_{xy} &= (C_{11} - C_{12})\varepsilon_{xy}
\end{aligned}\right\} \quad (3.4)$$

Where, the adsorption stress is given as:

$$s_i^a(p) = \int_0^p C_i(p) n_o(p) V_b(p) dp \quad (3.5)$$

Where, $n_o(p)$ is the number of moles adsorbed and $V_b(p)$ is the molar volume of gas at a given temperature and pressure. The basis for derivation of the above adsorption stress is energy conservation (first law of thermodynamics, Maxwell's relation for thermodynamic state functions and Gibbs-Duhem equation) (Espinoza et al., 2013) using $C_i(p)$ as a coefficient, coupling the volume of gas sorbed and the corresponding stress. Simplifying Equation (3.4) for methane gives the following:

$$\sigma_x = \sigma_y = -p = (C_{11} + C_{12})\varepsilon_x + C_{13}\varepsilon_z - s_x^a(p) \quad (3.6.a)$$

$$\sigma_z = -p = 2(C_{13}\varepsilon_x) + C_{33}\varepsilon_z - s_z^a(p) \quad (3.6.b)$$

Inverting the stiffness matrix to compliance matrix gives the following:

$$\begin{bmatrix}\varepsilon_x\\ \varepsilon_z\end{bmatrix} = \begin{bmatrix}\frac{1-\nu_x}{E_x} & \frac{-\nu_z}{E_z}\\ \frac{-2\nu_z}{E_z} & \frac{1}{E_z}\end{bmatrix}\begin{bmatrix}s_x^a(p) - p\\ s_z^a(p) - p\end{bmatrix} \quad (3.7)$$

Taking derivative of Equation (3.7) with respect to pressure gives the following:

$$\begin{bmatrix} \frac{ds_x^a(p)}{dp} & -1 \\ \frac{ds_z^a(p)}{dp} & -1 \end{bmatrix} = \begin{bmatrix} \frac{1-\nu_x}{E_x} & \frac{-\nu_z}{E_z} \\ \frac{-2\nu_z}{E_z} & \frac{1}{E_z} \end{bmatrix}^{-1} \begin{bmatrix} \frac{d\varepsilon_x}{dp} \\ \frac{d\varepsilon_z}{dp} \end{bmatrix} \tag{3.8}$$

Equation 3.8 was solved for ds_x^a/dp ands_z^a/dp. From the value of the derivative of adsorption stress, the coupling coefficient C_i (p) was calculated in both horizontal and vertical directions using Equation 3.5. The value of n(o)p in Equation (3.5) is the number of moles adsorbed by coal at zero strain and determined from the sorption isotherm data. V_b(p), that is, the calculated molar volume of gas as a function of pressure, was estimated using the Van der Waal's equation of state. The calculated value of C_i(p) is actually pressure-dependent and captures the coupling between adsorption and stress. It depends on fluid pressure, type of gas, pore shape and size distribution.

The values of the coupling coefficient, calculated for vertical and radial directions, are presented in Figure 3.4.

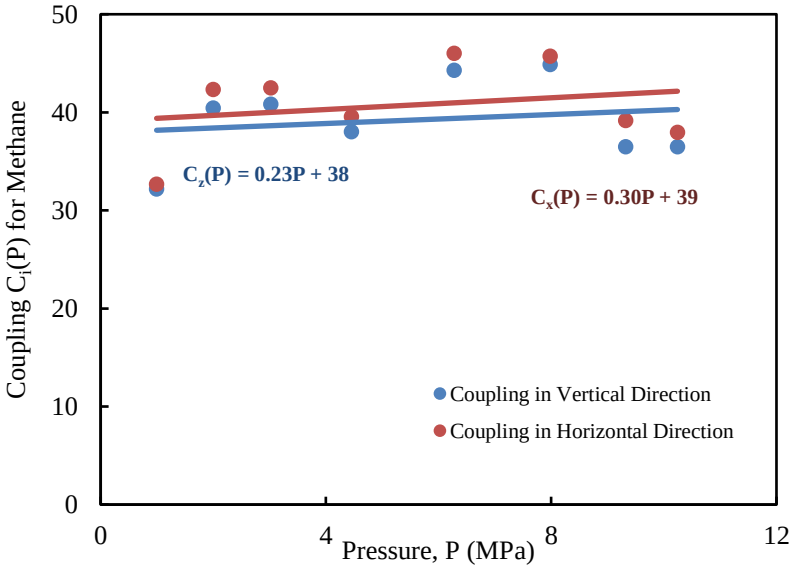

Figure 3.4 Variation of adsorption coupling in vertical and horizontal directions with depletion.

There is a significant scatter in the values, and this is expected given that it captures several parameters and its variation is not monotonic. In order to remedy the large scatter, Espinoza et al. (2013) proposed a Biot's-*like* coefficient, given as:

$$b_i(P) = ds_i^a/dp = C_i(P)n_o(P)V_b(P) \quad (3.9)$$

A good correlation was obtained between Biot's-*like* co-efficient and pressure, as shown in Figure 3.5. This was used extensively in the modeling exercise to determine the stress path followed by coal during depletion. It is important to note that the variation of Biot's-like coefficient depends on the nature of gas, coal type and temperature.

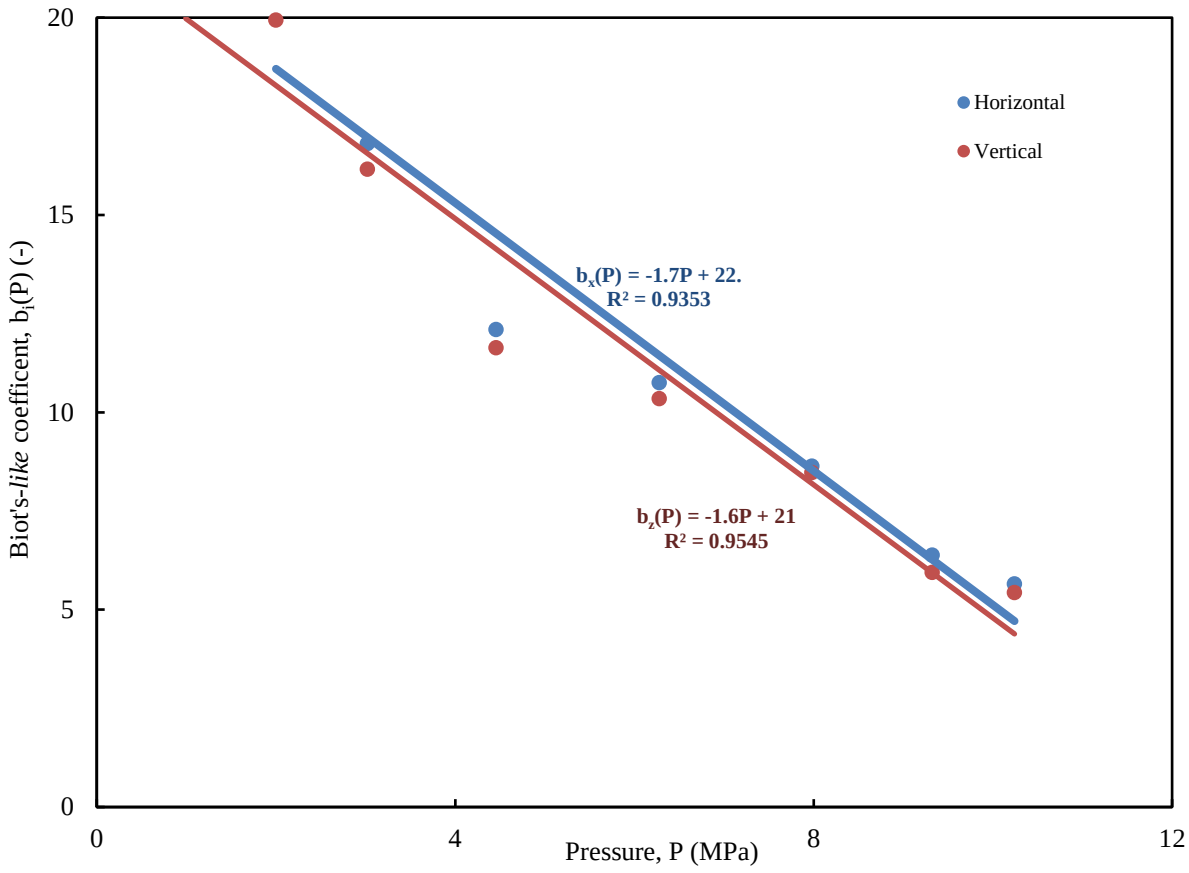

Figure 3.5 Biot-*like* coefficient in vertical and horizontal directions.

The appropriate nature of variation should be established based on experimental data, as was done in this study, or using the technique reported by Nikooshokhan (2012). In this study, a

linear fit for failure of coal was used since it provided a good approximation over the pressure range of the experiment. Using a non-linear fit is recommended for certain coal types but this would depend on the type of relationship obtained experimentally.

3.4.3. Failure Analysis Using Adsorption-coupled Poromechanical Model

Taking the adsorption stresses into account, the variation in horizontal stress and vertical strain can be written as follows (Espinoza et. al., 2015a):

$$\Delta\sigma_x = \left(\frac{C_{13}}{C_{33}}\alpha_z - \alpha_x\right)\Delta p_{c+}\left(\frac{C_{13}}{c_{33}}(1-\alpha_z) - (1-\alpha_x)\right)\frac{ds^a(p_m)}{dp_m}\Delta p_m \quad (3.10.a)$$

$$\Delta\varepsilon_z = \frac{1}{C_{33}}\alpha_z\Delta p_c + \frac{1}{C_{33}}(1-\alpha_z)\frac{ds^a(p_m)}{dp_m}\Delta p_m \quad (3.10.b)$$

The above equations assume reservoir to be under uniaxial strain condition and consider the total stress in the earth, that is, due to depth and tectonics. The constraints on the stresses in the earth described by Zoback (2007) were taken into account and the initial conditions for the experiments were estimated accordingly. Modeling was carried out for a normal faulting scenario. This study did not consider fault slipping and the resulting changes in tectonic stresses due to depletion.

The calculated compliance matrix constants were determined using a quadrant sample of coal. Using a full core scale would provide improved estimates but would take significantly longer to achieve pressure equilibrium. However, the elastic moduli estimated are well within the range of prior similar studies like (Hol and Spier, 2012). Changes in Biot-*like* co-efficient (ds_z^a/dp) and vertical strain were calculated as a function of pore pressure using Equation (3.10b). Finally, the vertical strain results were compared with those obtained in the laboratory. By matching the two strains and minimizing the residual error, the actual Biot's coefficient (α_z) was estimated. There were a few outlier data points and considering these resulted in 25 % residual error. However, eliminating two data points lowered this to 16% error. The

corresponding best matched Biot's coefficient value was used for all further work. Using the calculated value of Biot's coefficient (α_z) and measured changes in the horizontal stress, Biot's coefficient in the horizontal direction was estimated. The estimated Biot's coefficient values for the vertical and horizontal directions were $\alpha_z = 0.78$ and $\alpha_x = 0.93$, respectively. Using these values, the variation of effective horizontal and vertical stresses was calculated using Equation (3.10a). The results are shown in Figure 3.6.

The definition of Biot's effective stress used to estimate the effective stress for the analysis presented here is given as:

$$\sigma_{eff} = \sigma - \alpha P \qquad (3.10.c)$$

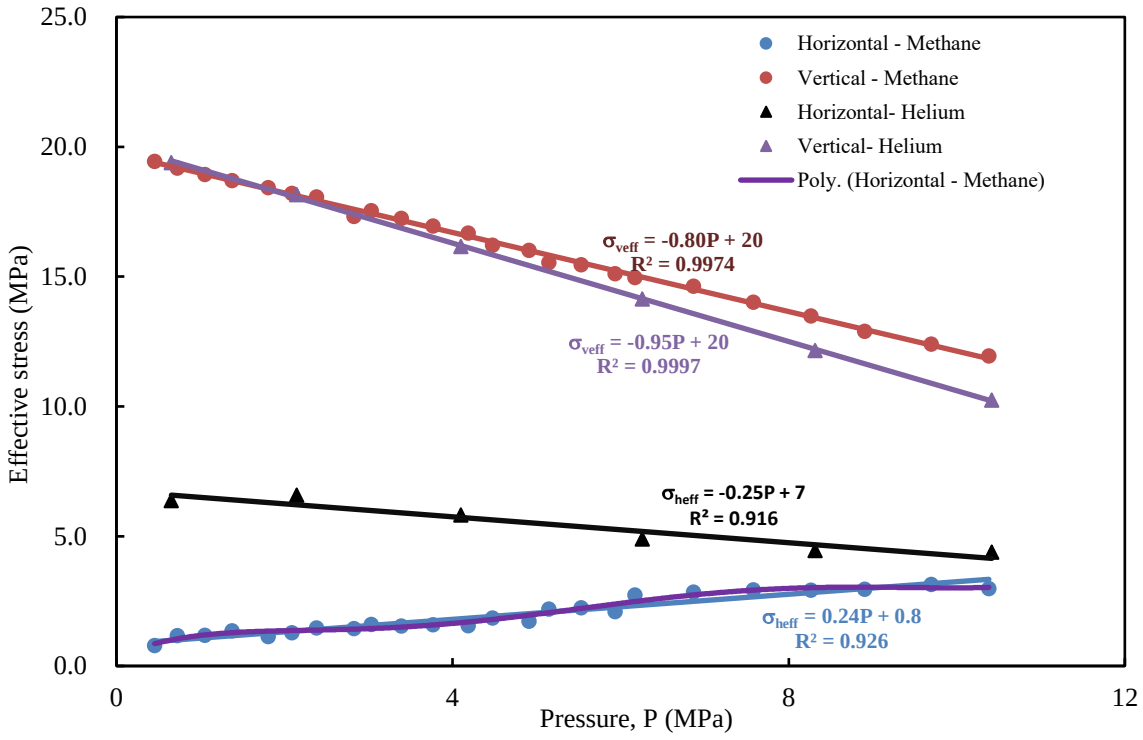

Figure 3.6 Variation of effective stresses with pressure for methane and helium depletion. (Uniaxial strain conditions).

The above interpretation of effective stress holds for non-sorptive gases and shows that pore pressure reduces the stress effectively acting on the grains of the porous solid. The parameter α (Biot's coefficient) captures the configuration of the contact between grains, holds for loosely consolidated material and is close to one for rocks like coal (Lu and Connell, 2016). They also presented a modified definition of effective stress for non-sorptive rocks, where the effect of swelling of grains and the corresponding change in the inter-granular contact with changes in pressure is considered. This definition of effective stress presents a more theoretically rigorous interpretation and can be very useful for history matching and field scale studies. However, for a laboratory scale study, where the associated pore volume is very small, this effect is almost negligible. The approximation of using the Biot's effective stress definition for sorptive rocks is considered valid and is simpler to model. This has served well in prior studies (Singh, 2014; Espinoza, 2015; Liu and Harpalani, 2014).

Coal is essentially an anisotropic rock and has been so treated for determining the poromechanical properties. However, coal has been often treated as an isotopic rock for the sake of simplicity when evaluating failure with depletion. Previous studies (Lu and Connell, 2016; Espinoza, 2015; Singh, 2014) considered coal as an isotropic solid for failure analysis and the results were accepted to be satisfactory. Hence, in light of the efforts made earlier, we used Drucker-Prager criterion for failure analysis of coal, which was proposed for isotropic solids. At this point, it is important to note that there are several failure criteria for anisotropic solids, such as, generalized Hill's criterion given in Chu (1995), anisotropic extension of Drucker- Prager yield criterion by Liu et al (1997), which can be used for failure analysis presented in this study. However, these criteria are for plastically deforming solids and require modification and validation by experimentation for coal, which is beyond the scope of this study. Also, a simple

failure model, like the Drucker-Prager, works well for deformation analysis in the coalbed reservoir domain, as demonstrated by previous field studies.

Next, the failure modeling was carried out using the Drucker-Präger criterion as follows:

$$\tau(oct) = a + b\sigma(oct) \quad (3.11)$$

Using the experimental results for helium and the calculated value of the Biot's coefficient, τ(oct) and $\sigma(oct)$ were estimated for the simplified case, $\sigma_x = \sigma_y$, as follows:

$$\tau\ (\text{oct}) = 0.47\ (\sigma_{veff} - \sigma_{heff}) \quad (3.12)$$

$$\sigma\ (\text{oct}) = 0.33(2\sigma_{heff} + \sigma_{veff}) \quad (3.13)$$

where, $\sigma_{h/veff}$ is effective horizontal/vertical stress in horizontal/vertical direction. The failure envelope, along with the stress path followed by coal under depletion of both helium and methane, were plotted with the calculated effective stress in the octahedral stress invariant plane (J_2 and I_1) where, I_1 is octahedral mean stress invariant and J_2 is the octahedral shear stress invariant. The stress path of methane clearly indicated that adsorption stresses play a significant role in causing the stress path to move towards the failure envelope, while the stress path of helium moves away from the failure envelope, as shown in Figure 3.7.

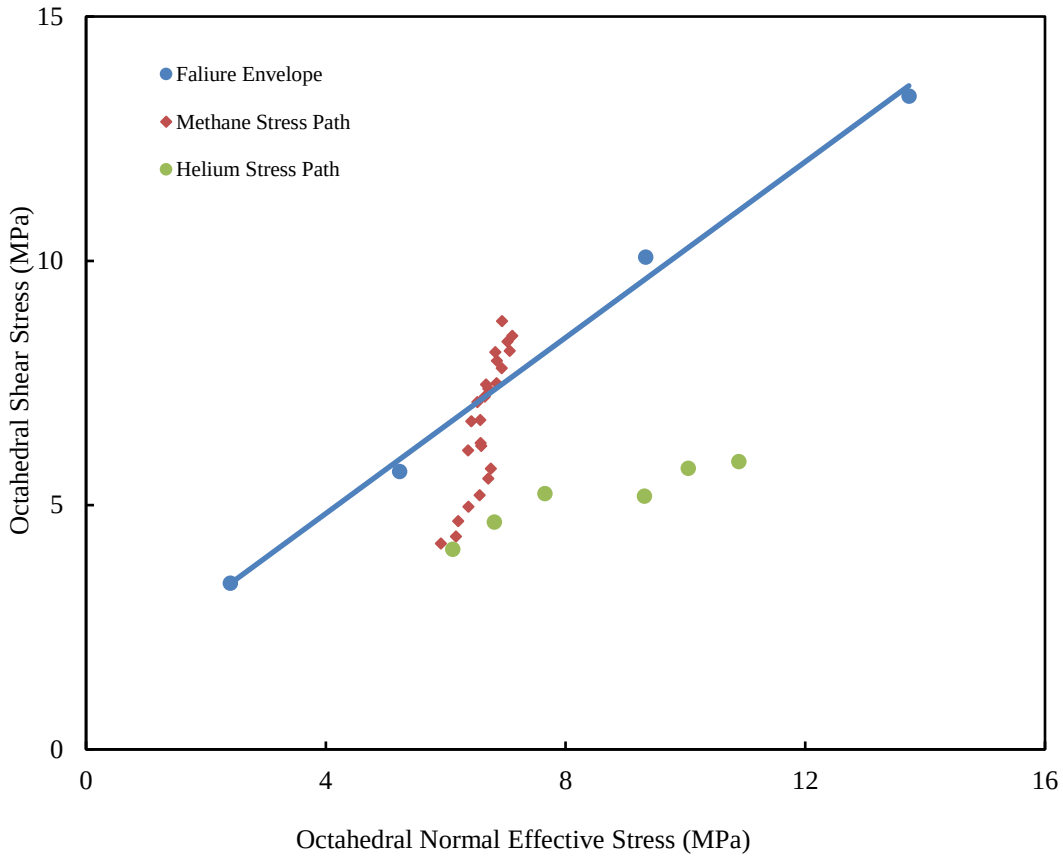

Figure 3.7 Stress invariant path with gas depletion in coal sample along with failure envelope.

Finally, a mathematical analysis was carried out in order to understand the condition which may lead to movement of the stress path towards the failure envelope. There are two components which govern the changes in effective horizontal stress, first being the pore pressure drawdown and the second one related to adsorption stresses in the coal matrix. When the component of horizontal stress related to sorptive stresses becomes higher than the component related to drawdown, the slope of the line becomes negative and the state of stress of coal moves towards the failure line. The path is a combination of the poromechanical response to depletion and desorption-induced stresses. A simple explanation for failure of coal is the high stress anisotropy developed during depletion of sorptive gases. During depletion, the effective vertical stress increases and the effective horizontal stresses decreases, leading to a highly anisotropic

stress loading condition, which eventually takes the stress path of coal towards the failure envelope. During experimental work, the coal failure was observed at ~4.1 MPa (600 psi), which is evidenced in the methane stress path. It is difficult to pinpoint the shear failure stress although, according to the stress path, coal failure initiated in shear at approximately ~4-4.5 MPa (650 - 600 psi).

3.4.4. Explaining Stress Paths

Figure 3.8, showing the octahedral shear stresses for methane and helium depletion, indicates that the shear stress is significantly higher for methane at low pressure. Although the effective vertical stress increases significantly for both gases, the effective horizontal stress increases only with helium depletion (Figure 3.6). For methane, it decreases, leading to stress anisotropic loading and consequently shear failure. It should be noted that effective horizontal stress for methane does increase slightly, or may be considered to remain numerically equal, up to a certain pressure during depletion. This can be attributed to the fact that the desorption phenomenon did not exceed the poroelastic response of rock to depletion. This is shown by a polynomial fit in the figure, which shows that the horizontal effective stress is constant or has increased slightly with depletion from 10 MPa to 8 MPa. There is generally a rebound point at which the slope of the plot of effective horizontal stress changes with pressure. This is explained later in this section.

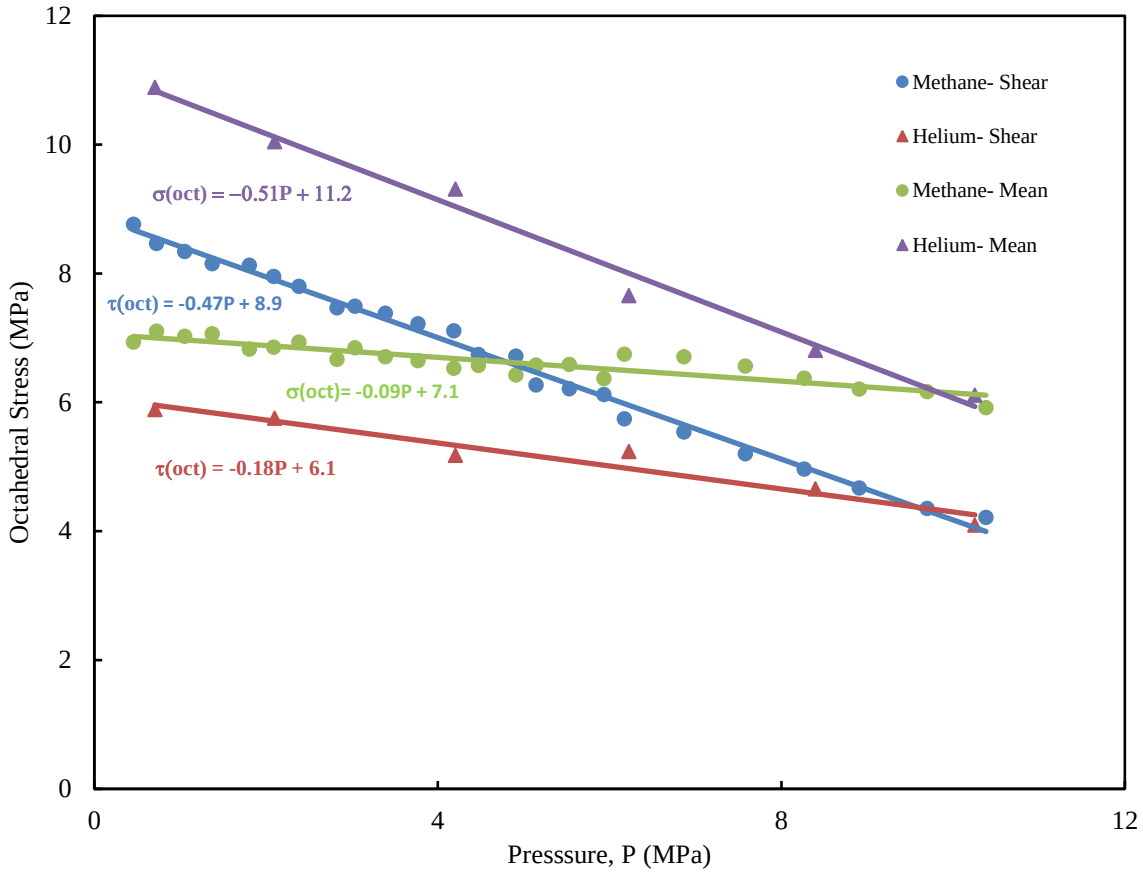

Figure 3.8 Variation in octahedral stresses with pressure with methane and helium depletion.

Also, taking all the principal stresses into account, Figures 3.7 and 3.8 show that the increase in the effective mean stress in case of methane is insignificant compared to helium (in the stress invariants plane). However, the change in octahedral shear stress is significant for methane compared to helium and this is apparent in Figures 3.7 and 3.8 (in the stress invariant plane). This can again be explained by the fact that there is a decrease in the effective horizontal stress with methane depletion, which compensates for the increase in the value of vertical stress in Equation (3.13), leading to a rather small variation in the value of J_1.

An attempt was made to mathematically define the unusual changes in horizontal stresses with methane depletion. Presenting the changes in horizontal stresses in a simplified form

(simplification of Equation 3.10), without transverse isotropy ($\nu_3 = \nu \; and \; E = E_3$) gives the following (Espinoza et. al, 2015 b):

$$\Delta\sigma_h = \alpha\left(\frac{1-2\nu}{1-\nu}\right)\Delta P + (1-\alpha)\left(\frac{1-2\nu}{1-\nu}\right)\left(\frac{ds^a}{dp(m)}\right)\Delta p(m) \tag{3.14}$$

Hence,

$$\Delta\sigma_{heff} = \alpha\left(\frac{-\nu}{1-\nu}\right)\Delta P + (1-\alpha)\left(\frac{1-2\nu}{1-\nu}\right)\left(\frac{ds^a}{dp(m)}\right)\Delta p(m) \tag{3.15}$$

The part of Equations (3.14) and (3.15) with (1-α) as multiplier is attributed to adsorption while the remaining part accounts for the poromechanical response of coal to depletion. A quick calculation shows that, for $\alpha = 0.93$ and $\nu = 0.3$, the effective horizontal stress increases at the rate of 0.39 times the helium pore pressure variation. Another important aspect of Equation 3.15 is that it can successfully predict the rebound point in the plot of changes in effective horizontal stress with pressure, effectively showing that the adsorption phenomenon exceeds the poroelastic response of rock. This can be estimated by modifying it to Equation (3.16) and solving for pressure P by setting the left side equal to zero.

The dynamics of the process is initiated with a pressure reduction in the cleats, which occurs very quickly under experimental conditions. This results in a helium concentration gradient between the cleats and coal matrix, thus inducing flow due to the chemical potential gradient of the gas, leading to diffusion of helium from the matrix to cleats. Given that the diffusion coefficient of helium is larger than that of methane, the time taken for helium to achieve the same reduced pressure in the coal matrix is short. This entire dynamic reduces the pore pressure and increases the effective horizontal stress for helium. Hence, the effective horizontal stress increases continuously with pressure for helium depletion. Going through the same exercise for methane and re-writing Equation (3.15) gives the following:

$$\frac{\mathrm{d}\sigma_{heff}}{\mathrm{dP}} = \alpha\left(\frac{-\nu}{1-\nu}\right) + (1-\alpha)\left(\frac{1-2\nu}{1-\nu}\right)\left(\frac{ds^a}{dp(m)}\right) \quad (3.16)$$

Substituting $\frac{ds^a}{dp(m)} = -1.7P + 22$ from figure 8 gives the following:

$$\frac{\mathrm{d}\sigma_{heff}}{\mathrm{dP}} = \alpha\left(\frac{-\nu}{1-\nu}\right) + (1-\alpha)\left(\frac{1-2\nu}{1-\nu}\right)(-1.7P + 22) \quad (3.17)$$

Plotting the experimental and modeled values of the rate of change of effective horizontal stresses as a function of pressure depletion demonstrates a clear interdependence. Figure 3.9 shows the modeled results using Equation (3.17) and Figure 3.10 shows the experimental results. However, there appears to be quite a bit of noise in the experimental data. This is expected given that the experimental process is extremely complex due to the combination of the poromechanical response and that due to adsorption process.

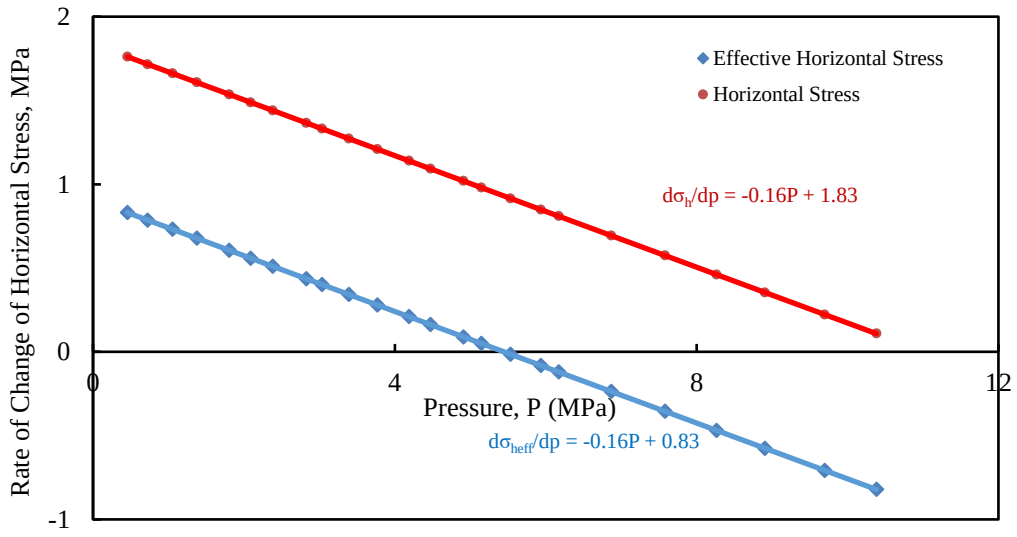

Figure 3.9 Calculated rate of change of horizontal stress with pressure depletion.

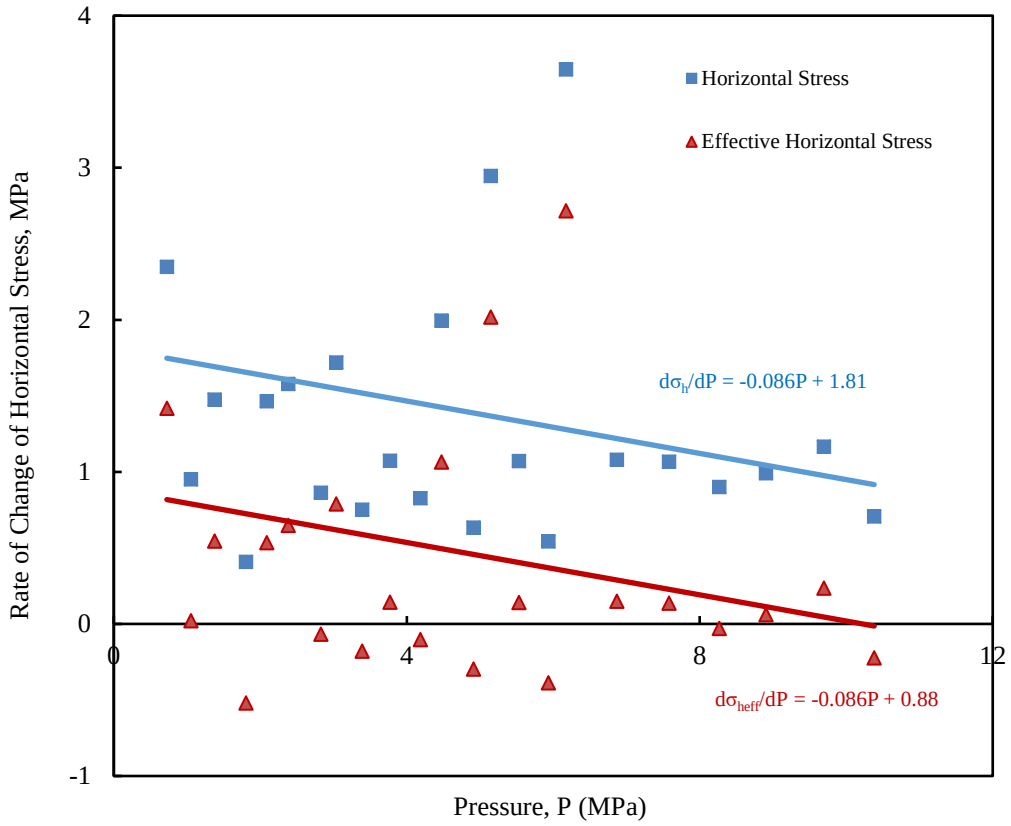

Figure 3.10 Experimental rate of change of horizontal stress with pressure depletion.

Figure 3.11 shows the change in horizontal stress with depletion using the modeled data presented in Figure 3.9. It also shows similar variation using data shown in Figure 3.10 (linear fit). In Figure 3.11, there is a difference in the slope of the graph of change in horizontal stress with depletion. However, both are fairly close to the slope value of 1.17, based on experimental results. It is, therefore, argued that the rate of change of horizontal stresses with pressure depletion is pressure-dependent, and it increases with depletion. This suggests that, at low pressures, the component of the rate of change of horizontal stress related to adsorption overshadows the poro-mechanical component. Espinoza et al. (2013) reported that, for CO_2 at low pressures, $b_i(p)$ $(or\ \frac{ds_i^a}{dp(m)})$ has a value close to 40 and it decreases to a minimum value close to 1 at very high pressure.

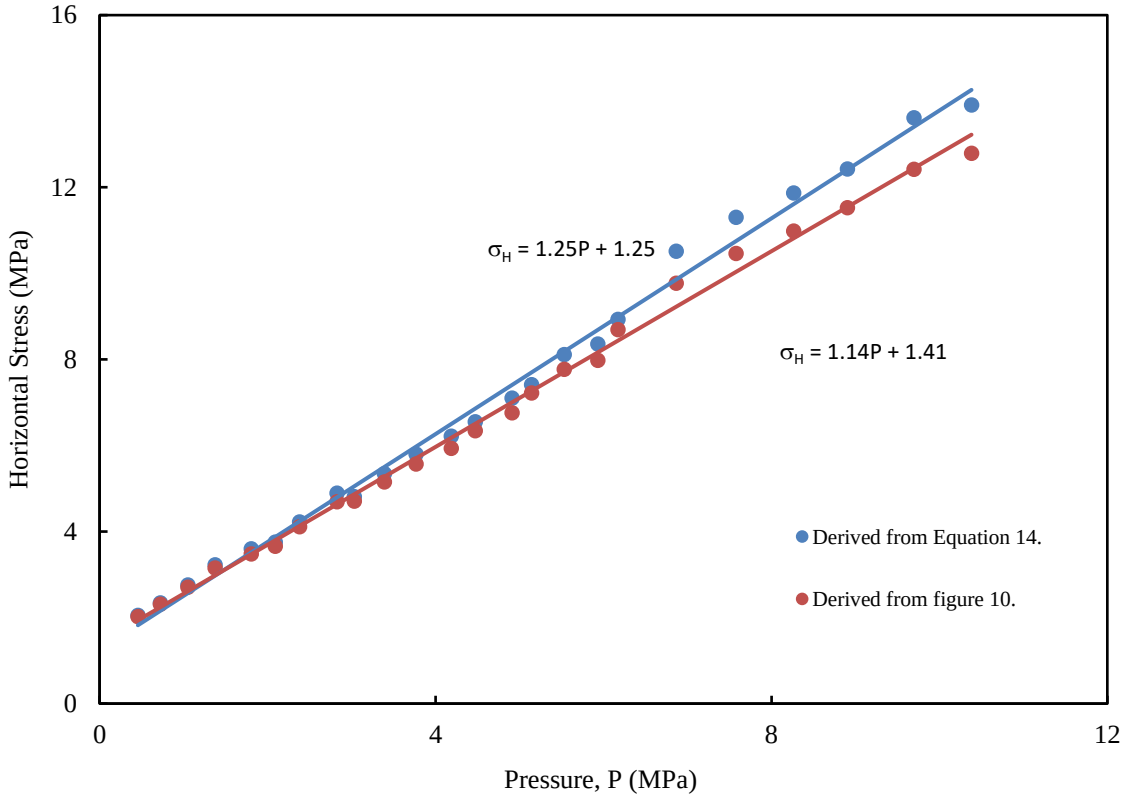

Figure 3.11 Integrated value of horizontal stress with pressure from Equation (3.14) and Figure 3.10.

A similar comparison can be drawn for methane – used in this study – although the experiments went down to only 100 psi and the calculated value of $b_i(p) or \frac{ds_i^a}{dp(m)}$ attained a maximum value of 22. However, due to the trend of the plot, the coefficient's value was extrapolated to lower pressure and concluded that its value would be higher, and coal is more likely to fail at lower pressures.

3.4.5. Permeability Modeling

The fundamental stress-strain relationship for coal at the scale of cleats, incorporating both mechanical and adsorptive properties, has been defined earlier in the form of Equations

(3.6a & 3.6b). These can be used to estimate the effective horizontal and vertical stresses acting on coal, which induce strain in the coal matrix with continued pressure depletion. It is believed that this strain is responsible for changes in the cleat aperture with pressure depletion and, hence, indirectly responsible for the changes in coal permeability. With improved understanding of stress-strain relationships for the reservoir, a pressure/stress-dependent-permeability (PdK) model was developed. The cubic relation between permeability and cleat porosity was used as the fundamental equation to estimate the permeability at any pressure. After assuming an initial value, the cleat porosity at different reservoir pressures was estimated using the stress-strain relationship defined earlier. Essentially, equations were developed, as shown later in this section, and used to calculate changes in the cleat aperture, perpendicular to the plane of the cleat. The horizontal strain in the cleats was estimated and added to the initial assumed cleat aperture, thus obtaining the variation in cleat aperture at any pressure. The cleat porosity of coal, represented as a bundle of matchsticks geometry, was taken as (Reiss, 1980):

$$\Phi = 2b/a \tag{3.18}$$

Major assumptions made in development of the model are as follows:

1. Coal geometry is best represented as a bundle of matchsticks. Furthermore, coal exhibits transverse anisotropy, based on experimental results presented earlier and this is supported by recent researchers (Moore, et al, 2014).
2. Cleat spacing (a) is very large compared to the cleat aperture (b). It is further assumed that the cleat spacing does not change with depletion and the only variable that changes is the cleat aperture (b).
3. Cleat width changes only due to desorption-based shrinkage of the matrix, expansion due to reduction in the horizontal stress and increase in the effective vertical stress.

3.4.5.1. Model for Coal Geometry

The bundle of matchsticks is a widely accepted geometry for coalbed methane reservoirs. This has been explained in detail by Reiss (1980), Palmer and Mansoori (1996), Pan and Connell, (2007), Liu and Harpalani, (2013a) and others in their work. Hence, a full-scale description of the geometrical structure is redundant. However, a brief description is warranted for better appreciation of the estimates presented using this model. In this geometrical representation, cleats are defined as spaces between the individual matchsticks in the bundle. In our model, the two sets of cleats are assumed to be perpendicular to each other. It is believed that, with depletion, the height of the matchstick bundle decreases and the spacing between the individual matchsticks increases due to desorption of gases and the associated shrinkage of coal matrix. Since coal is assumed to exhibit dual porosity behavior, this shrinkage can easily be related to the amount of gases leaving the matrix pore space at low pressure.

3.4.5.2. Mathematical Modeling

The exercise of modeling is initiated by considering four adjacent matrix blocks with a set of perpendicular cleats as our representative elemental volume. Since transverse anisotropy is assumed, strain estimated along x-axis is assumed to be same as that for y-axis. Figure 3.12 shows the schematic for the longitudinal section of the representative elemental volume (REV), where the width of the REV is along the x-axis in the horizontal plane and the height is along z-axis in the vertical plane.

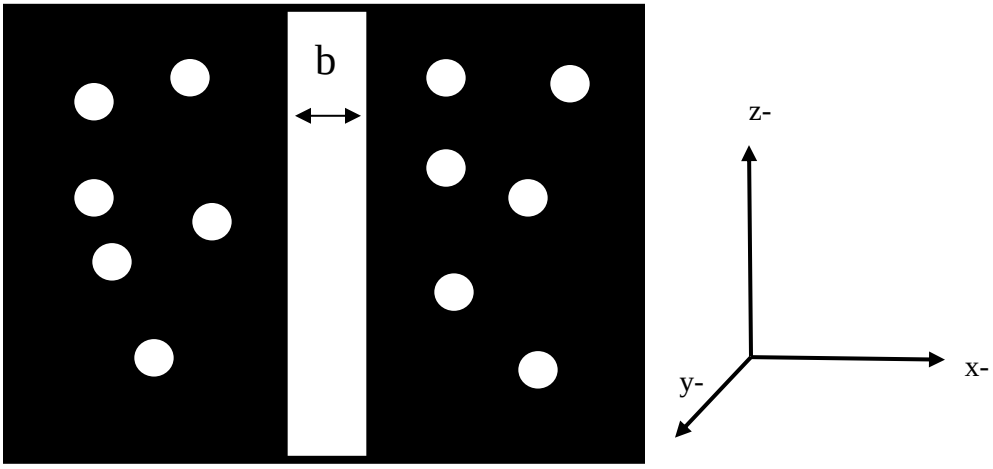

Figure 3.12 Schematic of coal matrix (with small pores) and cleat - longitudinal section of relative elemental volume used for permeability modelling.

The strain at the cleat level can be calculated using simple stress-strain relationship for coal as follows:

$$\varepsilon_{\mathrm{h}}^{\mathrm{m}} = \{C_m^h(\mathrm{p})\Delta\mathrm{p}\} - \left[\frac{(1-\nu_{\mathrm{h}})\Delta\sigma_{\mathrm{heff}}}{\mathrm{E_h}} + \frac{\upsilon_{\mathrm{v}}\Delta\sigma_{\mathrm{veff}}}{\mathrm{Ev}}\right] \quad (3.19)$$

where, superscript 'm' denotes that estimates are at the matrix scale. $\Delta\sigma_{heff}$ can be estimated using Equation (3.17) and $\Delta\sigma_{veff}$ can be calculated using the effective stress equation with vertical Biot's coefficient value of 0.78 (estimated earlier). $C_m^h(\mathrm{p})$ is the linear shrinkage compressibility term, defined and explained in Appendix II. Basically, it is the rate of change of horizontal strain with change in pressure in the matrix due to desorption-based shrinkage of the matrix. It is important to note that the first term on the right side of the equation (in curly parenthesis), that is, linear compressibility in horizontal direction, denotes change in the cleat aperture due to matrix shrinkage and desorption phenomenon. The second term (in square parenthesis) denotes the change in cleat aperture due to stress re-distribution around matrix with depletion. Once the horizontal strain was calculated for one matrix block, the change in b (cleat

aperture) was estimated by the following equation, assuming that adjacent matrix blocks show a similar strain in the two horizontal directions:

$$b = b_0 + 2(\varepsilon_h^m) \tag{3.20}$$

The initial cleat porosity value was written as:

$$\phi_0 = 2b_o/a$$

and the change in cleat porosity as:

$$\frac{\phi}{\phi_o} = \frac{b}{b_o} \tag{3.21}$$

Including Equation (3.19) in Equation (3.20), and using the b term obtained in Equation (3.21), the expression for change in cleat porosity with change in effective stresses can be written as:

$$\phi = \phi_o \left\{ \frac{b_0 + 2\left(\{C_m^h(p)\Delta p\} - \left[\frac{(1-\nu_h)\Delta\sigma_{heff}}{E_h} + \frac{\upsilon_v \Delta\sigma_{veff}}{Ev} \right] \right)}{b_0} \right\} \tag{3.22}$$

Finally, the change in permeability can be written as:

$$K = K_o \left\{ \frac{b_0 + 2\left(\{C_m^h(p)\Delta p\} - \left[\frac{(1-\nu_h)\Delta\sigma_{heff}}{E_h} + \frac{\upsilon_v \Delta\sigma_{veff}}{Ev} \right] \right)}{b_0} \right\}^3 \tag{3.23}$$

The modeled permeability variation using Equation (3.23) for San Juan coal type is shown in Figure 3.13.

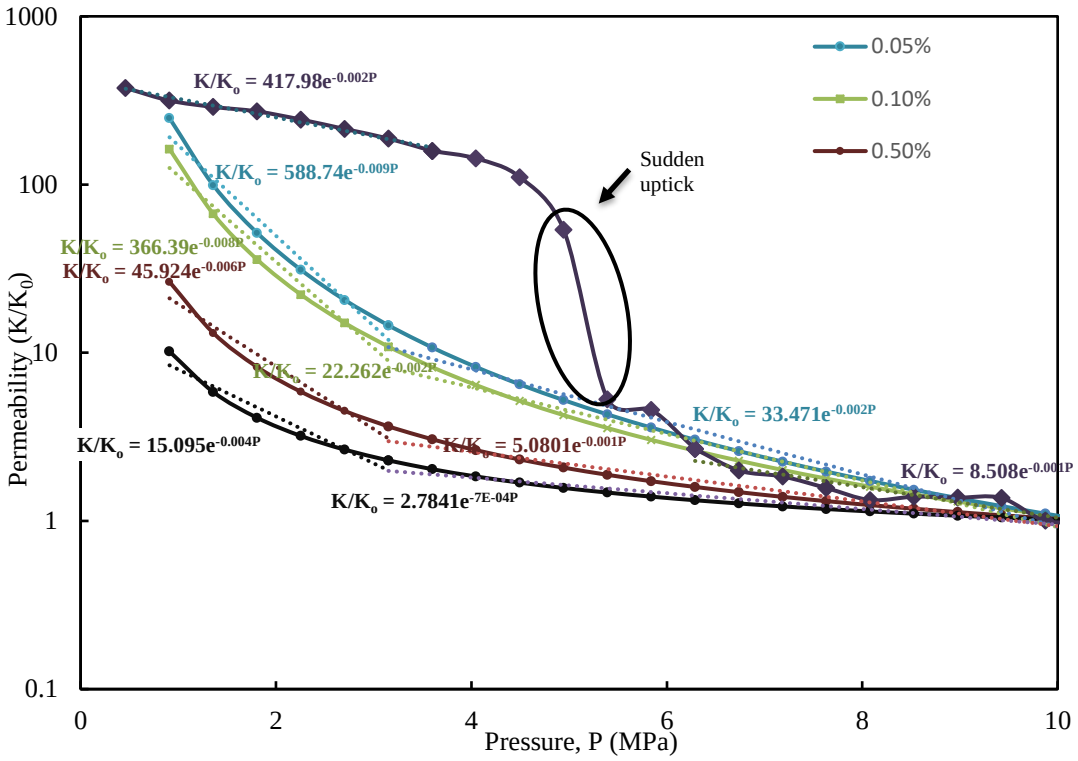

Figure 3.13 Permeability variation using proposed model compared and experimental data (Singh, 2014). (Bimodal variation for two pressure ranges).

The figure shows the modeled permeability with pressure variation for different values of cleat porosity. The model used pressure steps similar to those used in the experimental work in this study (Singh, 2014). It is important to note that, for modeling the permeability data, an exponential fit of the Biot-*like* co-efficient is required, since linear fit is not adequate for very low methane pressures, below 1 MPa (~150 psi) used. However, modeling exercise should be valid for the entire pressure range and, since the Biot-*like* coefficient varies non-linearly at very low pressures, a more general exponential fit was used. The exponential fit gave only a slightly better value of R^2 compared to the linear fit. This is illustrated in Figure 3.14.

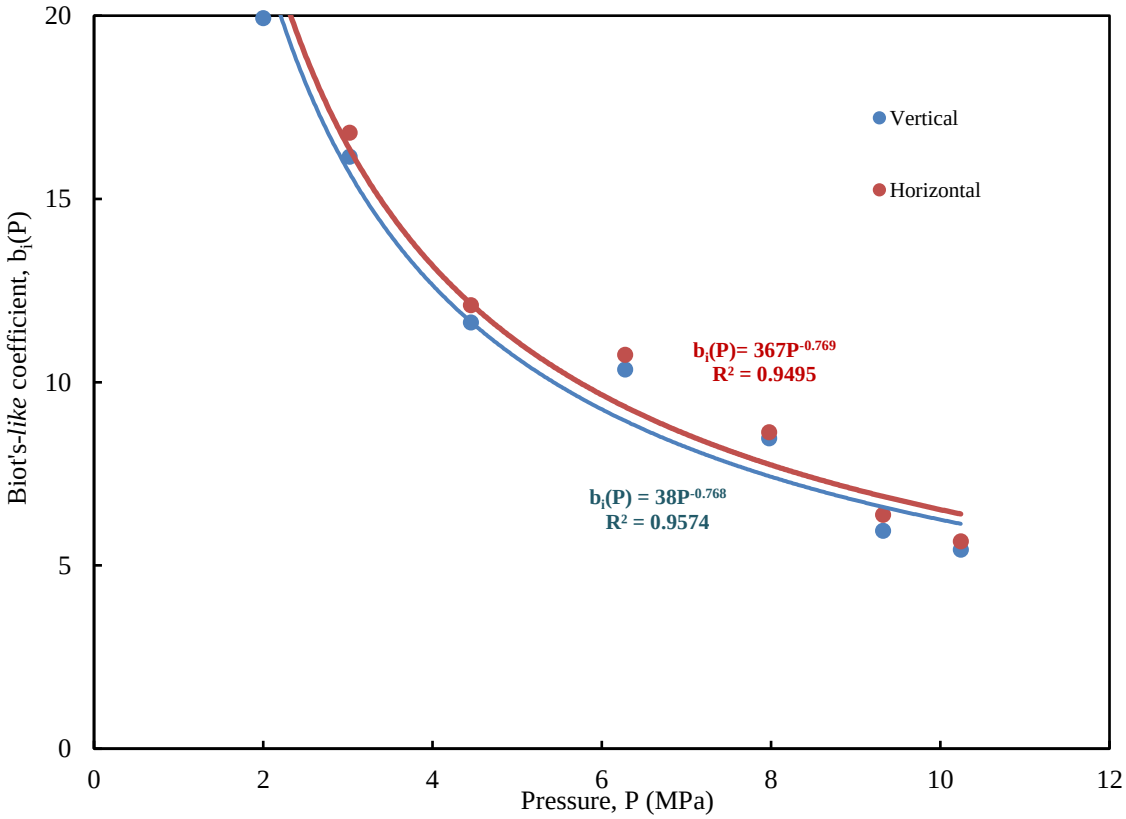

Figure 3.14 Exponential fit for the proposed Biot-*like* coefficient in vertical and horizontal directions.

Also, the parameters in Equation (3.23) have been defined and used for laboratory scale. It would take some history matching and validation exercise to modify the proposed permeability model (Equation 3.23) for field application.

It should be noted from the comparison between modeled and experimental permeability variation with pressure, as presented in Figure 3.13, that coal had an initial cleat porosity of 0.1 %. After 700-750 psi pressure, formation of cracks may have been initiated as can be interpreted from the failure model discussed earlier. According to the proposed permeability model, there is a sudden increase in the cleat porosity of coal, causing rapid increase in the permeability at ~650

psi. Hence, it can be concluded that the element which describes a sudden permeability uptick due to shear failure of coal is missing from this permeability model. This sudden uptick can be included in the permeability model by incorporating the failure model developed earlier. At this stage, this paper has set the fundamental stage for a permeability model that includes failure of coal with depletion. An improved permeability model with failure of coal incorporated in it, given that the impact of failure is significant on gas production, will be presented in a later paper.

3.5 Conclusions and Recommendations for Future Work

This paper has utilized the pressure-dependent-permeability and pressure-volumetric strain experimental data of Singh (2014) and analyzed it using the models developed by Espinoza et al. (2013; 2015). Based on the analysis presented, the following conclusions are made:

- Horizontal stresses in coal decrease with depletion in CBM reservoirs. However, the decrease is non-linear in nature, in contrast to what has been reported in the past (Liu and Harpalani, 2014). Using the modeling results presented, it is established that the nature of non-linearity is of second degree. It is also argued that, at low pressures, the proposed Biot-*like* coefficient responsible for non-linear changes is itself a non-linear parameter, depending on the maximum adsorption limit of gas on coal.
- Use of Biot-*like* coefficient translating the molar volume of adsorbed gas and the associated volumetric strain to adsorption stress serves as an excellent tool to estimate the changes in stress and, hence, the changes in permeability.
- The rate of decrease of horizontal stress depends on the sorption characteristics of the coal-type.

- Coal fails due to anisotropic loading condition under shear, which is in agreement with the findings presented by Espinoza et al. (2015) and Singh (2014). This is strongly dependent on the depth of coal since deeper coals are subjected to larger vertical stresses. The effective vertical stress goes up further with depletion, while the effective horizontal stresses decreases. Such conditions are more conducive to shear failure of coal during depletion and failure may even occur at higher reservoir pressures. This is a positive finding for deeper gas deposits. It should be noted that effective horizontal stress may occasionally increase initially in some cases, depending on the adsorption characteristics of coal, but there is a rebound point in the effective horizontal stress and pressure. This can be estimated using the equations presented in this study. Lu and Connell (2016) present one such study. However, a decrease in horizontal stress eventually occurs for every case reported to date.
- The reported increase in permeability of coal with depletion at a particular pressure can be explained to be the result of joining of pore spaces and formation of new factures and cracks, ultimately causing failure.

Based on the findings of this work, it is recommended that research be pursued in the following areas:

- Modeling of post-failure permeability is critical in evaluating the pressure-dependent-permeability behavior of coal. This is particularly valuable for deeper coals that are highly stressed since failure and the resulting uptick in permeability can be a game changer for development of gas recovery operations in such deposits.
- Since there are striking similarities between the gas storage, release and transport phenomena of coal and shales, and shale deposits are significantly deeper, similar

experimental and modeling effort should be carried out for shale formations. Although shale is typically a stronger and more competent rock, the phenomenon needs to be investigated given the potentially positive consequence.

CHAPTER 4

GENERALIZED STRESS-DEPENDENT PERMEABILITY MODELING

This Chapter is an exact copy (except for format change) of the journal paper entitled "Stress path with depletion in coalbed methane reservoirs and stress-based permeability modeling", published in *International Journal of Coal Geology*, 2018. DOI: 10.1016/j.coal.2017.11.005. Elsevier holds the copyright for this paper. This material may be downloaded for personal use only. Any other use requires prior permission of Elsevier.

Authors:

Suman Saurabh and Satya Harpalani

Abstract

That permeability is a critical parameter dictating the performance of naturally fractured reservoirs, like coalbed methane (CBM), is evident form the available field, experimental and permeability modeling information in the literature. Although modeling is often achieved at the expense of several input parameters, the exercise is typically unable to match sudden increases in coal permeability, encountered in deep coals after significant depletion. This paper is aimed at coupling stress and permeability in order to reduce the number of parameters required for modeling the permeability variation. Stresses in the reservoir are translated to invariants and stress path of coal is established in octahedral effective stress plane. Based on a detailed analysis of the stress path of three different coal types, a permeability model is presented in terms of stresses alone, that is applicable for elastic as well as inelastic deformations of coal. The model is validated using pressure-dependent-permeability experimental data for thee coal types along with the geomechanical testing data used to develop the failure envelope.

The primary implication of the study is improved capability to predict permeability of

deep coal deposits, given that they are likely to undergo inelastic deformation or shear failure with continued depletion, using one parameter only. Finally, realistic constraints on the values of the parameter are provided to enable operators with the necessary tools to use the model for field applications, particularly in the new and upcoming CBM fields.

Keywords: Stress path, Dilatancy, Shear failure, Permeability modeling, Coalbed methane

4.1 Introduction

Coal gas reservoirs are considered naturally fractured, typically with a well-developed fracture network known as the cleat system (Laubach et al., 1998). The cleats are primarily responsible for the permeability in coalbed methane (CBM) reservoirs and the performance of a reservoir depends largely on this parameter. Furthermore, it is well accepted that coal permeability changes dynamically throughout the life of a reservoir, depending on the variation in reservoir stresses. Two different dynamics are believed to affect the permeability of CBM reservoirs. First, the mean effective stress increases with depletion, inducing compaction in the reservoir and thus leading to a decrease in its permeability. Second, with depletion of methane, coal matrix shrinks, resulting in lateral relaxation of the coal matrix and fractures and, hence, in increased permeability. These two processes, dominant in the elastic deformation zone of the reservoir, occur simultaneously.

Sorption-induced coal matrix shrinkage is a well understood phenomenon, with tremendous amount of information in the literature describing it. Since methane is in adsorbed state in the coal matrix, there is an increase in the surface energy of pore surfaces of coal (Brochard et al., 2012; Espinoza et al., 2013; Kowalczyk et al., 2008; Pijaudier-Cabot et al., 2011). On macroscopic scale, this effect translates to swelling of the coal matrix. Hence, during depletion of methane, coal matrix shrinks, resulting in opening up of the cleats and increased

permeability (Ceglarska-Stefańska and Zarbska, 2002; Cui and Bustin, 2005; Harpalani and Chen, 1997; Harpalani and Schraufnagel, 1990; Karacan, 2007; Lin and Kovscek, 2014; Liu et al., 2011; Mazumder et al., 2006; Pan and Connell, 2007; Wang et al., 2010). The second effect of coal matrix relaxation is a reduction in the horizontal stress with continued depletion.

There have been several studies and permeability models presented in the literature, coupling the phenomena of stress and permeability of CBM reservoirs (Cui and Bustin, 2005; Liu et al., 2012; Palmer and Mansoori, 1998; Sawyer et al., 1990; Shi and Durucan, 2010, 2005, 2004). However, most modeling work has concentrated on the elastic deformation, with little on post-failure modeling. It is important to note that, deep coals (more than ~1000 m) like Indonesian coal, parts of San Juan, Greater Green River basin and some coal seams in China are typically under significant stress conditions (vertical stress more than 20 MPa, using lithostatic thumb rule), depletion may cause inelastic deformation.

Under appropriate conditions, this may also result in shear-induced failure in the reservoir (Chen et al., 2016; Liu and Harpalani, 2014; Saurabh et al., 2016). Some studies suggest that such inelastic deformation and shear failure result in significant permeability boost of CBM reservoirs (Chen et al., 2016; Espinoza et al., 2015; Liu and Harpalani, 2014; Singh, 2014). In deeper parts of the San Juan basin, such increases in permeability have been encountered in CBM operations (Okotie and Moore 2011). Sudden decrease in permeability is also known to occur, accompanied by production of large amounts of fines requiring well cleanouts, following which, permeability continues to increase. Previous attempts to delineate stress and deformation coupling in coal with depletion are fairly detailed (Espinoza et al., 2015; Liu and Harpalani, 2014; Lu and Connell, 2016). However, they lack completeness in terms of identifying the complete stress path of coal with depletion. In addition, past studies lack rigorous

validation in terms of application of the theory to different coal types.

There are only a few studies in open literature that address the variation in permeability over the range of elastic, inelastic and post-failure deformations. Chen et al. (2016) presented such a model although it was based on logistic function with the aid of three fitting parameters in order to achieve a good fit. The three parameters, however, were without constraints. In this paper, we first attempt to lay the ground by establishing the stress path for different coal types. Following this, we present a detailed analysis of the stress path to generalize the observations. The analysis is then used to discuss the nature of stress path of different coal types. The stress path analysis is shown to be coherently related to permeability data because several features of the variation of the two are strongly coupled. In light of the stress path investigation and observations made for the coal types, a general permeability model for coal is developed and presented. The proposed permeability model is useful in predicting permeability in elastic as well as inelastic deformation zones of CBM reservoirs. The model was able to predict experimental permeability variation accurately using a proposed modeling parameter, which encompasses the information on the stress path. Although the parameter is essentially a fitting parameter, effort to place constrains on its value within reasonable bounds, and using experimental data to estimate its value, is presented. This can be a useful guideline for the modeling exercise presented and serve as a tool for permeability and production modeling of the recent and upcoming CBM reservoirs in the San Juan basin.

4.2 Experimental Work and Results

4.2.1. Experimental Work

Experimental data used for the analysis presented in this paper is taken from a laboratory-based study completed at Southern Illinois University, aimed primarily at establishing the

pressure-dependent-permeability (PdK) of CBM reservoirs in the San Juan basin in the US and Sanga Sanga (SS) basin in Indonesia (Saurabh et al. 2016; Soni 2016; Singh 2014). The experimental work was carried out to determine the changes in permeability with pressure drawdown, ensuring best possible replication of *in situ* reservoir stress and uniaxial strain conditions. In-situ conditions were replicated using a triaxial setup, where sample was vertically stressed to in situ vertical stress condition. Laterally the two horizontal stresses were assumed to be equal and stressed to initial horizontal stress condition assuming normal faulting regime for the coal. The above assumptions are quite appropriate for Sanga Sanga (SS) and San Juan Coal (SJM/SJSJ) basins. Over the course of the experiments, stresses, strains, P-wave velocity and flowrates were recorded for a stepwise decrease in gas pressure, first using helium and then methane, for each depletion step. In addition, triaxial strength testing of the coal type was carried out under incremental confining stress conditions to establish the failure envelope for the coal type. The geo-mechanical test results also provided the mechanical parameters, Poisson's ratio and Young's modulus, cohesive strength and friction angle. Details of all experimental setups and testing procedures are presented in Saurabh et al. (2016) and Singh (2014).

4.2.2. Sample Characterization

The coal tested in this study was retrieved from different parts of the world and geologic settings. Table 4.1 presents the details of the sample location and geology. The rank of all coals tested was sub-bituminous. Table 4.2 presents the ash, moisture content and density of the coal types. Cores of coal, two inches in diameter and three inches long from San Juan basin (SJM and SJSJ), and four inches in diameter and six inches long from Sanga Sanga basin, were used for the flow, geomechanical testing and failure envelope experiments. Pictures of coal cores showing their cleated structure are presented in Figure 4.1.

Table 4.1 Sample location and rank of coals tested.

Sample Name	Location	Rank of Coal
SJM	Northwestern San Juan basin, US	Sub-bituminous
SJSJ	Northwestern San Juan basin, US	Sub-bituminous
SS	Sanga Sanga basin, Indonesia	Sub-bituminous

Table 4.2 Proximate analysis results for coals tested.

Sample Name	Density (g/cc)	Ash Content (%)	Moisture content (%)
SJM	1.34	5.1	7.9
SJSJ	1.31	7.9	1.4
SS	1.26	1.2	4.8

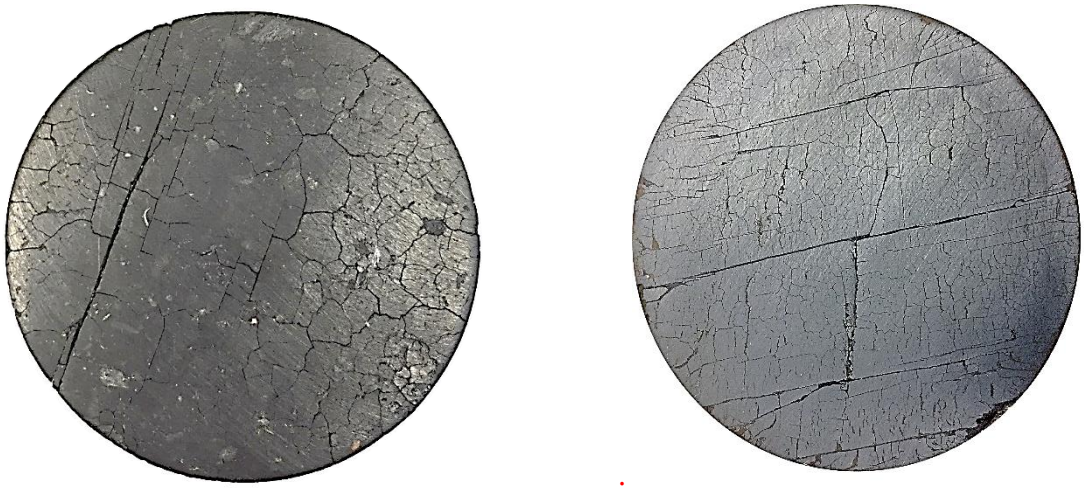

Figure 4.1 Pictures of coal cores showing the cleated structure of San Juan coal (SJM/SJSJ, left) and Indonesian coal (SS, right).

4.2.3. Experimental Results

Initial stress conditions for the experiments were based on normal stress regime (Zoback, 2007). The boundary condition for the flow experiments was uniaxial strain. Hence, the total vertical stress, replicating the depth of coal, was maintained constant throughout the experiment

and no horizontal strain was allowed during depletion. However, release of methane and its depletion resulted in matrix shrinkage, resulting in significant horizontal strain, which was compensated for by decreasing the total horizontal stress. Starting with initial horizontal/vertical stresses and pore pressure, the horizontal and vertical stresses were monitored with stepwise depletion of methane. The variation in the stresses over the duration of the experiments is shown in Figure 4.2. Since the primary aim of the study was to establish the PdK trend with methane depletion, permeability was estimated using the measured flowrates. Figure 4.3 presents the variation of permeability (k) with methane depletion as a function of the initial permeability (k_o). For the experiments using San Juan coal, the core did undergo shear failure whereas the SS coal did not.

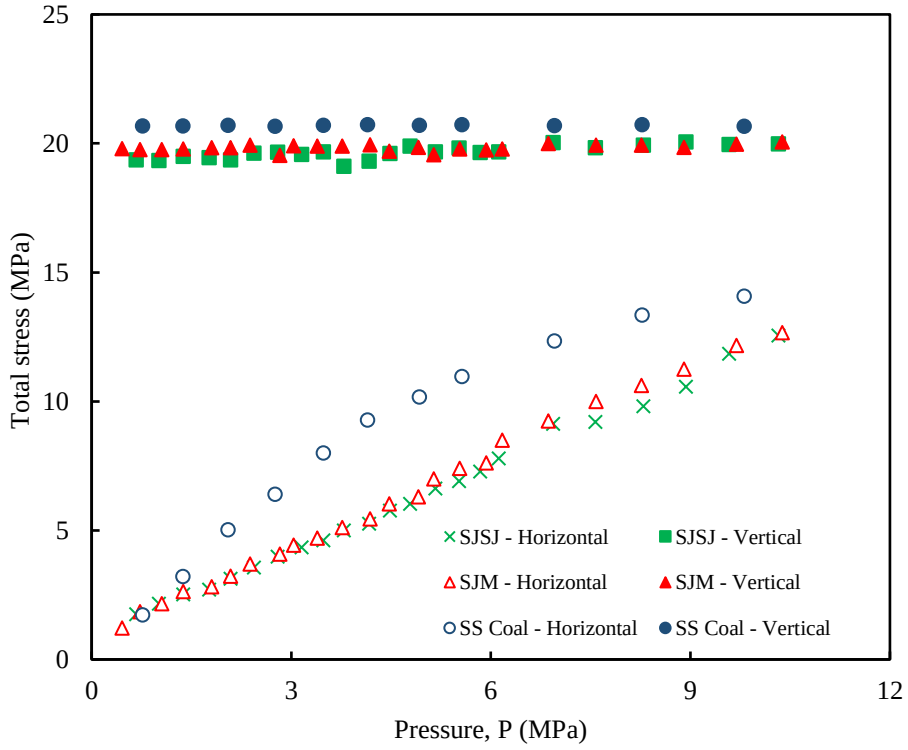

Figure 4.2 Variation of total stresses with methane depletion.

Figure 4.2 clearly exhibits a continuous decrease in the horizontal stress with methane depletion while the applied vertical stress remained constant, ensuring uniaxial strain condition.

The overall trend of decreasing horizontal stress with depletion is the same for all three cores tested although the rate of decrease is fairly similar for San Juan coals, but different for SS coal. This is to be expected given the entirely different locations and geologic settings of the two coals. The rate of decrease in the horizontal stress for SS-coal is gentle in the beginning, increasing with depletion. Figure 4.3 also shows that there is a significant increase in the permeability of San Juan coals, including one fairly sudden and significant jump. We hypothesize that the reason for this uptick in permeability is shear failure of coal. SS coal did not exhibit such an uptick in permeability, suggesting that there was no shear failure. Also, at the end of the experiment, SS core was intact.

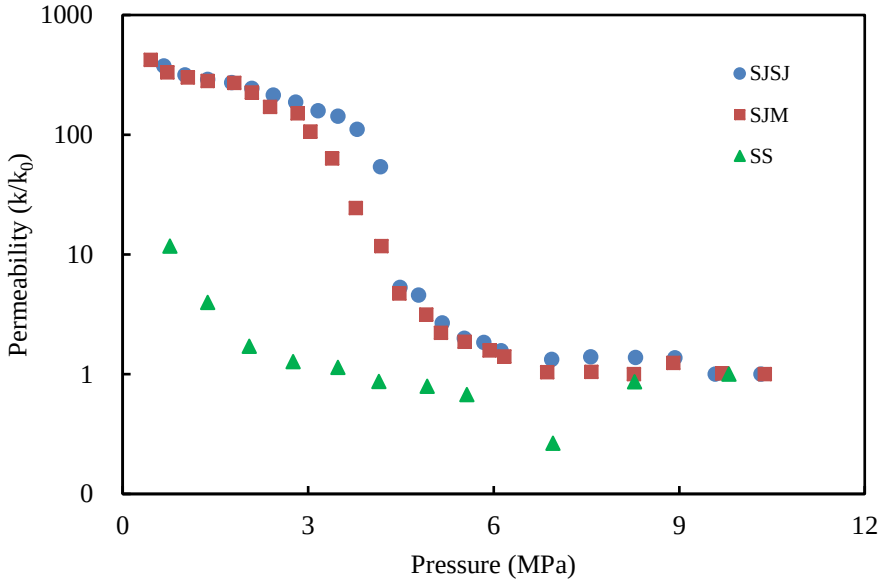

Figure 4.3 Variation in permeability with methane depletion.

4.3 Analysis and Discussion

This paper discusses the stress path of the three coal types with continued methane depletion. Coal undergoes deformation with depletion, which can be elastic or inelastic, the latter including dilatancy and coal failure. At this time, there is no shortage of evidence in the literature of only the elastic deformation. It is only recently that some effort has been made in the direction

of describing CBM reservoir permeability related to inelastic deformation. Shovkun & Espinoza (2017) and Chen (2016) presented the effect of dilation, or inelastic deformation, in the form of a permeability model for inclusion in a reservoir simulator (Shovkun & Espinoza, 2017). The effort in this paper achieves the same using experimental data. An attempt is made here to describe elastic as well as inelastic deformation and, using it, explain the corresponding impact on permeability.

4.3.1. Stress Path

Given that coal is a poroelastic medium, it is important to determine the effective stress when evaluating the deformations occurring in it in a dynamic stress environment. It is important to lay out the type of constitutive equations that are applicable to coal in elastic region and flow rule in plastic zone of deformation for complete stress-strain description of coal. Hence, the following three sub-sections are devoted to the definition of effective stress used in the study, scale dependent constitutive equations used for the elastic deformation in coal, and flow rules associated with plastic deformations.

4.3.2. Effective Stress Law for Stress Path

Stresses in both horizontal and vertical directions were measured during the PdK experiment. Since the core tested was cylindrical, stresses in the two horizontal directions were equal. In order to determine the stress path with depletion, estimation of effective stresses is required, and Terzaghi's definition of effective stress was used for this (Terzaghi, 1943). Mathematically, this is given as:

$$\sigma_i' = \sigma_i - p \tag{4.1}$$

where, σ_i' is the effective stress along ith direction, σ_i is the total stress along ith direction and p is the pore pressure. The expression is simple and has been shown to work fairly well for

most geomechanical applications (Coussy, 2003a; Espinoza et al., 2015; Shimin Liu and Harpalani, 2014). A more rigorous approach is possible by using the Biot's definition of effective stress (Biot, 1941). The authors carried out a study using estimated Biot's coefficient, determined for the coal type in a study (Saurabh et al., 2016), and found that the variation in the stress path was minimal. Given that the primary aim of this paper is not to *predict* the effective stress, additional complexities were avoided by using Terzaghi's definition.

4.3.3. Constitutive Equations for Coal

Coal has been treated as an isotropic medium in this paper for simplicity. Coal has been presented as anisotropic media in a number of studies before, but to integrate the elastic and inelastic deformation in coal and treating it as anisotropic media would require significant additional experimental work to evaluate the geomechanical characteristic strength and anisotropic flow of cleat structure of coal. The poroelastic constitutive equations for isotropic rocks presented by Coussy (2003a) were used in the analysis for elastic deformations. These are given as:

$$\Delta\sigma = K\epsilon - b\Delta p \tag{4.2}$$

$$\Delta s_{ij} = 2\mu e_{ij} \tag{4.3}$$

$$\Delta\,\phi = b\epsilon + \frac{\Delta p}{N} \tag{4.4}$$

where, $\Delta\sigma$ is the change in the mean stress tensor, K and μ are the grain bulk and shear modulus, b is Biot's coefficient (taken as 1 for simplicity), Δp is the change in pore pressure, Δs_{ij} is the change in deviatoric stress tensor, e_{ij} is deviatoric strain tensor, $\Delta\phi$ is the change in cleat porosity, N is the Biot's modulus, and ε is the volumetric strain. The constant N is called Biot's modulus and defined as the increase of the amount of fluid per unit volume of rock as a result of unit increase of pore pressure, under constant volume condition. Coal is a dual

porosity medium and micro-macro strain data must be coupled. The micro-macro scale strain coupling equation used is as follows (Coussy, 2003b):

$$\epsilon = (1 - \phi_0)\epsilon_s + \phi \quad (4.5)$$

where, ϵ is volumetric strain and ϵ_s is the volumetric strain in the solid part of coal, that is, coal grains. Since $\phi_0 << 1$ for coal, the equation can be simplified as (Coussy, 2003a):

$$\epsilon = \beta\phi \quad (4.6)$$

where, β is a proportionality constant. As a next step, the strain was separated as elastic and plastic, with the assumption that there is only elastic strain with helium depletion since it is a non-sorbing gas. Figure 4.4 presents the results of vertical strain with helium and methane depletion for SJM coal. A similar exercise was carried out for the other two coal types as well. The equation used to separate the strain in elastic and plastic components is as follows:

$$\varepsilon = \varepsilon_e + \varepsilon_p \quad (4.7)$$

The separation of the elastic and inelastic strains in coal enabled defining the zones of elastic and inelastic deformation in the stress path during gas depletion.

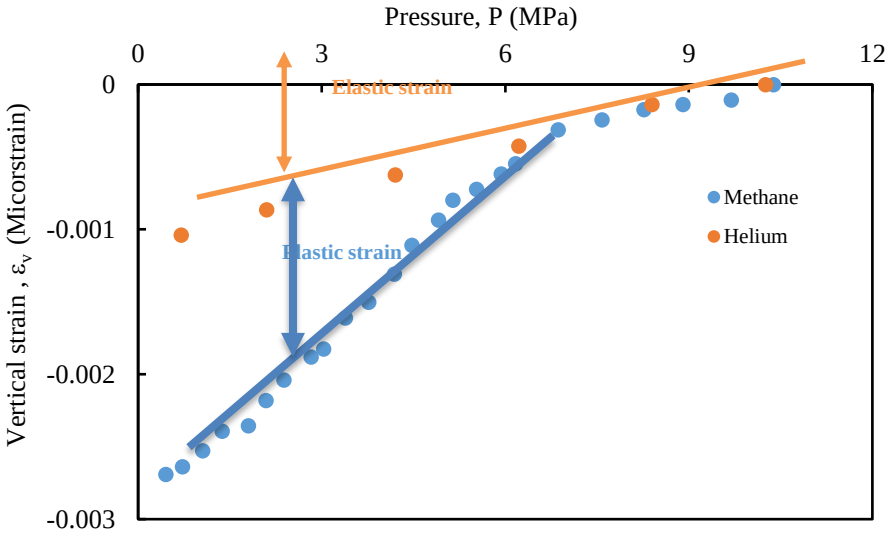

Figure 4.4 Strain data analysis for SJM coal with helium and methane depletion.

4.3.4. Flow Rule and Dilatancy Characterization

Complete description of stress-strain behavior of coal during the dynamic stress environment of gas depletion can be established using flow rules for the plastic deformation zone. The approach followed in this study is to evaluate deformation in the stress plane and identify the different deformation zones. The stress plane used for analysis is the octahedral shear stress/σ_s ($\sqrt{\frac{2}{3}J_2}$) and octahedral mean stress/σ_m (I_1), where, J_2 is the second deviatoric stress invariant and I_1 is first stress invariant. The variation of stress path in this plane is delineated into different deformation zones. The technique to do this and definitions of the deformation zones are discussed in the following sub-section (4.3.5). The study uses non-associative flow rule for plastic deformations in coal. Coal is treated as isotropic for this exercise, just as prior researchers did (Espinoza et al., 2015; Liu and Harpalani, 2014; Lu and Connell, 2016; Saurabh et al., 2016). The stress path of coal was established using the stress data collected during the experiments. The Drucker-Pr*ä*ger yield criterion was used for this and determine the yield surface (failure envelope) for coal (Drucker and Prager, 1952). Drucker-Prager yield criterion is basically a modified Tresca criterion, where intermediate principal stress also plays a role in strengthening the rock. The criterion can be mathematically defined as:

$$\sqrt{J_2} = A + B\, I_1 \tag{4.8}$$

where, J_2 is the second stress invariant, I_1 is the first stress invariant, A and B are constants determined experimentally.

Every experiment was initiated at *in situ* stress and pore pressure conditions and changes in the stresses were recorded during the entire experiment with depletion of gas. This enabled estimation of the stress path of coal in the octahedral shear stress and octahedral mean stress plane or, the Drucker-Pr*ä*ger plane. Similarly, geomechanical failure test data was used to

determine the failure envelope in the Drucker-Präger stress plane. The estimated effective stresses (Equation 4.1) were used to estimate $\sqrt{\frac{2}{3}J_2}$ (σ_s), and I_1 (σ_m), using the following:

$$J_2 = \frac{1}{6}\left[(\sigma_v' - \sigma_H')^2 + (\sigma_h' - \sigma_H')^2 + (\sigma_v' - \sigma_h')^2\right] \quad (4.9)$$

where, σ_v', σ_h' and σ_H', are the effective stresses

For axially symmetric conditions, defined as $\sigma_H' = \sigma_h'$, the above equation simplifies to:

$$J_2 = \frac{1}{3}(\sigma_v' - \sigma_h')^2 \quad (4.10)$$

Hence, σ_s is given as:

$$\sigma_s = \sqrt{\frac{2}{9}(\sigma_v' - \sigma_h')^2} \quad (4.11)$$

or, simply as:

$$\sigma_s = 0.47\,(\sigma_v' - \sigma_h') \quad (4.12)$$

Also, I_1 was estimated using the following:

$$I_1\,(or\ \sigma_m) = \frac{1}{3}[\Sigma(\sigma_v' + 2\sigma_h')] \quad (4.13)$$

Using Equations (4.12) and (4.13), the stress paths for the coal types were established. These are presented in Figures 4.5(a-c), along with the corresponding failure envelope. The yield surface was also obtained using Equations (4.12) and (4.13), using the geomechanical strength testing data. Hence, using the definition of effective stress and Drucker-Präger yield criterion, stress path of coal for methane depletion was estimated and plotted in octahedral stress plane, along with the failure envelope.

Dilatancy in rock is widely believed to be related to the factor, shear plastic strain (Υ^p), given as (Alejano and Alonso, 2005):

$$\Upsilon^p = \left|\varepsilon_1^p - \varepsilon_3^p\right| \quad (4.14)$$

where, ε_i^p are the principal plastic strains. This study uses stress data instead of strain to avoid the inherent scale dependency of strain. Dilatancy has been characterized using octahedral shear stress, which is proportional to the shear plastic strain (Υ^p) (Equation 4.14). In the section on permeability modeling, it is shown that the plastic permeability variations are also proportional to the shear plastic strains (Equation 4.13) or, the octahedral shear stress.

4.3.5. Discussion on Stress Path

As mentioned in section 4.2.3, the experimental conditions resulted in an increase in the vertical effective stress with continued depletion. In terms of effective stress, this resulted in an increased vertical effective stress. At the same time, there was a reduction in the total horizontal stress with methane depletion, the overall process leading to a decrease in the effective horizontal stress. The two processes together, therefore, resulted in increased stress anisotropy with continued depletion. Understanding this in terms of octahedral stress is more meaningful since it provides a three-dimensional picture. Hence, the stress path was plotted to explain the above behavior, as presented in Figures 4.5(a-c).

Stress paths for the three coal types exhibited similar behavior, qualitatively speaking. A comparison of the stress paths is presented here in order to understand how different coals behaved with depletion. The important features of the stress path are discussed first, followed by a discussion of the stress path for each coal type.

- Each coal type exhibited at least two major regions in the stress path, that is, elastic, dilatancy and inelastic deformation zones.
- Elastic zone (E-Z): The identification of the elastic zone was carried out by a linear fit from the start of the stress path until there was deviation from linearity. This is based on the assumption that the core fulfils the Drucker stability postulate, which implies that a

stable, strain-hardening material exhibits normality and convexity yield surface with respect to plastic strain (Drucker, 1957). Typically, for non-sorbing rocks, the stress path moves away, or remains parallel to, the failure envelope in this zone, implying that there is no plastic strain. This results in elastic compaction of the porosity, resulting in decreased permeability. However, the sorption induced elastic strain can also affect movement of the stress path in this region, as in the case of San Juan coals, resulting in the stress path moving a little towards the failure envelope. Hence, these two coal types did not undergo compaction from the start of depletion. For SS-coal, the phenomenon of sorption-induced strain was found to be weaker than that for the other two coal types and, hence, the difference in behavior.

- Dilatancy and inelastic deformation zone (D-Z): Identification of this zone was carried out with very high to negative slope in the octahedral effective stress plane. This signals the development of plastic strain in coal, based on the normality condition. It also signals plastic changes in the porosity structure. The movement of stress path towards failure envelope in this zone signals weakening, or dilatancy being initiated in the sample. The reason for this behavior is believed to be the anisotropic stress conditions, resulting from significant decrease in horizontal stress with depletion and further compounded by shrinkage of the coal matrix, leading to dilatancy.
- Post failure zone (PF-Z): This zone is identified as the zone lying beyond the failure envelope. The slope of the stress path is small in this region. However, it is still greater than the slope of the failure envelope. This denotes continued increase in permeability with further depletion, particularly in the absence of fines production and clogging of fractures.

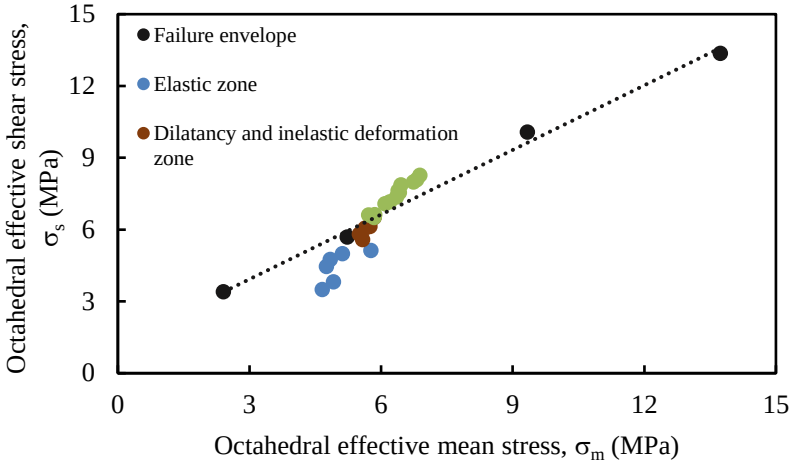

Figure 4.5a Stress path of SJSJ coal with depletion.

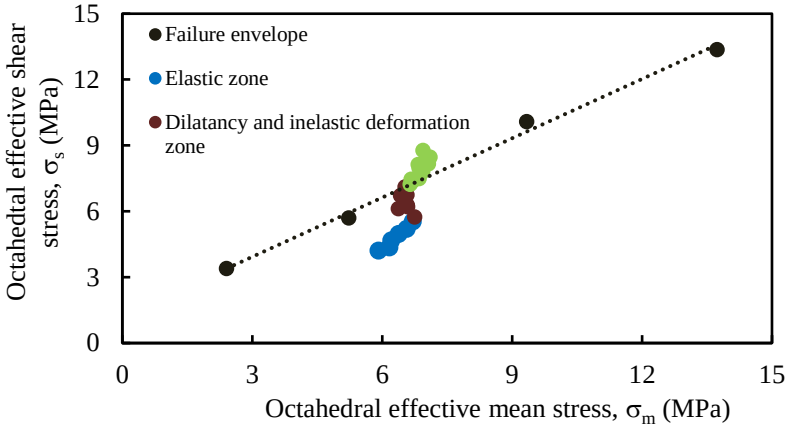

Figure 4.5b Stress path of SJM coal with depletion.

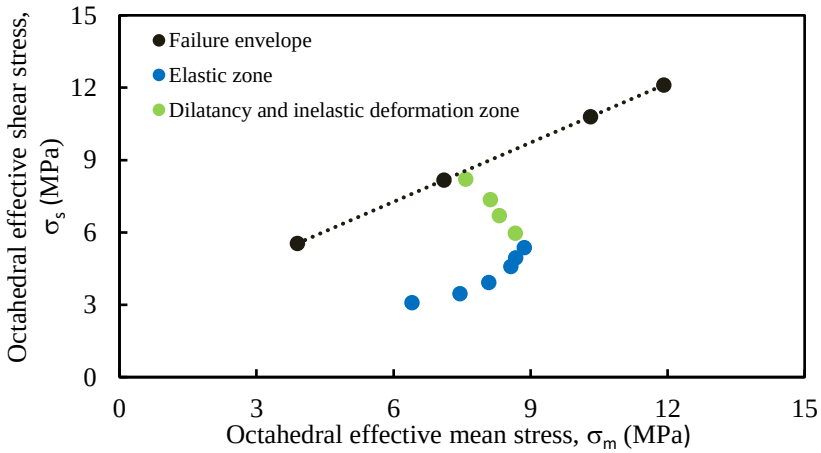

Figure 4.5c Stress path of SS coal with depletion.

Figure 4.5(a-c) Stress path of various coal types with depletion.

San Juan Coal

- **Elastic zone:** These two coal types exhibited three distinct zones in the stress path during depletion. Starting with linear elastic zone, the slope of the stress path was generally higher than that of the failure envelope. Hence, even in the elastic zone, there was no compaction and permeability increased for both coals. The exhibited behavior was probably the result of the non-linear elastic deformation in coal due to sorptive behavior of coal.
- **Plastic zone with dilatancy:** With continued depletion, the slope increased significantly in case of SJSJ coal and became negative for SJM coal. This can be explained with plastic deformation in coal due to increased octahedral shear stress on the sample. A negative or very high slope leads the stress path to move towards the failure envelope, which denotes introduction of plastic strain by normality condition. Hence, the stress path started moving towards the failure envelope at a faster pace, resulting in dilatancy and increased porosity and, ultimately, a rapid increase in the permeability.
- **Post-failure zone** - After failure, that is, when the stress path of coal reached the yield surface, coal retained the plastically increased porosity and the stress path moved beyond the failure envelope. This shows that coal exhibited strain-hardening behavior and it is able to move beyond the yield surface because of the increased octahedral mean stress, resulting in coal becoming stronger due to increased mean stress. It is important to note that, under stressed condition and with pore pressure, the coal remained intact even with a failure plane. Again, comparing the slopes of failure envelope and post-failure zone, the latter had a steeper slope. Hence, coal retained the

increased permeability due to failure and further increase in permeability was the result of continued matrix shrinkage as methane continued to desorb.

SS Coal:

- **Elastic zone:** This coal started with movement of the stress path away from the failure envelope, indicating compaction of coal. Hence, a reduction in permeability was observed to begin with.
- **Dilatancy zone-** The next three data points in the elastic zone moved towards the failure zone and, hence, the permeability increased during this period. This is explained by the non-linear elastic strain due to sorptive behavior of coal. This was followed by a negative slope and movement towards the failure envelope, which consequently caused a significant increase in the permeability. Again, both phenomena can be explained using the normality condition, implied by fulfilment of the Drucker postulate and development of dilatancy with plastic straining of coal.

This explanation of the stress path and its inherent coupling with permeability variation (in elastic and inelastic zones, including the post-failure zone) calls for a mathematical link between the two parameters. Such a modeling exercise would not only help in understanding the behavior but also projecting the permeability variation in terms of stresses existing in the reservoir. The stress path discussed in the study only considers the steady-state condition of rock and transient process. The case where pressure in matrix is not equal to pressure in fractures, like in slow sorbing coals, is not considered. It is also important to mention at this point that the thrust of this paper is not to model dilatancy with depletion of methane in coal given a plethora of excellent literature on modeling of dilatancy under various boundary conditions in coal. This study is aimed at developing a technique to establish the stress path in the laboratory in order to

understand the elastic and plastic deformations developed in coal with methane depletion, all based on definitions of elastic and plastic deformations available in the current literature. In addition, the experimentally established stress path is used to model the changes in coal permeability with depletion.

4.4 Permeability Modeling

The permeability model presented in this paper attempts to couple the phenomena occurring in terms of reservoir stresses. We argue that all variations in the reservoir parameters ultimately translate to a change in reservoir stresses and that effective stress is the sole parameter dictating changes in the permeability. It is believed that changes in permeability are controlled by shear and normal stiffness of fractures, frictional dilation of fractures, moduli of the rock, initial permeability and the state of stress (Bai et al., 1999). Specifically, this paper addresses coal permeability variation with depletion. Coal is a dual porosity medium with most of the gas stored in its matrix and the flow taking place primarily in the cleat system. It is a widely believed in scientific literature that only changes in cleat properties of coal are responsible for changes in coal permeability. The above being said, cleat aperture of coal changes with variation in pore pressure and shrinkage of coal with methane depletion. Both phenomena, coupled together, produce changes in the state of stress and are reflected in terms of increased permeability. There are several permeability models in the current literature, where mean effective stress and horizontal stress, in addition to the fracture permeability, are believed to be the primary factors controlling changes in permeability with depletion. In this paper, we propose a combination of effective vertical and horizontal stresses, call it the *differential octahedral effective shear stress*, and that this is the primary permeability-controlling factor in coal reservoirs with continued depletion.

Several assumptions are made to start the modeling exercise. These are presented below:

- The model assumes uniaxial strain condition in the reservoir. Since 1995 (Seidle et al. 1995), this is believed to best replicate the actual *in situ* conditions in CBM reservoirs. Also, based on this, the experiments were carried out under uniaxial strain condition. Hence, this assumption is inherent in the modeling exercise.
- The model does not assume the bundle of matchstick geometry (Reiss, 1980) and this is a deviation from most recent models presented. In fact, we propose that the basic geometrical structure of coal can be anything and the presented model is free of the assumptions of a geometrical structure. Of course, the model would work for the bundle of matchsticks geometry.
- We assume that the permeability achieved by coal at failure is retained and any further increase in its value is based on the newly retained porosity structure.

We define differential octahedral effective shear stress ($\Delta\sigma_s$) as the difference between octahedral effective shear stresses (y-axis in the plots) for the failure envelope and stress path, as the key and sole parameter dictating the permeability variation with continued depletion. We further propose that this parameter has an inverse relation to changes in permeability. If it increases, compaction of coal takes place and permeability decreases. On the other hand, if the parameter decreases, permeability increases as a result of dilatancy. If it remains constant, permeability does not change. Figure 4.6 shows these assumptions schematically. It is important to note that the octahedral mean stress affects permeability as well.

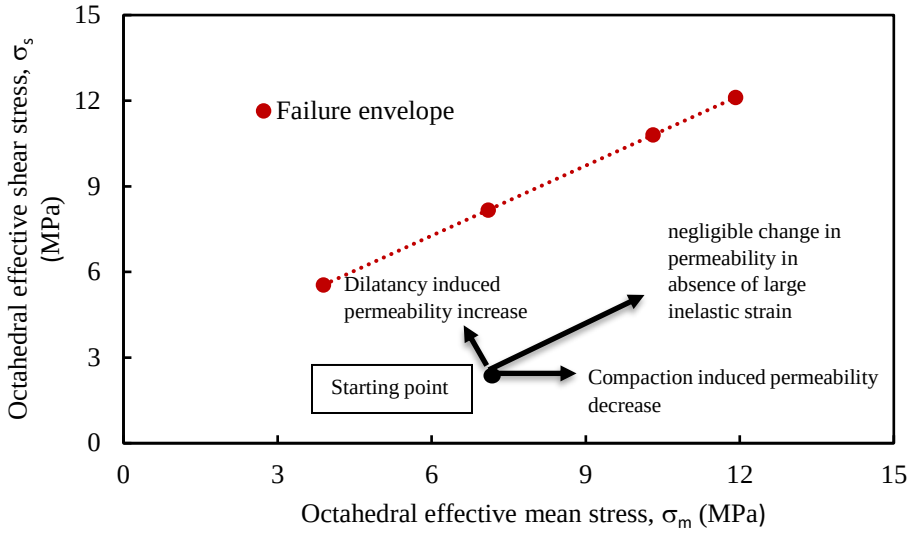

Figure 4.6 Schematic presentation of assumptions for permeability changes.

In fact, the differential octahedral effective shear stress is not only a function of octahedral shear stresses at failure envelope and that in the sample at any point, it is also dependent on the octahedral mean stress since, with depletion, octahedral mean stress typically increases. In general, with increase in octahedral mean stress alone, permeability is expected to decrease. For all experiments completed, the change in octahedral mean stress was small. This aids to simplify the permeability model and define it only in terms of the octahedral effective shear stress. The effect of octahedral mean stress is encompassed in the differential octahedral shear stress compressibility term, explained later. The differential octahedral effective shear stress is given as:

$$\Delta\sigma_s = \sigma_s^f - \sigma_s^{sp} \tag{4.15}$$

where, σ_s^f is the octahedral shear effective stress at failure and σ_s^{sp} is the octahedral shear effective stress acting on the sample at a particular value of the octahedral mean effective stress. Since coal permeability is believed to depend on its cleat porosity alone (Liu and Harpalani, 2013b; Ma et al., 2011; Palmer, 2009; Pan and Connell, 2012b; Saurabh et al., 2016),

the following general expression is given as:

$$k \propto b^n \tag{4.16}$$

where, b denotes the cleat aperture and n denotes the structure dependence. The b and n terms can be different for different geometries. For example, the value of n would take a value of 3 for the bundle of matchstick geometry and 4 for the bundle of capillaries (Bai et al., 1997; Reiss, 1980) geometry. Using a constant of proportionality, Equation (4.16) is written as:

$$k = Ab^n \tag{4.17}$$

The deformation in coal, leading to changes in its cleat aperture, can be written as follows:

$$b = b_0 + X\varepsilon_m^h \tag{4.18}$$

where, b_o is the initial cleat aperture, ε_m^h is the matrix scale strain in coal and X is the strain multiplier depending on the coal structure. Hence, as defined in sub-section 4.3.4, if there is linear elastic strain in coal, then b changes linearly with depletion. This is signaled as linear variation of permeability with depletion. However, in case of coal, there is the additional non-linear elastic strain related to its sorption behavior and b changes non-linearly with depletion, resulting in some non-linearity in the variation in permeability with depletion. In addition, there is plastic strain in coal, as discussed in determination of the stress path of each coal by its movement towards the failure envelope. This causes plastic deformation in the matrix, probably because of axial splitting or other modes of introduction of dilatancy in the sample, significantly changing the cleat spacing, a. This can be expressed by change in the cleat aperture by modifying Equation (4.18) as:

$$b = b_0 + X'\left\{(\varepsilon_m^h)_{elastic} + (\varepsilon_m^h)_{plastic}\right\} \tag{4.19}$$

The above equation can be modified and expressed in terms of the shear plastic strain or

as:

$$b = b_0 + X'\{(\varepsilon_m^h)_{elastic} + p(\gamma)_{plastic}\} \quad (4.20)$$

where, p is the proportionality coefficient. Since differential octahedral effective shear stress is believed to be an indicator for both elastic and plastic deformations in coal as well as permeability changes in the experiment, permeability modeling is carried out in terms of this parameter.

Differentiating Equation (4.17) with respect to $\Delta\sigma_s$ gives the following:

$$\frac{\partial k}{\partial \Delta\sigma_s} = Anb^{n-1}\frac{\partial b}{\partial \Delta\sigma_s} \quad (4.21)$$

We now define the octahedral effective shear stress compressibility (C_s) as:

$$C_s = -\frac{n}{b}\frac{\partial b}{\partial \Delta\sigma_s} \quad (4.22)$$

(the C_s parameter is explained in detail later in this section.)

Combining Equations (4.17, 4.21 and 4.22) gives the following:

$$\frac{\partial k}{\partial \Delta\sigma_s} = -C_s k \quad (4.23)$$

Integrating Equation (4.23) gives the following:

$$k = k_i \exp\{-C_s(\Delta(\Delta\sigma_s))\} \quad (4.24)$$

Using the above, permeability modeling gave good fits for all three coal types, as presented in Figures 4.7(a-c). The values of octahedral effective shear stress compressibility, C_s, used to fit the modeled results to the experimental data are presented in Table 4.3.

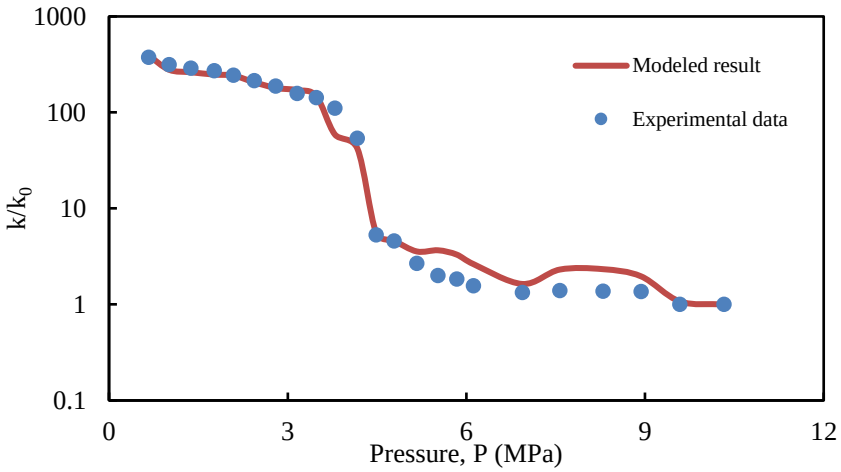

Figure 4.7a Experimental and modeled permeability for SJSJ coal.

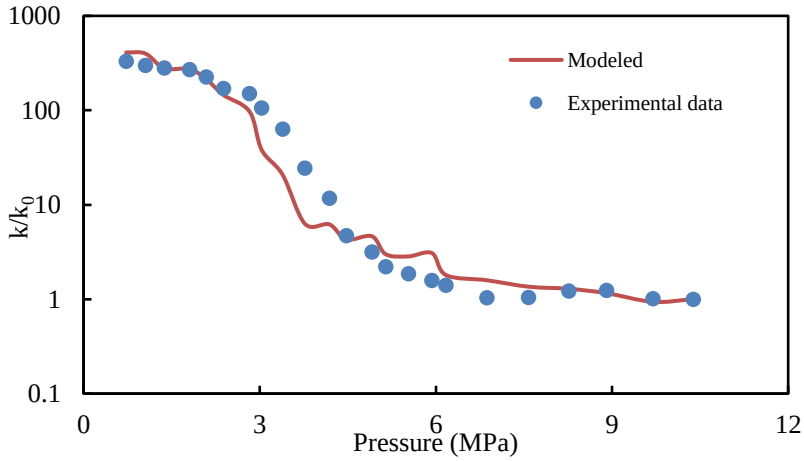

Figure 4.7b Experimental and modeled permeability for SJM coal.

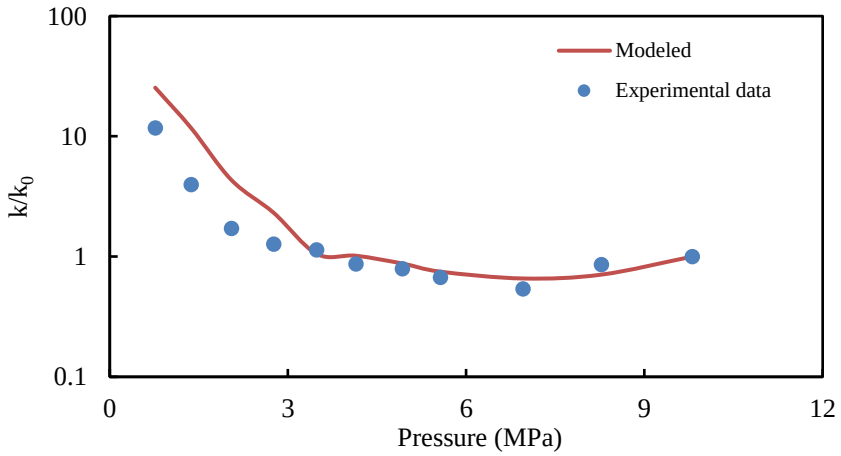

Figure 4.7c Experimental and modeled permeability for SS coal.

Figure 4.7(a-c) Experimental and modeled permeability for various coal types.

Table 4.3 Values of C_s used for permeability modeling.

Octahedral effective shear stress compressibility (C_s) , (MPa^{-1})			
Sample Name	**Elastic Zone**	**Dilatancy Zone**	**Post failure Zone**
SJSJ	0.76	9.6	4.7
SJM	0.69	11.36	5
SS	0.59	0.74	--

4.5 Octahedral Effective Shear Stress Compressibility (C_s)

The octahedral effective shear stress compressibility, introduced in Section 4.3.2, is explained in detail here. We first attempt to provide a general outlook of what is captured by this parameter, that is, its physical significance. After that, a brief discussion on the variation in the magnitude of this parameter is presented. Lastly, experimental work that can be carried out to estimate this parameter is presented.

As apparent from Equation (4.22), the unit of C_s is MPa^{-1}. Hence, it is introduced as a compressibility term. Our first attempt is to define the term using a mathematical definition. The octahedral effective shear stress compressibility (C_s) is the relative change in the cleat aperture per unit change in the differential octahedral effective shear stress $\Delta(\Delta\sigma_s)$, where differential octahedral shear effective stress is the difference between the octahedral effective shear stress at a pressure and the octahedral effective shear stress required for failure at that pressure. It is important to mention that differential octahedral effective shear stress is a function of the octahedral effective mean stress, octahedral effective shear stress and the failure envelope. Hence, the definition can be re-worded as: octahedral effective shear stress compressibility is the

relative change in the cleat aperture with change in the state of stress in an octahedral effective stress plane with respect to failure envelope.

Conventionally, the exponential permeability model contains a compressibility term, either the pore volume compressibility with respect to pore pressure (Seidle et al. 1995) or, with respect to effective horizontal stress (Shi & Durucan 2004; 2005). In the model presented here, C_s takes the analogous role of pore volume compressibility. C_s is defined in terms of b (cleat aperture) instead of porosity (ϕ,) to make our statement more general since b and ϕ are related, depending on the geometry used. Again, using the definition of b at a particular pressure in the form of Equation (4.20), it can be said that the C_s parameter captures the elastic as well as plastic deformation caused by the developed dilatancy in coal. In addition, in the previous models, the pore volume compressibility was either measured with respect to pore pressure or horizontal stress and neither of these two parameters signal any indication of dilatancy or failure. Hence, this parameter is replaced by differential octahedral effective shear stress, which is a function of both vertical/horizontal stress, pore pressure and the failure envelope. This certainly helps in modeling the permeability induced due to shrinkage as well as in tracking dilatancy and failure-induced permeability (Zoback and Byerlee 1975; Simpson et al. 2001; Souley et al. 2001), which can be due to slipping of cracks under shear stress, a phenomenon overlooked by previous models.

Next, we use the mathematical definition (Equation 4.22) to look at the magnitude of the values that C_s can take during depletion. It is proposed that the limiting value that the "n" parameter can have in Equation (4.22) is 10, based on existing literature where n has been reported not to exceed 10. For example, for a bundle of matchstick geometry, the value of n is three and for the bundle of capillaries, it is four. Also, from Figures 4.4(a-c), it is estimated that

$\partial\Delta\sigma_s$ lies between 10 and 100 for the coals tested.

To determine the order of magnitude of $\frac{\Delta b}{b}$, Equation (4.17) is re-written for the bundle of matchstick geometry as:

$$\frac{k}{k_0} = \left(\frac{b}{b_0}\right)^3 \tag{4.25}$$

where, k_o is the initial permeability. Expanding Equation (4.25) gives the following:

$$\frac{k}{k_0} = \left(\frac{b_0 + \Delta b}{b_0}\right)^3 \tag{4.26}$$

or, $$\frac{k}{k_0} = \left(1 + \frac{\Delta b}{b_0}\right)^3 \tag{4.27}$$

Assuming that change in the cleat aperture is very small, Equation (4.27) can be approximated as:

$$\frac{k}{k_0} = 1 + \frac{3\Delta b}{b_0} \tag{4.28}$$

For an increase in permeability of between 10 and 100, the ratio $\frac{\Delta b}{b_0}$ lies between 3 and 33. Hence, the order of magnitude of C_s can be estimated as follows:

$$C_s = n\ (\text{between 1 and 10}), \frac{\partial b}{b_0}\ (\text{between 10 and 100}), \frac{1}{\partial\Delta\sigma_s}\ (\text{between 0.01 and 0.1}) \tag{4.29}$$

Based on Equation (4.29), the value of C_s can vary from 0.1 to 100 MPa^{-1}. Although empirical, this range provides a constraint for the values of C_s to be used as a guideline.

An experiment to measure the octahedral effective shear stress compressibility can be carried out in the laboratory by replicating the same stress path as that obtained in the experiments presented in this paper and using sonic velocities to measure changes in the elastic moduli, which signal changes in the porosity (Walsh, 1965). The effect of pore pressure induced increase in stiffness of the sample when using ultrasonic wave velocity can be avoided by conducting the experiment without any pore pressure and tracing the effective stress path

obtained in the permeability experiments.

This approach has been mentioned in the literature (Mavko et al. 2009; Bourbié and Coussy 1987). Equation (4.22) then transforms to the following:

$$c_s = -n\left\{\frac{\partial f(v_p,v_s)}{f_0(v_p,v_s)\partial\Delta\sigma_s}\right\} \tag{4.30}$$

where, $f(v_p,v_s)$ is some function relating ϕ (total porosity) to the measured ultrasonic compressional and shear velocities (v_p and v_s). However, it is clear from its mathematical definition that this parameter (C_s) measures the effect of octahedral shear stress on porous structure of coal and it can be especially helpful in quantifying dilatancy in coal with methane depletion. To validate the trend of values used in the modeling above for C_s, the ultrasonic velocity (v_p- P-wave velocity) measured during depletion was used in Equation (4.30). P-wave velocity data was available only for one San Juan sample (SJM). Figure 4.8 shows the variation of P-wave velocity for SJM sample with methane pressure depletion. The values of the P-wave velocity were used in a simple function, given as:

$$f(V_p) = (V_p)^m \tag{4.31}$$

where, m is a material constant. It was taken to be 1 for undamaged coal and 4.5 for damaged coal. P-wave velocity is directly related to porosity of coal and the function used in Equation (4.30) is a defined to be indicative of porosity variation.

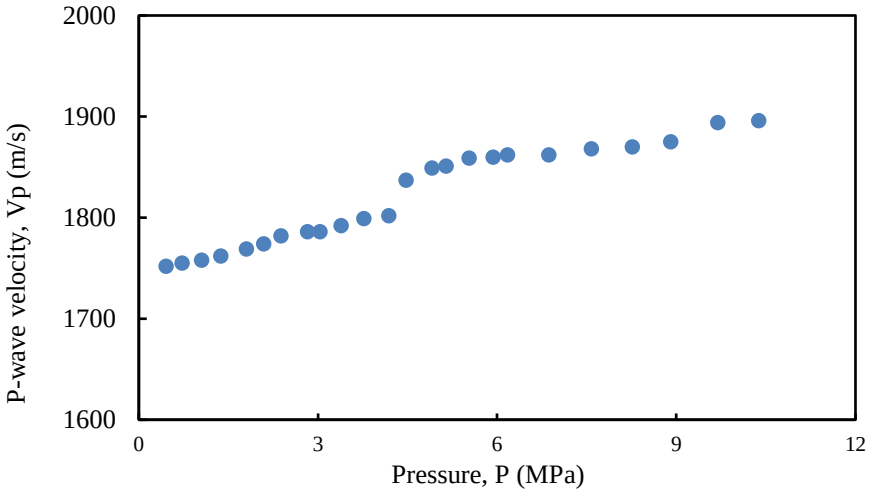

Figure 4.8 Ultrasonic P-wave velocity with methane depletion (SJM).

However, the functional values need some fitting to match the experimental data and m was defined separately for intact and damaged coal in lines of parameter D (Disturbance factor) defined for intact and damaged rock in Hoek and Brown criterion (Eberhardt, 2012).

The estimated slope of the $(d(V_p)^m)/\left((V_p)^m\right)_0$ versus the octahedral shear stress was used in Equation 4.19, with n = 1 and scaled with a multiplication of 100 to compare it with the values used in the fitting of model data (Figure 4.9). The scaled values so obtained were plotted against those used in the modeling in Figure 4.10. The figure provides a convincing argument, justifying the values used in the model, and further justifies the trend of values.

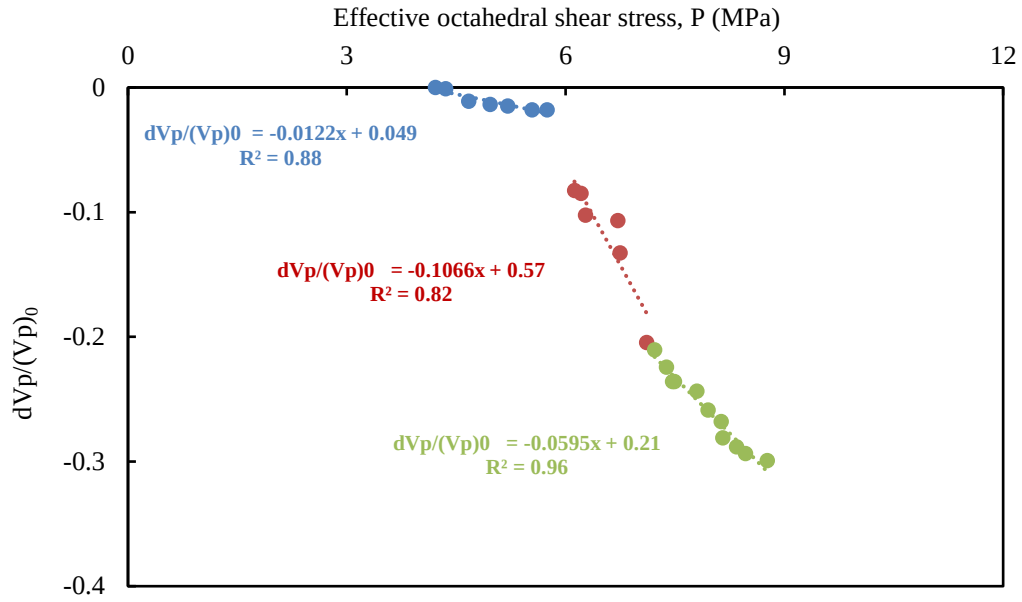

Figure 4.9 $(d(V_p)^m)/\left((V_p)^m\right)_0$ vs effective octahedral shear stress.

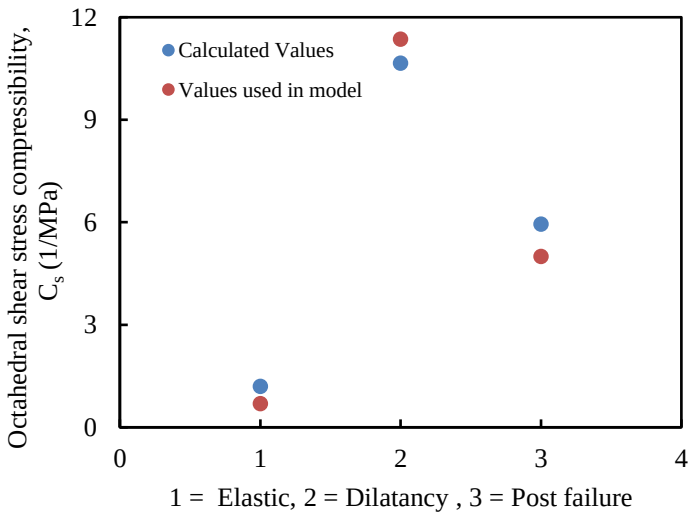

Figure 4.10 Comparison of calculated and values used in the permeability modeling for SJM coal.

4.6 Conclusions

In light of the investigation of stress path and the consequent permeability modeling, several important conclusions are made. These are listed below:

- Based on the stress paths presented, it can be conclusively said that the nature of permeability variation in coal is inherently coupled with stresses existing in the reservoir. Hence, permeability modeling using stress path is all-inclusive and can be a powerful tool in modeling. This paper presents a transition from modeling of coal permeability in elastic regime to inelastic regime. At the same time, it highlights the importance of geomechanics in flow modeling in coalbed methane reservoirs. The striking feature of the model presented in the paper is that the permeability model depends on only one independent parameter, that is, octahedral effective shear stress compressibility (C_s) and can be used for all regimes, that is, elastic as well as inelastic.
- Movement of stress path away from the failure envelope causes permeability reduction by compaction and movement towards the failure envelope causes dilation. It is important to note that the movement towards the failure envelope signals initiation of the phenomenon of matrix shrinkage, which, in turn, results in development of dilatancy. Implication of this is that the model provides improved understanding of the reasons behind changes in permeability and when it occurs. In other words, it can be predicted if the coal would develop dilatancy or failure induced sudden permeability uptick, based on the stress path with depletion.
- Post-failure behavior, showing permeability increase and its ability to withstand stress, suggests that coal does not fail completely and is able to withstand stresses. Its permeability continues to increase due to the phenomenon of matrix shrinkage. An extrapolation of this result is that, with further larger stress anisotropy, complete failure of sample can take place until it becomes rubble. At that point, the permeability in the reservoir will be strikingly high. However, this may be accompanied by production of a

significant amount of fines, which can be a serious problem.

- Of the coal types studied, two-showed failure and one only exhibited dilatancy zones. However, SS coal, which only showed elastic and dilatancy zones, was very close to failing and had started showing significant increase in permeability. It does demonstrate that not every coal would exhibit dilatancy and failure induced permeability surge. The behavior will depend on the strength of coal, depth of coal and the sorption characteristics of the coal.
- Octahedral shear effective stress compressibility (C_s), introduced in the paper, takes a lower value in the elastic zone, increasing in the dilatancy and post failure zones. It shows that it is inherently related to the coal porosity structure, which is altered in different zones.

Acknowledgements

The authors wish to thank Southern Illinois University for giving permission to publish this paper using the data acquired as a part of work funded by various sponsors. The authors would also like to express gratitude to researchers who worked in the laboratory on the experimental phase of the presented work, particularly Aman Soni and Vivek Singh.

CHAPTER 5

EFFECTIVE STRESS LAW FOR TRANSVERSELY ISOTRPIC, STRESS-SENSITIVE ROCKS

This Chapter is an exact copy (except for format change) of the journal paper entitled “The effective stress law for stress-sensitive transversely isotropic rocks”, published in *International Journal of Rock Mechanics and Mining Science*, 2018. DOI: 10.1016/j.ijrmms.2017.11.015.

Authors:

Suman Saurabh and Satya Harpalani

Abstract

This paper first presents a review of the development of the concept of effective stress, followed by major experimental and theoretical studies carried out to estimate the Biot’s coefficient. It then uses the constitutive equations for vertically transverse isotropic (VTI) reservoirs, like coal, derived using the principles of thermodynamics for estimation of the Biot’s coefficients in the vertical and horizontal directions. Laboratory data for tests conducted on two coal types retrieved from different geologic settings and geographical locations were used to carry out the modeling and validation exercise. Evidence is presented that values of Biot’s coefficient can be greater than one, proposed by Biot to be the limiting value, for sorptive rocks. To address this, the term Biot’s coefficient is replaced with “effective stress coefficient”. Finally, this paper discusses the pressure- and stress- dependent behavior of the Biot’s coefficient. The results clearly show that the estimated values of Biot’s coefficients in both vertical and

horizontal directions are different, varying with pressure for methane depletion but remaining constant for helium depletion. At the same time, the nature of Biot's coefficient, re-termed as effective stress coefficient, was found to be greater than unity for methane depletion. As a last step, a conceptual physical model is proposed to explain the pressure-dependent variation of effective stress/Biot's coefficients in terms of the contact area between grains. Based on the findings that the effective stress coefficient decreases with pressure, it is concluded that the effective vertical stress would increase significantly with depletion which, in turn, would result in shear failure and increased permeability.

Keywords: Effective stress law; Biot's coefficient; Transversely isotropic rocks; Sorptive rock-effective stress coefficient; Variable Biot's coefficient.

5.1 Introduction

The concept of effective stress is central and critical to reservoir geomechanics when dealing with porous rocks with fluid partially or fully residing in it. It is fundamental to several applications in reservoirs, like compressibility, flow problems, PV problems, temperature changes and other rock responses that are applicable to, and measured in, a reservoir (be it water, oil or natural gas). The concept of effective stress, over ninety years old, was first defined as the difference between external stress and pore pressure (Terzaghi, 1943). The concept has since been revised several times and researchers continue to work on it, given its importance and criticality during modeling and simulation of oil/gas production in order to make reliable future projections. The laws of effective stress have evolved over the years from ones dealing with soil to isotropic rocks, followed by anisotropic rocks and, finally, for sorptive media, like coal and shales. Dealing with the last two problems, anisotropy and sorptive media, poses a major challenge that is somewhat recent and continues to be a topic of research worldwide.

The term was originally developed to deal with saturated and unsaturated rocks, just like for any other solid media, by substituting the total stress by effective stress. By definition, it is the stress acting on the matrix of the porous solid, estimated by cancelling the effect of pore pressure. A correct expression for effective stress can help in dealing with saturated media by replacing the total stress in constitutive equations, failure criterion and flow problems with it. This paper first presents a brief review of the effective stress laws and their evolution over time. It then presents a means to estimate the effective stress for transversely isotropic, sorptive media, like coal.

5.2 Overview

5.2.1. Fundamental studies

The first concept of effective stress was presented by Terzaghi (1943) and was related primarily to soil mechanics. His findings, based on study of columns, had practical applications in soil mechanics. Terzaghi's definition of effective stress, however, was for one-dimensional stress only. In addition to being one dimensional, the definition was for constant load condition and saturated soils with incompressible grains. The definition of effective stress was simply the difference between applied stress and pore pressure in soil, given as:

$$\sigma^{eff} = \sigma - p \tag{5.1}$$

where, σ_{eff} is the effective stress, σ is the total applied stress and p is the pore pressure. This definition is still widely used for rocks and soils as a good approximation. The first complete and rigorous attempt to define and explain the theory behind effective stress was made by Biot (1941). The assumptions associated with treatment of effective stress definition by Biot were: 1) isotropy of the material; 2) reversibility of stress-strain; 3) linear stress-strain behavior; 4) small strains; 5) incompressible water and unsaturated conditions; and 6) applicability of

Darcy's law. Biot's extension of the effective stress theory of Terzaghi was to three dimensions is given as:

$$\sigma_{ij}^{eff} = \sigma_{ij} - \alpha p \delta_{ij} \quad (5.2)$$

where, σ_{ij}^{eff} is the effective stress tensor, σ_{ij} is the total stress tensor, p is the pore pressure, δ_{ij} is the Kronecker delta symbol and α is the Biot's coefficient. This is the most general and widely accepted expression for effective stress. The expression to estimate the Biot's coefficient is given as:

$$\alpha = \frac{E}{3\,(1-2\upsilon)H} \quad (5.3)$$

where, E is the Young's modulus, υ is the Poisson's ratio and H is the effective modulus, defined for the porous media. H is the modulus of the grain or, the inverse of grain compressibility. Skempton (1961) and Bishop (1954) presented an expression for the Biot's coefficient in terms of contact area between particles per unit gross area of the material. Geertsma (1957) proposed another expression for the coefficient for Biot's effective stress law as:

$$\alpha = 1 - \frac{K}{K_s} \quad (5.4)$$

where, K and K_s are the bulk modulus and grain modulus of the media respectively. A similar expression was proposed by Skempton (1961), given as:

$$\alpha = 1 - \frac{C_s}{C} \quad (5.5)$$

where, C_s and C are the grain and bulk compressibilities of the porous media. Suklje (1969) modified the above expression with addition of the porosity term (ϕ) as:

$$\alpha = 1 - (1 - \phi)\frac{K}{K_s} \quad (5.6)$$

Nur and Byerlee (1971) provided the experimental validation for Equation 5.4 and

theoretical derivation for the expression of Biot's coefficient. Using the results of a series of experiments conducted on weber sandstone, they concluded that using the expression of Biot (1941) and Equation 5.4 gives better results than that obtained using Terzaghi's expression.

5.2.2. Variation of Biot's Coefficient

Researchers worldwide have reported experimental work suggesting that Biot's coefficient varies with changes in confining stress and pore pressure conditions. Fatt (1959) measured values of the Biot's coefficient for Boise sandstone using kerosene as the pore fluid and reported that, with varying confining stress, the value of α varied between 0.77 to 1.0. Todd and Simmons (1972) studied the effect of pore pressure and confining stress on seismic velocity through the sample and their derivation of α was later extended as (Christensen and Wang, 1985; Hornby, 1996; Sarker and Batzle, 2008):

$$\alpha = 1 - \frac{\frac{\partial Q}{\partial p}\Big|_{\sigma}}{\frac{\partial Q}{\partial \sigma}\Big|_{p}} \tag{5.7}$$

where, Q is any measured physical quantity[16]. Christensen and Wang (1985) reported values of α ranging from 0.5 at high stresses to 0.89 at low stresses for Berea sandstone by measuring the dynamic properties and deformations. Warpinski and Teufel (1992) reported the variation of α with stress and pore pressure for tight sandstone and chalk from 0.65 to 0.95. Franquet and Abass (1999) conducted experiments on sandstone to propose that the value of α decreases with increase in confining pressure. A recent study by Ma and Zoback (2016) also reported, based on experimental work on samples from Middle Bakken, that there is dependence of Biot's coefficient on confining stress and pore pressure. Ma and Zoback (2016) concluded that the variation of α is significant at higher pore pressure and stress conditions, resulting in failure of Terzaghi's effective stress law. They used the method proposed by Christensen and Wang

(1985) for estimation of the Biot's coefficient using dynamic as well as static measurements, a modification of the method first proposed by Todd and Simmons (1972). However, they commented that using dynamic method is not suitable for estimation of the coefficient because both elastic and non-elastic strains occur in a reservoir and using a static test is, therefore, better for estimating the value of α.

5.2.3. Anisotropy of Biot's coefficient

Since most of the above experimental work and theoretical derivation dealt with isotropic rocks, like sandstone and limestone, the above form of effective stress law cannot be accepted in its current form for anisotropic rocks, like coal and shales. These exhibit a special kind of anisotropy, termed vertical transverse isotropy (VTI), exhibiting isotropy in the two horizontal directions but vertical anisotropy. Hence, defining an effective stress law for these rock-types would be more appropriate for use in reservoir geomechanics problems in shale and coalbed methane reservoirs. Carroll (1979) developed equations for anisotropic effective stress law for elastic deformation. The derivation is simple and follows the same procedure as that followed by Nur and Byerlee (1971). Carroll (1979) proposed that effective stress law requires two constants for transversely isotropic medium and three for an orthotropic medium. Considering both anisotropic pore geometry and intrinsic anisotropy, he proposed that using six material constants, two of which are for solid material and four porous media constants, the two Biot's coefficients can be estimated for a transversely isotropic medium.

Coussy (2003b) presented a set of poroelastic equations, derived thermodynamically and based on energy balance for transversely isotopic media, as:

$$
\left.
\begin{aligned}
\sigma_{11} &= C_{11}\varepsilon_{11} + C_{12}\varepsilon_{22} + C_{13}\varepsilon_{33} - b_1 N[(\phi_c - \phi_{c0}) - b_1(\varepsilon_{11} + \varepsilon_{22}) - b_3\varepsilon_{33}] \\
\sigma_{22} &= C_{12}\varepsilon_{11} + C_{11}\varepsilon_{22} + C_{13}\varepsilon_{33} - b_1 N[(\phi_c - \phi_{c0}) - b_1(\varepsilon_{11} + \varepsilon_{22}) - b_3\varepsilon_{33}] \\
\sigma_{33} &= C_{13}\varepsilon_{11} + C_{13}\varepsilon_{22} + C_{33}\varepsilon_{33} - b_3 N[(\phi_c - \phi_{c0}) - b_1(\varepsilon_{11} + \varepsilon_{12}) - b_3\varepsilon_{33}] \\
\sigma_{23} &= 2C_{44}\varepsilon_{23} \\
\sigma_{31} &= 2C_{44}\varepsilon_{31} \\
\sigma_{12} &= 2\frac{(C_{11} - C_{12})}{2}\varepsilon_{12} \\
p_c &= N[(\phi_c - \phi_{c0}) - b_1(\varepsilon_{11} + \varepsilon_{22}) - b_3\varepsilon_{33}]
\end{aligned}
\right\} \quad (5.8)
$$

where,

$$b_1 = 1 - \frac{C_{11}+C_{12}+C_{13}/3}{K_m}$$

$$b_3 = 1 - \frac{(2C_{13}+C_{33})/3}{K_m}$$

$$\frac{1}{N} = \frac{(2b_1 + b_3)/3 - \phi_{c0}}{K_m}$$

where, σ_{ij} is the total stress along i-j direction, C_{ij} is the i-jth component of compliance matrix, ε_{ij} is the strain in i-jth direction, b_i is the Biot's coefficient in the ith direction, ϕ_c is the cleat porosity and p_c is the pore pressure in the cleat system of coal, K_m is the bulk modulus of coal matrix and N is defined as the reservoir Biot modulus. The above set of equations proposes that there should be two Biot's coefficients for a transversely isotropic media (b_1 and b_3). However, the equations lack the adsorption term, which must be included for sorptive rocks, like coal and shales, since these rock types interact with sorptive gases, like methane and carbon dioxide.

5.2.4. Sorption and Biot's Coefficient

Brochard et al. (2012) presented a theory to account for the adsorption-induced stress on microporous media and concluded that Biot's coefficient can be greater than one or less than

zero. The theory presented was used to develop a set of adsorption-coupled, thermodynamically-derived, poromechanical equations for microporous media with inclusion of cleats (fractures) by Nikoosokhan et al. (2012) and Espinoza et al. (2013, 2014). The set of equations proposed by Espinoza et al. (2014) is the most rigorous and complete of the above since it includes poroelasticity, adsorption-coupling, micro-macro (matrix-cleat behavior) scaling as well as the transverse isotropy for rocks, like coal and shale. The set of equations proposed by Espinoza et al. (2014) also contain the sorption dependent terms, presented as:

$$\left.\begin{aligned}
&\sigma_{11} = C_{11}\varepsilon_{11} + C_{12}\varepsilon_{22} + C_{13}\varepsilon_{33} - b_1 p_c - (1-b_1)s_m^{a1}(p)\\
&\sigma_{22} = C_{12}\varepsilon_{11} + C_{11}\varepsilon_{22} + C_{13}\varepsilon_{33} - b_1 p_c - (1-b_1)s_m^{a1}(p)\\
&\sigma_{33} = C_{13}\varepsilon_{11} + C_{13}\varepsilon_{22} + C_{33}\varepsilon_{33} - b_3 p_c - (1-b_3)s_m^{a3}(p)\\
&\sigma_{23} = 2C_{44}\varepsilon_{23};\ \sigma_{31} = 2C_{44}\varepsilon_{31};\ \sigma_{12} = 2\frac{(C_{11}-C_{12})}{2}\varepsilon_{12}\\
&p_c - s_m^a(p) = N[(\phi_c - \phi_{c0}) - b_1(\varepsilon_{11}+\varepsilon_{22}) - b_3\varepsilon_{33}]\\
&n_T = (1-\phi_{c0})n_m + \phi_c\rho_b
\end{aligned}\right\} \quad (5.9)$$

where, all the symbols defined in Equation (5.8) holds, with the addition of $s_m^{ai}(p)$, a pressure-dependent quantity coupling the sorption-based stress and strain in a microporous media. This was first proposed by Brochard et al. (2012), where n_T is the total adsorbed moles of gas on coal and ρ_b is the bulk density of coal.

5.2.5. Biot's Coefficient and Boundary Conditions

It is proposed here that the value of Biot's coefficient is dependent on the boundary condition of stress and strain in the reservoir, given its dependency on stress and pore pressure. Hence, the boundary conditions, such as, uniaxial strain, constant volume and constant triaxial stress conditions affect the value of Biot's coefficient. In this paper, the general equation for finding anisotropic Biot's coefficient for transversely isotropic sorptive media, like coal and shale, is derived using the equations proposed by Espinoza et al. (2014) for uniaxial strain

conditions. Applying the two boundary conditions of uniaxial strain conditions, shown below as Equations (5.10 & 5.11), to Equation (5.9) results in Equations (5.12 & 5.13).

$$\sigma_{33} = constant \text{ or } \frac{d\sigma_v}{dp} = 0 \tag{5.10}$$

$$\varepsilon_{11} = \varepsilon_{22} = 0 \text{ or } \frac{d\varepsilon_h}{dp} = 0 \tag{5.11}$$

$$b_1 = \frac{C_{13}\frac{d\varepsilon_3}{dp} - \frac{d\sigma_h}{dp} - \frac{ds_m^{a1}(p)}{dp}}{1 - \frac{ds_m^{a1}(p)}{dp}} \tag{5.12}$$

$$b_3 = \frac{C_{33}\frac{d\varepsilon_3}{dp} - \frac{ds_m^{a3}(p)}{dp}}{1 - \frac{ds_m^{a1}(p)}{dp}} \tag{5.13}$$

Expression for the Biot's coefficient will be different (Equations5.12 and 5.13), if different boundary conditions are used instead of uniaxial strain conditions. The effective stress depends not only on the pore pressure, but the boundary conditions as well, which determine variation in macroscopic properties like strain, compressibility, etc. These macroscopic properties boil down to changes in the microstructure of the rock and support the proposition that Biot's coefficient depends on the contact area between grain surfaces in porous media, as suggested by Skempton (1961) and Bishop (1954).

5.3 Experimental Work

Experimental data used for the analysis presented in this paper was taken from a laboratory-based study, aimed primarily at establishing the pressure-dependent-permeability (PdK) of CBM reservoirs in the San Juan basin in the US (Singh, 2014) and Sanga Sanga basin in Indonesia (Soni, 2017). Three different kinds of experiments were carried out as a part of these two studies. First, sorption characteristics of the coal type for methane were established. Using the sorption data, Langmuir Constants, P_L and V_L, were estimated. Second, quadrants of end pieces of the coal core were utilized to measure the volumetric shrinkage/swelling strains

under incremental hydrostatic pressure for unconstrained condition (unjacketed). This was first carried out for a non-sorbing gas (helium) and then repeated for a sorptive gas (methane).

Third, a flow experiment was carried out replicating the in situ reservoir stresses and uniaxial strain condition during depletion. As a part of this experiment, stresses, volumetric strains and flowrates were measured for a stepwise decrease in pore pressure for each step of depletion, for both sorptive and non-sorptive gases independently. As a final step, strength of the coal type was estimated. Details of all experimental setups used and testing procedures are presented in Singh (2014) and Soni (2017).

5.3.1. Sample Characterization

The coal tested in this study was retrieved from different parts of the world and geologic settings. Details of the sample location and geology are presented in Table 5.1. The rank of coals used in the study is sub-bituminous. The ash/moisture content and density of the samples are presented in Table 5.2.

Table 5.1 Sample location and rank of coals tested

Sample Name	Location	Rank of Coal
SJ Coal	Southwestern part of San Juan basin	Sub-bituminous
SS Coal	Sanga Sanga basin, Indonesia	Sub-bituminous

Table 5.2 Proximate analysis results for coals tested

Sample Name	Density (g/cc)	Ash Content (%)	Moisture content (%)
SJ Coal	1.34	5.1	7.9
SS Coal	1.26	1.2	4.8

For sorption experiments, pulverized sample, 0.0425–0.0149 cm in diameter, was used. For matrix shrinkage experiments, coal quadrants were prepared by trimming off the ends of the coal core. Each sample was approximately 1.9 cm thick and 2.5 cm in radius for San Juan coal and five cm in radius for Sanga Sanga coal. The remaining portions of the coal core, of diameter 5 cm and 7.5 cm long for San Juan coal, and 10 cm diameter and 15cm long for Sanga Sanga coal, were used for the PdK experiment. In addition, uniaxial compressive strength testing was carried out for each coal type.

5.3.2. Experimental results

The adsorption isotherms for the coal types are presented in Figure 5.1. The adsorption characteristics of both SJ- and SS- coals were different, SJ coal exhibiting superior sorptive behavior.

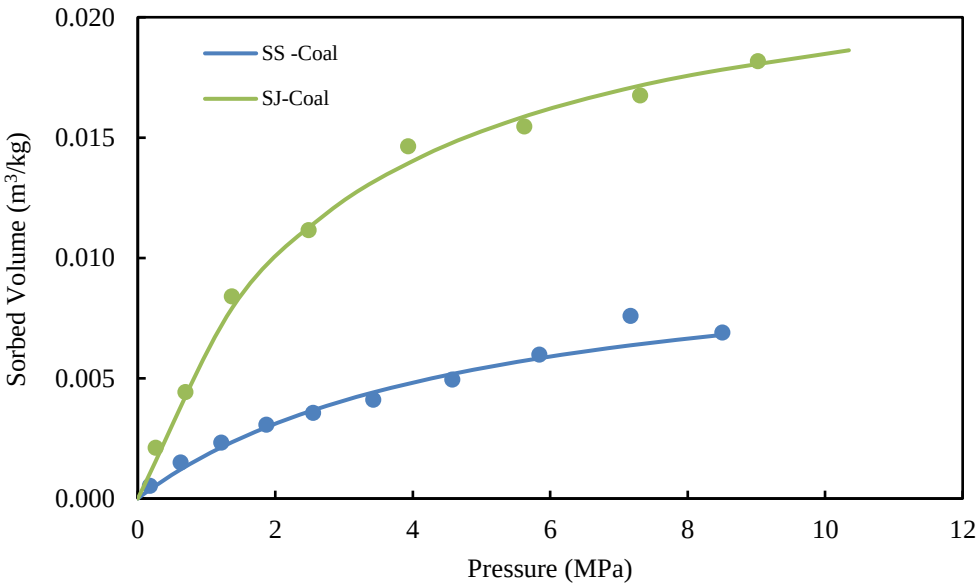

Figure 5.1 Adsorption isotherms for coal types.

The matrix shrinkage experiments included measurement of strains in the three principal directions under unconstrained conditions with gradual flooding with helium and methane.

Helium results provided the change in matrix volume of solid coal associated with changes in pressure while methane results provided the total strain resulting from the combined effects of matrix volumetric strain due to depletion as well as that associated with matrix shrinkage. Figures 5.2(a-b) show the results of the unconstrained drained experiment for helium flooding. For SS-coal, the vertical and horizontal strains were close, which is somewhat unusual for a vertical transversely isotropic rock. With helium depletion, the volume of solid coal increased as the pressure decreased from ~10 MPa (1500 psi) to atmospheric. The results in Figures 5.2(a-b) are shown on different scales, negative strain and positive strain, because Figure 5.2a shows the results for injection and Figure 5.2b for depletion result. However, with helium, the change is completely reversible given its inert nature.

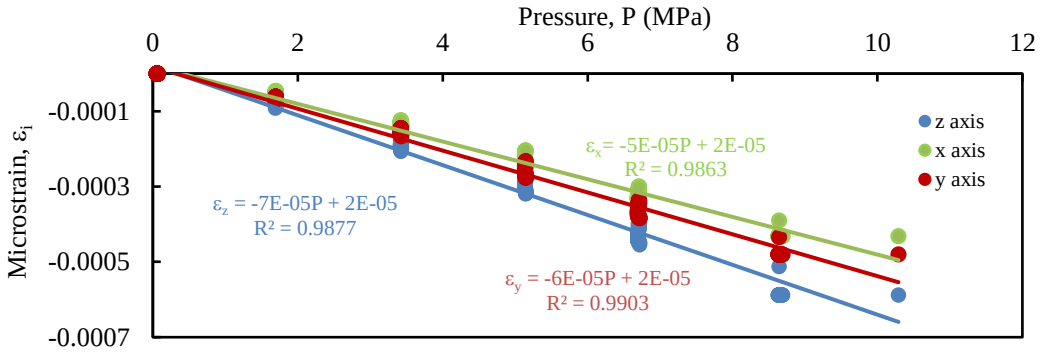

(a) Strain with helium injection for SJ coal.

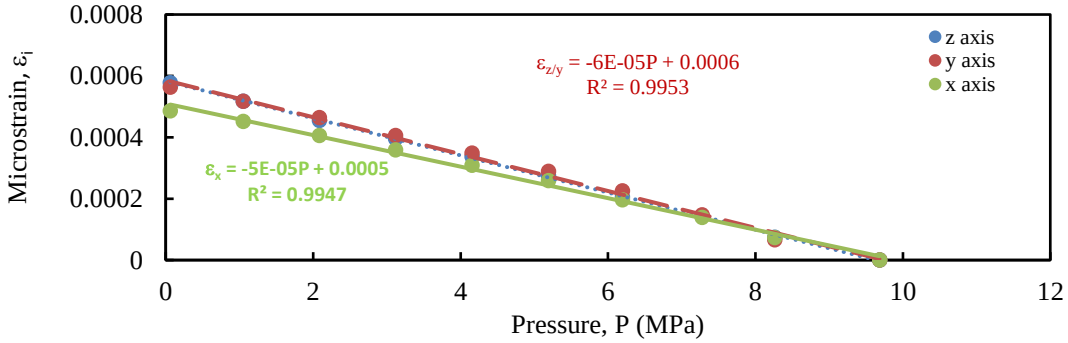

(b) Strain with helium depletion for SS coal.

Figure 5.2 Unconstrained matrix experiment for coal types using helium. (a) SJ coal, (b) SS coal.

Figs. 5.3(a-b) show the results of the unconstrained drained experiment for the coal types with methane depletion. For methane, the volume of solid coal decreased with depletion due to the dominant effect of sorption-induced matrix shrinkage (Durucan et al., 2009; Gorucu et al., 2007; Harpalani and Schraufnagel, 1990; Levine, 1996; Liu and Harpalani, 2013a; Pan and Connell, 2011; Siriwardane et al., 2009).

For permeability experiments, the coal sample was initially stressed to *in situ* reservoir conditions prior to depletion. For SJ coal, the sample was stressed vertically to 20 MPa and horizontally to 12.8 MPa with an initial pore pressure of 10.2 MPa (Singh, 2014). For of SS Coal, the sample stresses were ~21/14.1 MPa in the vertical/horizontal directions with initial pore pressure of 10.4 MPa (Soni, 2017). Gas was then depleted in a stepwise manner for declining pressure, recording the strain and stresses continuously, and measuring the flowrate for each step after attaining equilibrium. Using the flowrate, permeability was calculated for each step, thus establishing the pressure-dependent-permeability trend for the entire depletion. Throughout the experiment, uniaxial strain condition was maintained, that is, the horizontal strain was zero and vertical stress was maintained constant.

In order to compensate for the horizontal strain associated with matrix shrinkage, the horizontal stress was adjusted throughout the experiment. The pressure-dependent-permeability or constrained, drained experiment was conducted for both helium (non-sorptive) and methane (sorptive). The relevant experimental statistics for the pressure-dependent-permeability experiments for helium and methane depletion are presented in Table 5.3. The results showing the change in horizontal stress and vertical strain with helium depletion for the PDK experiments are shown in Figures 5.4 and 5.5.

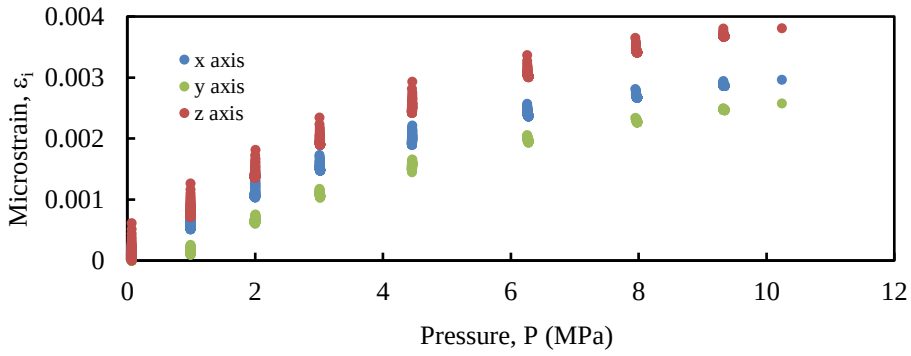

(a) Strains with methane injection for SJ-coal.

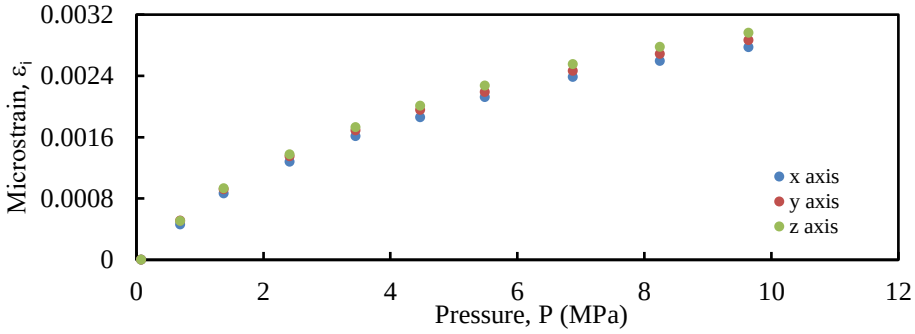

(b) Strains with methane injection for SS-coal.

Figure 5.3 Unconstrained matrix experiment for coal types. (a) SJ coal, (b) SS coal.

Table 5.3 Relevant data for pressure-dependent-permeability experiments.

Relevant statistics for pressure-dependent-permeability for helium depletion		
Sample	SJ Coal(Singh, 2014)	SS Coal(Soni, 2017)
Parameters	Range	Range
Pressure (MPa)	10.2 - 0.7 Step size: 2 MPa	10.7 - 0.8 Step size: 1.7 MPa
Vertical stress (MPa)	20.0 - 19.9	20.9 – 20.9
Horizontal stress (MPa)	12.8 - 7.5	14.1 - 8.2
Permeability Ratio (k/k_o)	1 - 0.13	1 - 0.02
Relevant statistics for pressure-dependent-permeability for methane depletion		
Sample	SJ Coal	SS Coal
Parameters	Range	Range
Pressure (MPa)	10.4 - 0.5 Step size: 10.8 - 6 MPa: 1 MPa 6 - 0.6 MPa: 0.3 MPa	9.8 - 0.8 MPa Step size: 1 MPa
Vertical stress (MPa)	20.0 – 19.8	20.7 – 20.7
Horizontal stress (MPa)	12.7 - 1.2	14 - 1.8
k/k_0	1 - 421	1 - 12

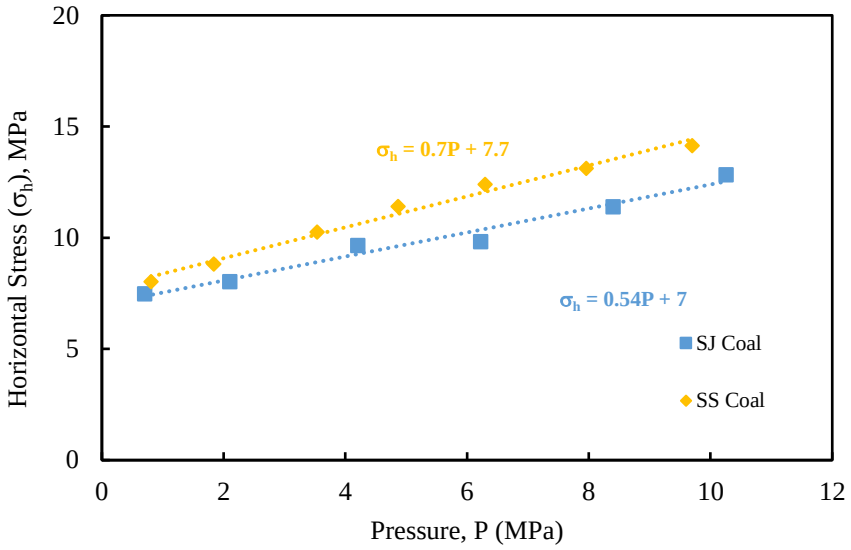

Figure 5.4 Horizontal stress variation with helium depletion.

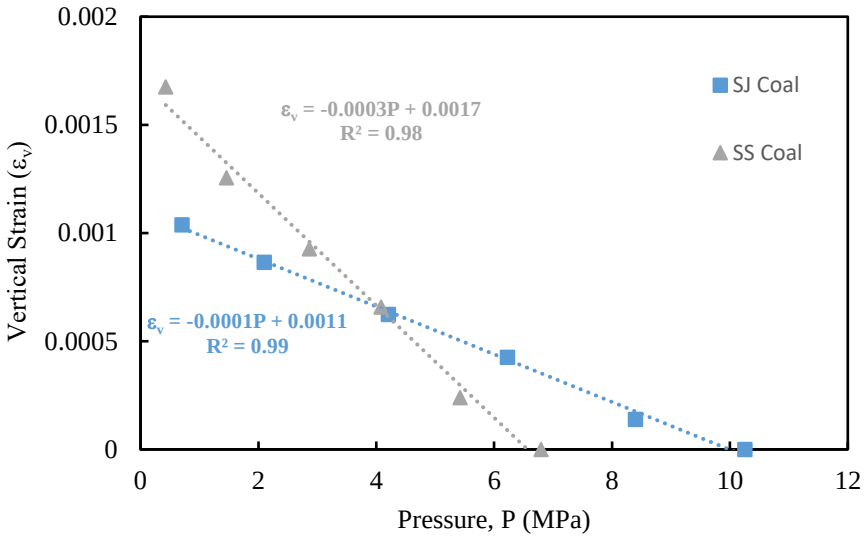

Figure 5.5 Vertical strain with helium depletion.

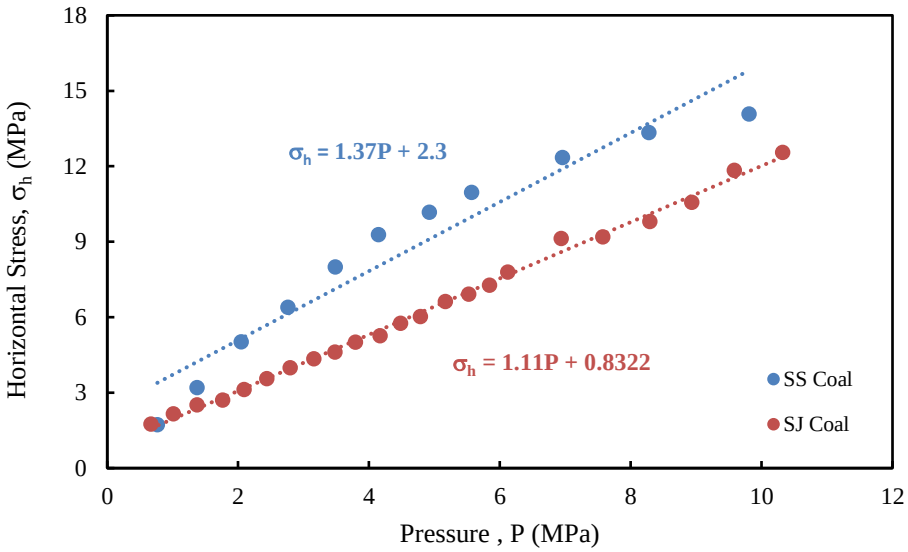

Figure 5.6 Horizontal stress variation with methane depletion.

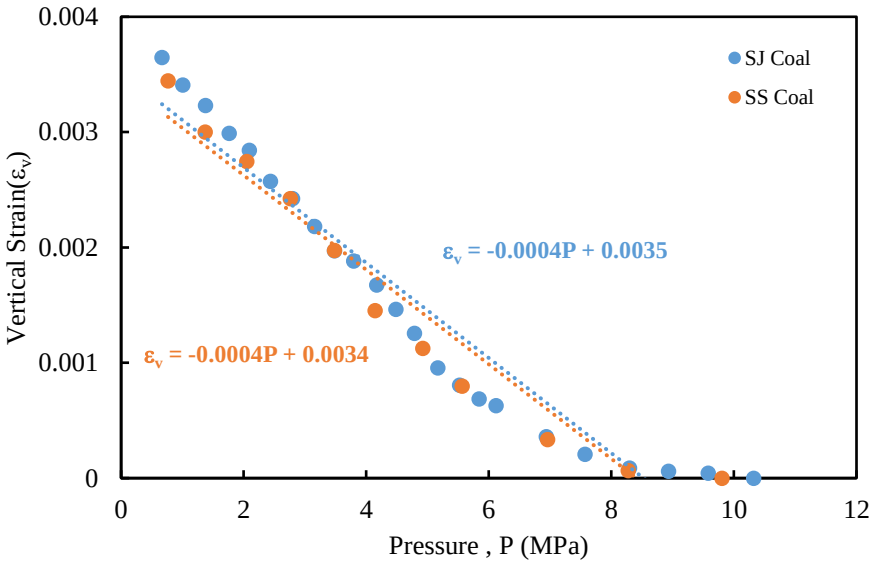

Figure 5.7 Vertical strain with methane depletion.

5.4 Analysis

This paper is concerned primarily with the definition of anisotropic Biot's coefficient for sorptive, transversely isotropic media, like coals and shales. The anisotropic Biot's coefficient was derived as Equations (5.12 & 5.13), as presented in Section 5.2.5. The terms in the two equations are a combination of terms that are required at the scales of matrix and bulk.

The terms at matrix scale are marked with subscript "m", for example, Biot's-like

coefficient defined by Espinoza et al. (2013). The Biot's-like coefficient is a parameter that was introduced by Brochard (Brochard et al., 2012). It can be obtained using the adsorption isotherm and unconstrained experiment results for methane or any other sorptive gases. It depends on the sorption characteristics, mechanical properties and pore structure of the microporous media. Determination of Biot's-like coefficient is explained in more detail in Section 5.4.1.1. All other parameters must be estimated at the scale of bulk rock. These were obtained from the pressure-dependent-permeability results. The anisotropic Biot's coefficient for different coal types is presented in section 5.4.2. We first begin to determine the matrix scale parameters required in the Equation (5.12 & 5.13).

5.4.1. Matrix Scale Parameter Estimation

Two matrix scale parameters have to be determined for estimation of Biot's coefficient using Equations (5.12 & 5.13). These parameters are Biot's like coefficient - a matrix scale parameter - and the second is the matrix scale elastic moduli.

5.4.1.1. Determination of Biot's-like Coefficient

In order to determine the Biot's-like coefficient, results of the unconstrained hydrostatic (flooding) experiment were used. The set of equations presented as Equation (5.9) is simplified, given that external stresses were equal to pore pressure, as:

$$\sigma_1 = \sigma_2 = -p = (C_{11} + C_{12})\varepsilon_{11} + C_{13}\varepsilon_{33} - s_m^{a1}(p) \quad (5.14)$$

$$\sigma_3 = -p = 2(C_{13}\varepsilon_{11}) + C_{33}\varepsilon_{33} - s_m^{a3}(p) \quad (5.15)$$

Inverting the above compliance matrix to stiffness matrix gives the following:

$$\begin{bmatrix}\varepsilon_{11}\\ \varepsilon_{33}\end{bmatrix} = \begin{bmatrix}\frac{1-\nu_1}{E_1} & \frac{-\nu_3}{E_3}\\ \frac{-23}{E_3} & \frac{1}{E_3}\end{bmatrix}\begin{bmatrix}s_m^{a1}(p)-p\\ s_m^{a3}(p)-p\end{bmatrix} \tag{5.16}$$

Taking the derivative of Equation (5.16) with respect to pressure and inverting the stiffness matrix gives the following:

$$\begin{bmatrix}\frac{ds_m^{a1}(p)}{dp} & -1\\ \frac{ds_m^{a3}(p)}{dp} & -1\end{bmatrix} = \begin{bmatrix}\frac{1-\nu_1}{E_1} & \frac{-\nu_3}{E_3}\\ \frac{-2\nu_3}{E_3} & \frac{1}{E_3}\end{bmatrix}^{-1}\begin{bmatrix}\frac{d\varepsilon_1}{dp}\\ \frac{d\varepsilon_3}{dp}\end{bmatrix} \tag{5.17}$$

The inverse matrix on the right-hand side of the equation can be determined using the results of the helium unconstrained experiment (Figures 5.2(a-b)) and the column matrix can be obtained from the results of the unconstrained methane experiment. The compliance matrix used here is different from that used in Equations (5.12 & 5.13) because Equation (5.16) is defined at the matrix scale, whereas Equations (5.12 & 5.13) use the constants from the compliance matrix, which have been determined for the bulk scale. The first matrix on the right-hand side of Equation (5.17) can be estimated using the data presented in Figures 5.2(a-b). This is further explained in following sub-section.

The column matrix on the right-hand side of the equation is obtained from the results of methane hydrostatic unjacketed/unconstrained experiment (Figures 5.3a-b). Using the results presented in Figures 3(a-b), Biot's-like coefficient was estimated for each coal type. Since Biot's-like coefficient is a pressure-dependent quantity, it can be presented easily as a graph. Figures 5.6 and 5.7 present the Biot's-like coefficient for two coal types as a function of pressure. The figure shows linear as well as non-linear fit for the variation of Biot's-like coefficient to demonstrate that, although the variation of Biot's-like coefficient in our study can be approximated to vary linearly for the pressure ranges in our experiment, it is expected to increase significantly at low pressures and is better represented as a non-linear fit (Espinoza et

al., 2013).

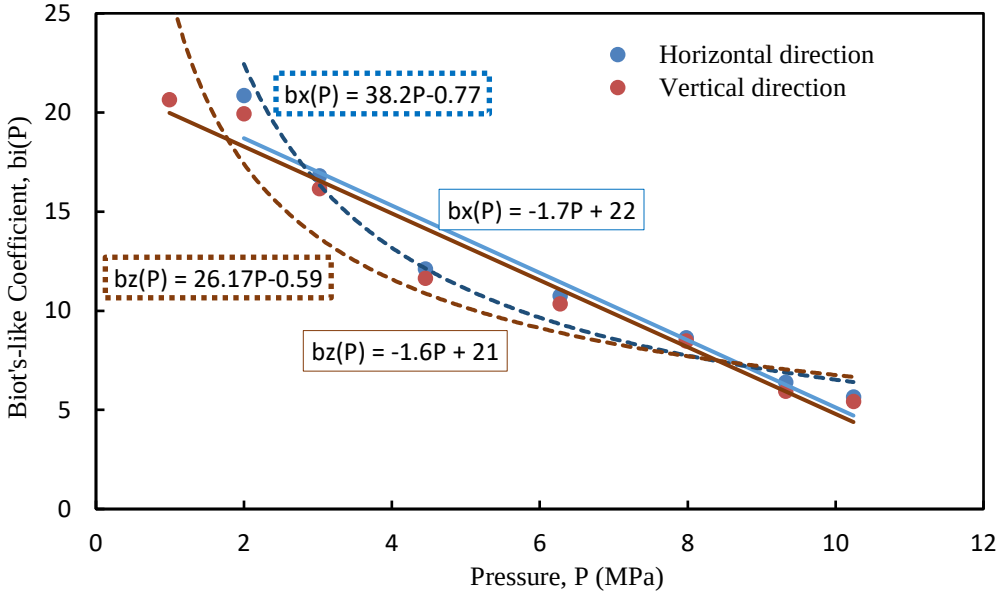

Figure 5.8 Biot-like coefficient in vertical and horizontal direction for SJ coal.

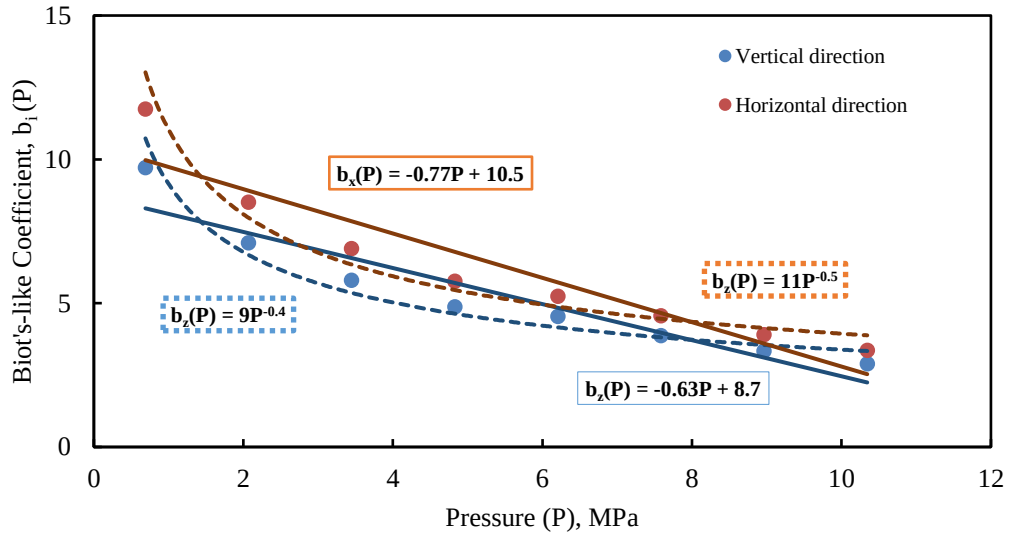

Figure 5.9 Biot-like coefficient in vertical and horizontal directions for SS coal.

5.4.1.2. Determination of Matrix Scale Elastic Moduli

Table 5.4 summarizes the estimated moduli of coal at matrix scale using Equation 5.16 and Figures 5.2(a-b) (with values of v_1 and v_3 assumed), with $s_m^{ai}(p) = 0$ because Figures 5.2(a-b) are for helium. For purpose of computation, the elastic moduli at matrix scale were first

determined using helium results, followed by determination of the Biot's-like coefficient using Figure 5.3(a-b) (methane data) and the estimated matrix scale moduli.

Table 5.4 Estimated moduli of coal at matrix scale. (*assumed values).

	E_1 (GPa)	E_3 (GPa)	ν_1^*	ν_3^*
SJ Coal	8.5	6.0	0.4	0.2
SS Coal	8.6	6.5	0.4	0.2

5.4.2. Bulk Scale Parameters

5.4.2.1. Determination of Bulk Scale Elastic Moduli

Geomechanical testing was carried out to estimate the Young's modulus and Poisson's ratio in the two directions (vertical and horizontal). Table 5.5 shows the results for the two coal types.

Table 5.5 Estimated moduli of coal at bulk scale.

	E_1 (GPa)	E_3 (GPa)	ν_1^*	ν_3^*
SJ Coal	1.70	1.11	0.42	0.22
SS Coal	4.1	2.7	0.42	0.22

5.4.2.2. Determination of Other Bulk Scale Parameters

Other bulk scale parameters, like $\frac{\mathrm{d}\varepsilon_3}{\mathrm{dp}}$ and $\frac{d\sigma_h}{dp}$, required in Equations (5.12 & 5.13), were estimated using the pressure-dependent-permeability results, presented in Figures 5.4 and 5.5. These parameters evaluate the variation of the macroscopic properties like, strains, microscopic deformation and microstructure variation of rock grain contacts with depletion and affect the value of Biot's coefficient.

5.4.3. Determination of Biot's Coefficient for Helium Depletion

The equations, presented once again for reference, are as follows:

$$b_1 = \frac{C_{13}\frac{d\varepsilon_3}{dp} - \frac{d\sigma_h}{dp} - \frac{ds_m^{a1}(p)}{dp}}{1 - \frac{ds_m^{a1}(p)}{dp}} \tag{5.12}$$

$$b_3 = \frac{C_{33}\frac{d\varepsilon_3}{dp} - \frac{ds_m^{a3}(p)}{dp}}{1 - \frac{ds_m^{a1}(p)}{dp}} \tag{5.13}$$

The above Equations can be simplified, given that helium is non-sorbing and the parameter $\frac{ds_m^{a1}(p)}{dp}$ becomes zero, to the following:

$$b_1 = C_{13}\frac{d\varepsilon_3}{dp} - \frac{d\sigma_h}{dp} \tag{5.18}$$

$$b_3 = C_{33}\frac{d\varepsilon_3}{dp} \tag{5.19}$$

Using the values presented in Table 5.3, Figures 5.4 and 5.5, Equations (5.18 & 5.19), b_1 and b_3 were calculated. Table 5.6 summarizes the values of Biot's coefficient estimated in both directions.

Table 5.6 Estimated Biot's coefficient for coal types at bulk scale.

Coal Type	b_1	b_3
SJ Coal	0.83	0.36
SS Coal	0.95	0.85

5.4.4. Pressure/Stress Dependent Biot's Coefficient

Since the bulk scale parameters have been approximated to be linearly dependent on pressure, Equations (5.18 & 5.19) yield constant values for Biot's coefficient in both directions. However, treating the two coefficients as pressure-dependent variables presents Biot's coefficient as a pressure- and stress- dependent parameter. It has been proposed by previous

researchers that elastic moduli changes with variations in effective stress or pressure (Walsh, 1965). Since the experiments were conducted under hydrostatic conditions, this change is expected to be reversible due to negligible friction effect. However, under uniaxial strain condition, there is a deviatoric stress component in the total stress tensor in addition to the hydrostatic component. Hence, there should be slippage of microcracks and treating the values of bulk scale moduli constant throughout the depletion is essentially an approximation (Walsh, 1965).

If these parameters are taken to be pressure-dependent, and estimated by measuring the dynamic moduli changes, the Biot's coefficient would come out to be anisotropic as well as variable with pressure within the sample. This supports the recent studies reported by Ma and Zoback (2016).

5.4.5. Determination of Effective Stress Coefficient for Methane Depletion

Biot's coefficient has been conventionally defined for non-sorbing rocks. Hence, in this paper, effective stress coefficient is defined as a parameter when dealing with sorptive rocks, like coal and shales. The data presented in Tables 5.4 and 5.5, Figure 5.6, 5.7, 5.8 and 5.9 were used in Equations (5.12 & 5.13) to estimate the effective stress coefficient (χ_{sc}). The estimated value of χ_{sc} is a pressure-dependent parameter and is presented for SJ and SS coals in Figures 5.10 and 5.11 respectively.

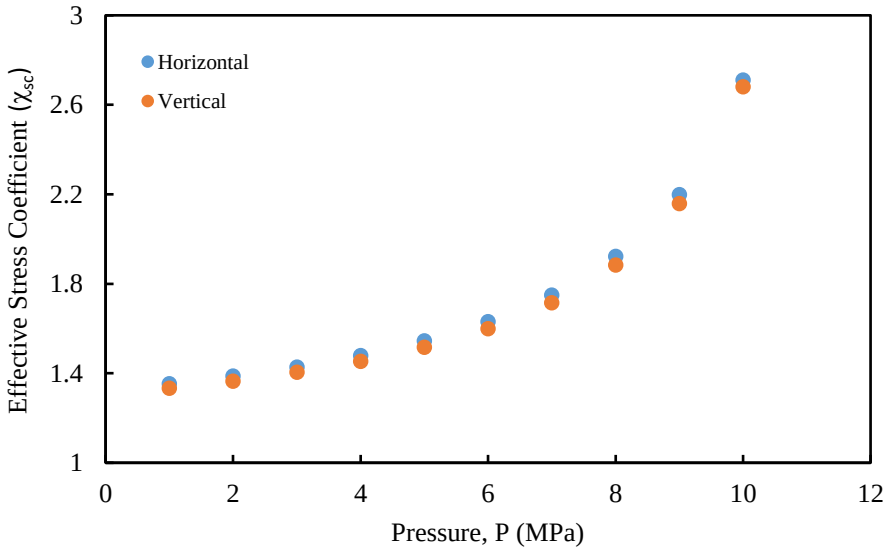

Figure 5.10 Effective stress coefficient with methane depletion for SS coal.

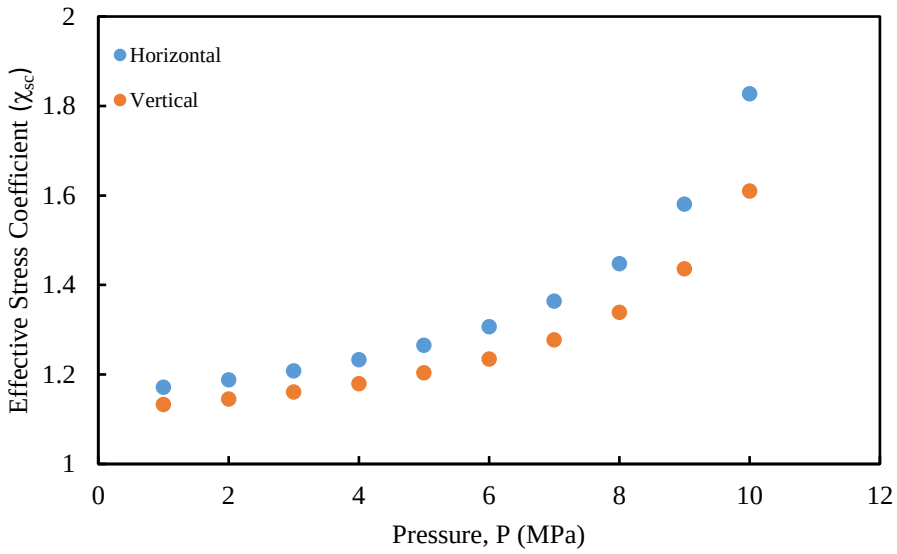

Figure 5.11 Effective stress coefficient with methane depletion for SJM coal.

5.5 Discussion

5.5.1. Discussion of Biot's Coefficient

Biot's coefficients in both vertical and horizontal directions were presented in the analysis section using experimental results. The results of adsorption, unconstrained and constrained experimental work on coal cores helped determine the matrix scale and bulk scale

parameters required for estimation of the Biot's coefficient. Fundamental, linear, poroelastic equations developed for transversely isotropic rocks were used (Espinoza et al., 2014). The uniaxial boundary conditions, together with the constitutive equations used, helped in extracting an expression for Biot's coefficient in the two directions. Since the experimental results (constrained) were for uniaxial boundary condition, this paper is limited to estimating the values of Biot's coefficient in both the directions under uniaxial boundary condition only. A comparative study of variation of Biot's coefficient under different boundary condition would yield further important information about how the boundary conditions affect the microstructure of the rock with depletion.

A closer look at the results presented in Table 5.6 shows that variation of effective stress with pore pressure is not simply the difference between total stress and pore pressure(Terzaghi, 1943). The value of Biot's coefficient estimated for coal varied between 0.83 and 0.95 in the horizontal direction and 0.36 and 0.85 in the vertical direction.

5.5.2. Discussion on Effective Stress Coefficient (χ_{sc})

In Figures 5.8 and 5.9, both coals exhibit similar behavior with depletion. The interesting feature that is consistent in both SJ and SS coals is that the value of the horizontal effective stress coefficient $(\chi_{sc})_h$ is greater than the one for vertical. Both decrease sharply with continued depletion. The value of χ_{sc}, however is greater for SS coal in the beginning than for SJ coal, the trend consistent with the values of Biot's coefficient in Table 5.6. In addition, it is worth mentioning that the value of χ_{sc} never goes below unity during depletion. Furthermore, the values of the coefficient do not vary much at lower pressures. One striking feature is that the anisotropy in the values of χ_{sc} for SJ is larger than SS coal, which is also apparent in the experimental data presented in Figure 5.3(a-b). Finally, the anisotropy in the coefficient values

diminishes at low pressure for both coal types. Hence, it is concluded that, at higher pore pressure and greater penetration of gas in the pores, anisotropy becomes significant. In other words, the anisotropy is due to pore structure of the rock.

5.5.3. Application of The Study

5.5.3.1. Stress Path Determination and In Situ Strength of Rocks

Establishing the stress path of the reservoir with depletion is an important geomechanical exercise, which helps in evaluation of the ongoing macroscopic phenomenon in reservoir like, compaction and failure. This can be done in an octahedral effective stress plane (octahedral effective shear stress σ_{octs} – octahedral effective mean stress σ_{octm}). Since stress path and *in situ* strength of rocks in a reservoir depends on the effective stress, the results of this study incorporating transverse isotropy will be helpful in improved simulation or estimation of both, mean effective stress invariant (I_1) and deviatoric stress invariant (J_2), in a reservoir. Assuming isotropy, these are written as:

$$I_1 = (S_1 - bp) + (S_2 - bp) + (S_3 - bp) \tag{5.20}$$

$$J_2{}^{1/2} = \frac{1}{6}[(S_1 - S_2)^2 + (S_2 - S_3)^2 + (S_3 - S_1)^2] \tag{5.21}$$

It can be seen that I_1 is affected by the values of Biot's coefficient for isotropy (all *b*s having same value), but deviatoric stress is not. Since it is believed that sedimentary deposits, like coal and shale, are transversely isotropic media, different Biot's coefficients should be considered in the vertical and horizontal directions. Treating such rocks as isotropic can yield inaccurate results when shear stress in reservoirs causes significant dilation and requires improved modeling/ simulation. Hence, it is concluded that isotropy underestimates the shear stress in reservoirs. Such underestimation of shear stress can affect the results of shear-induced failure in sorptive reservoirs. Sudden shear failures have been reported to cause permeability

boost or drop in coalbed methane reservoirs(Espinoza et al., 2015; Okotie and Moore, 2011; Saurabh et al., 2016).

5.5.3.2. Effective Stress Coefficient

Since coal and shales are sorptive rocks, the concept of Biot's coefficient fails. Hence, this paper has introduced the concept of effective stress coefficient. Furthermore, it is seen that effective stress coefficient is greater than one and it decreases with depletion. The implication of this can be significant effective stress increase in vertical direction with depletion, and coupled with decrease in effective horizontal stress, can result in significant stress anisotropy leading to shear failure in coal as reported by Singh(2014) and Saurabh et al.(2016).

5.5.3.3. Sudden Permeability Increase

The results support that there can be severe stress anisotropy with depletion and can cause shear failure, which has been reported to cause sudden increase in permeability of coal with depletion (Saurabh et al., 2016).

5.6 Conclusions

The review and modeling exercise suggest that Biot's coefficient values are not isotropic parameters and different values of Biot's coefficient should be used for horizontal and vertical directions for a transversely isotropic rock. This would lead to improved simulation of all poroelastic properties and properties dependent on effective stress like, compressibility, permeability and failure properties.

The value of Biot's coefficient calculated after including the sorption behavior of coal results in somewhat of a controversy given that the value comes out to be greater than one. Hence, the term *effective stress coefficient* (χ_{sc}) is introduced for the coefficient. It is important to note that the value of this χ_{sc} decreases with depletion and its value approaches one at complete

depletion. Implication of this is that there can be significant increase in vertical effective stress and reduction in horizontal effective stress leading to stress anisotropy and ultimately failure. Such failure has been held responsible for sudden increases in the permeability in several areas in the San Juan basin.

The estimated values of Biot's coefficient and χ_{sc} (effective stress coefficient) are anisotropic, with the value in the horizontal direction being higher than that in the vertical direction. According to the qualitative theory presented, higher Biot's coefficient in horizontal direction suggests higher porosity or, smaller contact between grains in the horizontal direction as a result of swelling of grains on the surface of cleats. This swelling decreases with depletion and the contact area increases, closing the gaps in the cleats of coal and resulting in an overall decrease in the effective stress coefficient. Similar argument also goes for the vertical direction. However, in vertical direction, grain contact is higher, that is, grains are well compacted under vertical stress, explaining the lower values of Biot's coefficient as well as effective stress coefficient.

The model proposed in this paper depends on both matrix scale parameters and fractured scale parameters. This points to the scale dependent behavior of Biot's coefficient for rocks, in accordance with the concept of scaling Biot's coefficient to reservoir scale from sample scale, as presented by Nikoosokhan et al.(2012). The Biot's coefficient values presented in this paper are on the scale of laboratory sample and these can be scaled up to reservoir scale, as proposed earlier by Nikoosokhan et al. (2012).

The upscaling and anisotropy of Biot's coefficient value points to the dependence of its value on the cleat behavior, or pore structure, in case of coal. Since coal exhibits anisotropy in terms of pore structure and scale-dependent heterogeneity, values of Biot's coefficient are

different in vertical and horizontal directions and these would vary with scale. In fact, for field condition, due to anisotropy of butt and face cleats, there may be a total anisotropy of Biot's coefficient. Hence, three different values of Biot's coefficient or χ_{sc} (effective stress coefficient) should be used for simulation work. In our experimental results and modeling exercise, the total anisotropic behavior was approximated to relatively simpler transversely isotropic behavior.

CHAPTER 6

SUMMARY AND FUTURE RESEARCH

6.1 Summary of Work

This dissertation was aimed at establishing the variations in permeability and effective stress with depletion in unconventional reservoirs, especially in transversely isotropic reservoirs like, coal and shale. With depletion of shallow gas and oil reservoirs, the unexploited reservoirs are the ones that are deeper and under higher stressed conditions. Typically, such reservoirs have very low permeability and are very stress sensitive. The study presented in this dissertation paves the path to unlock such deeper and low permeability reservoirs. The objectives achieved in this dissertation are:

1. Transverse isotropy of rock was characterized, and an experimental technique was developed to measure the anisotropy of such rocks. Based on the results of the study, trend in the variation of anisotropy with depletion was established.
2. The permeability model for transversely isotropic rocks, validated for coals, was developed for the elastic zone. A theory of sudden uptick of permeability due to shear failure of coal because of severe matrix shrinkage and anisotropic stress loading was developed.
3. A generalized stress-dependent-permeability model for transversely isotropic rocks, validated for three different coal types, was developed for elastic, dilatant and inelastic zone.
4. An effective stress law for transversely isotropic rocks was developed. It was validated for two different coal types. The effective stress law, developed for Barnett shale, was also studied and presented at the Sixth Poromechanics conference.

6.2 Future Research and Preliminary Results

In addition to the work presented above, another study was carried out on tighter coals. Three sets of experiments, sorption, shrinkage/ swelling and pressure dependent permeability of San Juan coal, outside the fairway region, were completed. The results are presented below:

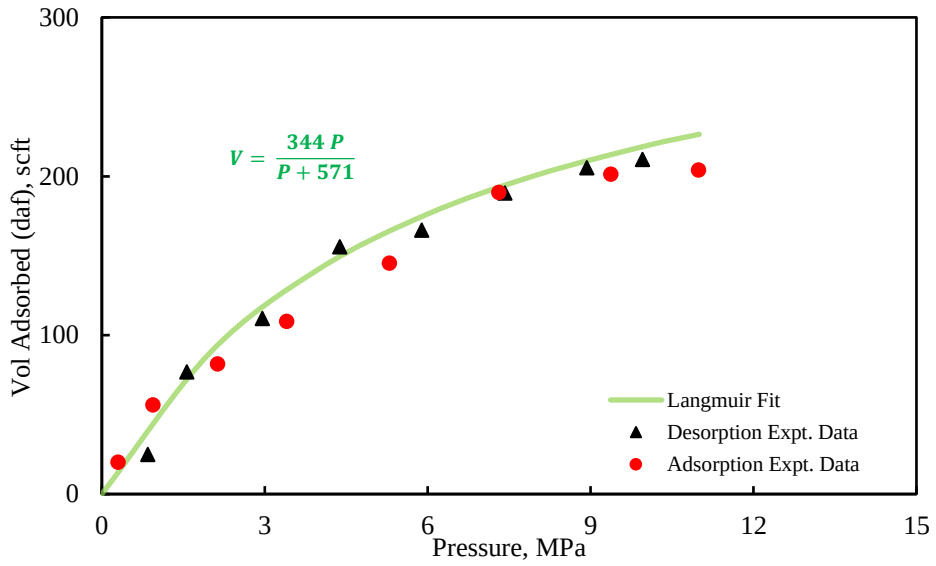

Figure 6.1 Sorption behavior of San Juan coal, south of fairway.

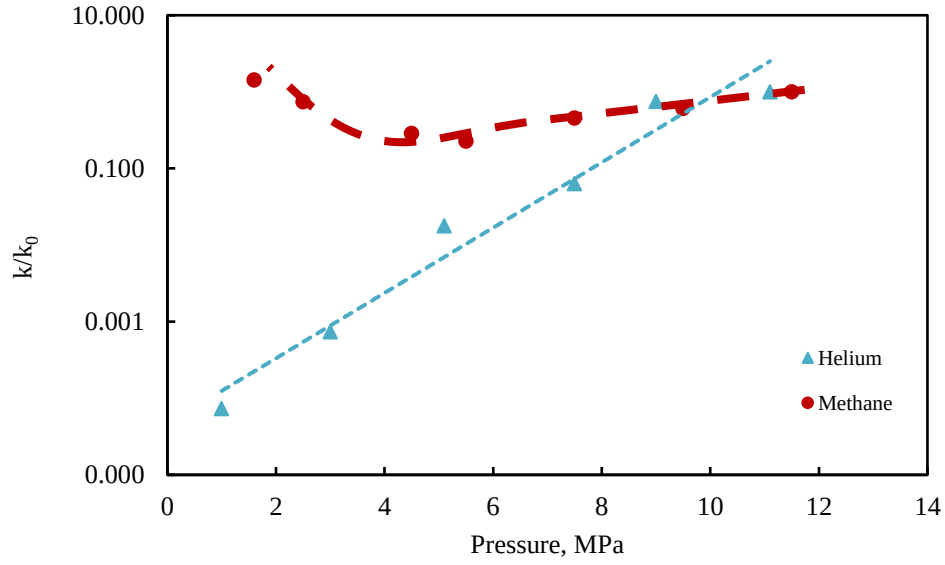

Figure 6.2 Pressure-dependent-permeability for helium and methane depletion for San Juan coal, south of fairway.

The results are substantially different and the wells in the area have performed poorly so far. The analysis presented in the dissertation can be translated to future studies when exploring the factors resulting in poor performance of these reservoirs and developing possible technologies which can unlock deeper/tighter reservoirs.

REFERENCES

Alejano, L.R., Alonso, E., 2005. Considerations of the dilatancy angle in rocks and rock masses. Int. J. Rock Mech. Min. Sci. 42, 481–507. https://doi.org/10.1016/j.ijrmms.2005.01.003

Bae, J.S., Bhatia, S.K., Rudolph, V., Massarotto, P., 2009. Pore accessibility of methane and carbon dioxide in coals. Energy and Fuels 23, 3319–3327. https://doi.org/10.1021/ef900084b

Bai, M., Meng, F., Elsworth, D., Roegiers, J.-C., 1999. Analysis of Stress-dependent Permeability in Nonorthogonal Flow and Deformation Fields. Rock Mech. Rock Eng. 32, 195–219. https://doi.org/10.1007/s006030050032

Bai, M., Meng, F., Elsworth, D., Zaman, Z., Roegiers, J.C., 1997. Numerical modeling of stress-dependent permeability. Int. J. rock Mech. Min. Sci. Geomech. Abstr. 34, 446. https://doi.org/10.1016/S1365-1609(97)00056-7

Balan, H.O., Gumrah, F., 2009. Assessment of shrinkage-swelling influences in coal seams using rank-dependent physical coal properties. Int. J. Coal Geol. 77, 203–213. https://doi.org/10.1016/j.coal.2008.09.014

Biot, M.A., 1941. General theory of three-dimensional consolidation. J. Appl. Phys. 12, 155–164. https://doi.org/10.1063/1.1712886

Bishop, A.W., 1954. The Use of Pore-Pressure Coefficients in Practice. Géotechnique 4, 148–152. https://doi.org/10.1680/geot.1954.4.4.148

Bourbié, T., Coussy, O., 1987. Acoustics of Porous Media, Institut français du pétrole publications. Editions Technip.

Brochard, L., Vandamme, M., Pellenq, R.J.M., 2012. Poromechanics of microporous media. J. Mech. Phys. Solids 60, 606–622. https://doi.org/10.1016/j.jmps.2012.01.001

Busch, A., Gensterblum, Y., Krooss, B.M., Littke, R., 2004. Methane and carbon dioxide

adsorption-diffusion experiments on coal: Upscaling and modeling. Int. J. Coal Geol. https://doi.org/10.1016/j.coal.2004.05.002

Ceglarska-Stefańska, G., Zarbska, K., 2002. The competitive sorption of CO2 and CH4 with regard to the release of methane from coal. Fuel Process. Technol. 77–78, 423–429. doi:10.1016/S0378-3820(02)00093-0

Carroll, M.M., 1979. An effective stress law for anisotropic elastic deformation. J. Geophys. Res. Solid Earth 84, 7510–7512. https://doi.org/10.1029/JB084iB13p07510

Chen, D., Pan, Z., Shi, J.Q., Si, G., Ye, Z., Zhang, J., 2016. A novel approach for modelling coal permeability during transition from elastic to post-failure state using a modified logistic growth function. Int. J. Coal Geol. 163, 132–139. doi:10.1016/j.coal.2016.07.007

Christensen, N.I., Wang, H.F., 1985. The influence of pore pressure and confining pressure on dynamic elastic properties of Berea Sandstone. Geophysics 50, 207 LP – 213.

Chu, E., 1995. Generalization of Hill's 1979 anisotropic yield criteria. Journals of Materials Processing Technology. 50, 207-215

Coussy, O., 2003a. Poromechanics, Handbook of Agricultural Economics. https://doi.org/10.1002/0470092718

Coussy, O., 2003b. Problems of Poroelasticity, in: Poromechanics. John Wiley & Sons, Ltd, pp. 113–150. https://doi.org/10.1002/0470092718.ch5

Cui, X., Bustin, R.M., 2005. Volumetric strain associated with methane desorption and its impact on coalbed gas production from deep coal seams. Am. Assoc. Pet. Geol. Bull. 89, 1181 LP-1202.

Day, S., Fry, R., Sakurovs, R., 2008. Swelling of Australian coals in supercritical CO2. Int. J. Coal Geol. 74, 41–52. https://doi.org/10.1016/j.coal.2007.09.006

Drucker, D.C., 1957. A Definition of Stable Inelastic Material. J. Appl. Mech. 26, 101–106. https://doi.org/10.2307/1146143

Drucker, D.C., Prager, W., 1952. Soil Mechanics and Plasticity Analysis of Limit Design. Q. Appl. Math. 10, 157–165.

Durucan, S., Ahsanb, M., Shia, J.Q., 2009. Matrix shrinkage and swelling characteristics of European coals, in: Energy Procedia. pp. 3055–3062. https://doi.org/10.1016/j.egypro.2009.02.084

Eberhardt, E., 2012. The Hoek-Brown failure criterion. Rock Mech. Rock Eng. 45, 981–988. https://doi.org/10.1007/s00603-012-0276-4

EIA (Coal bed methane), 2015. (EIA) US Information Administration: https://www.eia.gov/dnav/ng/NG_ENR_COALBED_DCU_NUS_A.htm. (Accessed – 05/ 04/2016)

Espinoza, D.N., Pereira, J.M., Vandamme, M., Dangla, P., Vidal-Gilbert, S., 2015. Desorption-induced shear failure of coal bed seams during gas depletion. Int. J. Coal Geol. https://doi.org/10.1016/j.coal.2014.10.016

Espinoza, D.N., Vandamme, M., Dangla, P., Pereira, J.M., Vidal-Gilbert, S., 2013. A transverse isotropic model for microporous solids: Application to coal matrix adsorption and swelling. J. Geophys. Res. Solid Earth 118, 6113–6123. https://doi.org/10.1002/2013JB010337

Espinoza, D.N., Vandamme, M., Pereira, J.M., Dangla, P., Vidal-Gilbert, S., 2014. Measurement and modeling of adsorptive-poromechanical properties of bituminous coal cores exposed to CO2: Adsorption, swelling strains, swelling stresses and impact on fracture permeability. Int. J. Coal Geol. 134–135, 80–95.

https://doi.org/10.1016/j.coal.2014.09.010

Evans, I. and Pomeroy, C. D., 1966. The strength, fracture and workability of coal: a monograph on basic work on coal winning carried out by the Mining Research Establishment. National Coal Board. 1st ed. Pergamon Press Ltd

Fatt, 1959. The Biot-Willis Elastic Coefficients for a Sandstone. J. Appl. Mech. 26, 296–297.

Franquet, J.A., Abass, H.H., 1999. Experimental evaluation of Biot's poroelastic parameterThree different methods

Geertsma, J., 1957. The Effect of Fluid Pressure Decline on V olumetric Changes of Porous Rocks. Soc. Pet. Eng. 210, 10.

Gorucu, F.B., Jikich, S.A., Bromhal, G.S., Sams, W.N., Ertekin, T., Smith, D.H., 2007. Effects of Matrix Shrinkage and Swelling on the Economics of Enhanced-Coalbed-Methane Production and CO2 Sequestration in Coal. SPE Reserv. Eval. Eng. SPE 97963, 382–392. https://doi.org/10.2118/97963-pa

Harpalani, S., Chen, G., 1997. Influence of gas production induced volumetric strain on permeability of coal. Geotech. Geol. Eng. 15, 303–325. https://doi.org/10.1007/bf00880711

Harpalani, S., Schraufnagel, R.A., 1990. Shrinkage of coal matrix with release of gas and its impact on permeability of coal. Fuel 69, 551–556. https://doi.org/10.1016/0016-2361(90)90137-F

He, L., Melnichenko, Y.B., Mastalerz, M., Sakurovs, R., Radlinski, A.P., Blach, T., 2012. Pore accessibility by methane and carbon dioxide in coal as determined by neutron scattering. Energy and Fuels 26, 1975–1983. https://doi.org/10.1021/ef201704t

Hillis, R. R., 2001. Coupled changes in pore pressure and stress in oil fields and sedimentary

basins, Pet. Geosci.71, 419-425

Hol, S., Spiers, C.J., 2012. Competition between adsorption-induced swelling and elastic compression of coal at CO 2 pressures up to 100 MPa. J. Mech. Phys. Solids 60, 1862–1882. https://doi.org/10.1016/j.jmps.2012.06.012

Hornby, B., 1996. An experimental investigation of effective stress principles for sedimentary rocks, in: SEG Technical Program Expanded Abstracts 1996, SEG Technical Program Expanded Abstracts. Society of Exploration Geophysicists, pp. 1707–1710. https://doi.org/doi:10.1190/1.1826458

Hudson, J.A., 1981. Wave speeds and attenuation of elastic waves in material containing cracks. Geophys. J. R. Astron. Soc. 64, 133–150. https://doi.org/10.1111/j.1365-246X.1981.tb02662.x

Karacan, C.Ö., 2007. Swelling-induced volumetric strains internal to a stressed coal associated with CO2 sorption. Int. J. Coal Geol. 72, 209–220. doi:10.1016/j.coal.2007.01.003

Kowalczyk, P., Ciach, A., Neimark, A. V., 2008. Adsorption-induced deformation of microporous carbons: Pore size distribution effect. Langmuir 24, 6603–6608. doi:10.1021/la800406c

Krooss, B.M., Van Bergen, F., Gensterblum, Y., Siemons, N., Pagnier, H.J.M., David, P., 2002. High-pressure methane and carbon dioxide adsorption on dry and moisture-equilibrated Pennsylvanian coals. Int. J. Coal Geol. https://doi.org/10.1016/S0166-5162(02)00078-2

Laubach, S.E., Marrett, R.A., Olson, I.E., Scott, A.R., 1998. Characteristics and origins of coal cleat: a review. Int. J. Coal Geol. 35, 175–207. doi:10.1016/S0166-5162(97)00012-8

Levine, J.R., 1996. Model study of the influence of matrix shrinkage on absolute permeability of coal bed reservoirs. Geol. Soc. London, Spec. Publ. 109, 197–212.

https://doi.org/10.1144/GSL.SP.1996.109.01.14

Lin, W., Kovscek, A.R., 2014. Gas Sorption and the Consequent Volumetric and Permeability Change of Coal I: Experimental. Transp. Porous Media 105, 371–389. doi:10.1007/s11242-014-0373-9

Liu, C., Huang, Y., Stout, M. G., 1997. On the asymmetric yield surface of plastically orthotropic materials: A phenomenological study. Acta Materialia. 45(6), 2397-2406

Liu, J., Chen, Z., Elsworth, D., Miao, X., Mao, X., 2011. Evolution of coal permeability from stress-controlled to displacement-controlled swelling conditions. Fuel 90, 2987–2997. doi:10.1016/j.fuel.2011.04.032

Liu, S, Harpalani, S., 2014. Compressibility of sorptive porous media: Part 1. Background and theory. Am. Assoc. Pet. Geol. Bull. 98, 1761–1772. https://doi.org/Doi 10.1306/03241413133

Liu, Shimin, Harpalani, S., 2014. Evaluation of in situ stress changes with gas depletion of coalbed methane reservoirs. J. Geophys. Res. B Solid Earth 119, 6263–6276. https://doi.org/10.1002/2014JB011228

Liu, S., Harpalani, S., 2013a. A new theoretical approach to model sorption-induced coal shrinkage or swelling. Am. Assoc. Pet. Geol. Bull. 97, 1033–1049. https://doi.org/10.130/12181212061

Liu, S., Harpalani, S., 2013b. Permeability prediction of coalbed methane reservoirs during primary depletion. Int. J. Coal Geol. 113, 1–10. https://doi.org/10.1016/j.coal.2013.03.010

Liu, S., Harpalani, S., Pillalamarry, M., 2012. Laboratory measurement and modeling of coal permeability with continued methane production: Part 2 - Modeling results. Fuel 94, 117–

124. https://doi.org/10.1016/j.fuel.2011.10.053

Liu, S., Wang, Y., Harpalani, S., 2016. Anisotropy characteristics of coal shrinkage/swelling and its impact on coal permeability evolution with CO2injection. Greenh. Gases Sci. Technol. 6, 615–632. https://doi.org/10.1002/ghg.1592

Liu, Y., Cao, S., Li, Y., Wang, J., Guo, P., Xu, J., Bai, Y., 2010. Experimental study of swelling deformation effect of coal induced by gas adsorption. Yanshilixue Yu Gongcheng Xuebao/Chinese J. Rock Mech. Eng. 29.

Lu, M., Connell, L., 2016. Coal failure during primary and enhanced coalbed methane production - Theory and approximate analyses. Int. J. Coal Geol. 154–155, 275–285. https://doi.org/10.1016/j.coal.2016.01.008

Ma, Q., Harpalani, S., Liu, S., 2011. A simplified permeability model for coalbed methane reservoirs based on matchstick strain and constant volume theory. Int. J. Coal Geol. 85, 43–48. https://doi.org/10.1016/j.coal.2010.09.007

Ma, X., Zoback, M.D., 2016. Laboratory investigation on effective stress in Middle Bakken: implications on poroelastic stress changes due to depletion and injection, in: 50th US Rock Mechanics/Geomechanics Symposium. American Rock Mechanics Association.

Mazumder, S., Karnik, A., Wolf, K.-H., 2006. Swelling of Coal in Response to CO2 Sequestration for ECBM and Its Effect on Fracture Permeability. SPE J. 11. https://doi.org/10.2118/97754-PA

Mazumder, S., Wolf, K.H., 2008. Differential swelling and permeability change of coal in response to CO2 injection for ECBM. Int. J. Coal Geol. 74, 123–138. https://doi.org/10.1016/j.coal.2007.11.001

Melnichenko, Y.B., He, L., Sakurovs, R., Kholodenko, A.L., Blach, T., Mastalerz, M., Radliński,

A.P., Cheng, G., Mildner, D.F.R., 2012. Accessibility of pores in coal to methane and carbon dioxide. Fuel 91, 200–208. https://doi.org/10.1016/j.fuel.2011.06.026

Mitra, A., Harpalani, S., Liu, S., 2012. Laboratory measurement and modeling of coal permeability with continued methane production: part 1 laboratory results. Fuel. 94, 110–116

Moore, R., Palmer, I., Higgs, N., 2014. Anisotropic Model For Permeability Change In Coalbed Methane Wells, in: Society of Petroleum Engineers. Society of Petroleum Engineers, Denver. https://doi.org/10.2118/169592-MS

Nikoosokhan, S., Vandamme, M., Dangla, P., 2012. A Poromechanical Model for Coal Seams Injected with Carbon Dioxide: From an Isotherm of Adsorption to a Swelling of the Reservoir. Oil Gas Sci. Technol. – Rev. d'IFP Energies Nouv. 67, 777–786. https://doi.org/10.2516/ogst/2012048

Nur, A., Byerlee, J.D., 1971. An exact effective stress law for elastic deformation of rock with fluids. J. Geophys. Res. 76, 6414. https://doi.org/10.1029/JB076i026p06414

Nur, A., Simmons, G., 1969. Stress-induced velocity anisotropy in rock: An experimental study. J. Geophys. Res. 74, 6667. https://doi.org/10.1029/JB074i027p06667

Okotie, V.U., Moore, R.L., 2011. Well-production challenges and solutions in a mature, very-low-pressure coalbed-methane reservoir. SPE Prod. Oper. 26, 149–161. https://doi.org/10.2118/107705-MS

Palmer, I., 2009. Permeability changes in coal: Analytical modeling. Int. J. Coal Geol. 77, 119–126. https://doi.org/10.1016/j.coal.2008.09.006

Palmer, I., Mavor, M.J., Gunter, B., 2007. Permeability changes in coal seams during production and injection, in: International Coalbed Methane Symposium. University of Alabama,

Tuscaloosa, p. 20.

Palmer, I., Mansoori, J., 1996. How permeability depends on stress and pore pressure in coalbeds: a new model. In the proceedings of SPE Annual Technical Conference and Exhibition. Society of Petroleum Engineers.539-544

Palmer, I., Mansoori, J., 1998. How Permeability Depends on Stress and Pore Pressure in Coalbeds: A New Model. SPE Reserv. Eval. Eng. 1, 539–544. doi:10.2118/52607-PA

Pan, Z., Connell, L.D., 2012. Modelling permeability for coal reservoirs: A review of analytical models and testing data. Int. J. Coal Geol. https://doi.org/10.1016/j.coal.2011.12.009

Pan, Z., Connell, L.D., 2011. Modelling of anisotropic coal swelling and its impact on permeability behaviour for primary and enhanced coalbed methane recovery. Int. J. Coal Geol. 85, 257–267. https://doi.org/10.1016/j.coal.2010.12.003

Pan, Z., Connell, L.D., 2007. A theoretical model for gas adsorption-induced coal swelling. Int. J. Coal Geol. 69, 243–252. doi:10.1016/j.coal.2006.04.006

Pijaudier-Cabot, G., Vermorel, R., Miqueu, C., Mendiboure, B., 2011. Revisiting poromechanics in the context of microporous materials. Comptes Rendus - Mec. 339, 770–778. doi:10.1016/j.crme.2011.09.003

Reiss, L.H., 1980. The Reservoir Engineering Aspects of Fractured Formations. Gulf Publishing Company., Houston, Texas.

Sarker, R., Batzle, M., 2008. Effective stress coefficient in shales and its applicability to Eaton's Equation Lead. Edge 27, 798. https://doi.org/10.1190/1.2944167

Saurabh, S., Harpalani, S., 2018. The effective stress law for stress-sensitive transversely isotropic rocks. Int. J. Rock Mech. Min. Sci. 101, 69–77. https://doi.org/10.1016/J.IJRMMS.2017.11.015

Saurabh, S., Harpalani, S., Singh, V.K., 2016. Implications of stress re-distribution and rock failure with continued gas depletion in coalbed methane reservoirs. Int. J. Coal Geol. 162, 183–192. https://doi.org/10.1016/j.coal.2016.06.006

Sawyer, W.K., Paul, G.W., Schraufnagel, R.A., 1990. Development And Application Of A 3-D Coalbed Simulator, in: International Technical Meeting Jointly Hosted by The Petroleum Society of CIM and The Society of Petroleum Engineers. Petroleum Society of Canada, Calgary. doi:10.2118/90-119

Sayers, C.M., 1994. The elastic anisotrophy of shales. J. Geophys. Res. 99, 767. https://doi.org/10.1029/93JB02579

Seidle, J.R., Huitt, L.G., 1995. Experimental Measurement of Coal Matrix Shrinkage Due to Gas Desorption and Implications for Cleat Permeability Increases, in: SPE International Meeting on Petroleum Engineering. Society of Petroleum Engineers. https://doi.org/10.2118/30010-MS

Shovkun, I., Espinoza, D.N., 2017. Coupled fluid flow-geomechanics simulation in stress-sensitive coal and shale reservoirs: Impact of desorption-induced stresses, shear failure, and fines migration. Fuel 195, 260–272. https://doi.org/10.1016/j.fuel.2017.01.057

Shi, J.-Q., Durucan, S., 2010. Exponential Growth in San Juan Basin Fruitland Coalbed Permeability With Reservoir Drawdown: Model Match and New Insights. SPE Reserv. Eval. Eng. 13, 914–925. doi:10.2118/123206-PA

Shi, J.-Q., Durucan, S., 2005. A model for changes in coalbed permeability during primary and enhanced methane recovery. SPE Reserv. Eval. Eng. 8, 291–299. doi:10.2118/87230-PA

Shi, J.Q., Durucan, S., 2004. Drawdown induced changes in permeability of coalbeds: A new interpretation of the reservoir response to primary recovery. Transp. Porous Media 56, 1–

16. doi:10.1023/B:TIPM.0000018398.19928.5a

Simpson, G., Gueguen, Y., Schneider, F., 2001. Permeability enhancement due to microcrack dilatancy in the damage regime. J. Geophys. Res. Earth 106, 3999–4016. http://dx.doi.org/10.1029/2000JB900194.

Singh, V.K., 2014. Assessment of sudden permeability uptick with depletion in coal bed. Southern Illinois University.

Siriwardane, H.J., Gondle, R.K., Smith, D.H., 2009. Shrinkage and swelling of coal induced by desorption and sorption of fluids: Theoretical model and interpretation of a field project. Int. J. Coal Geol. 77, 188–202. https://doi.org/10.1016/j.coal.2008.08.005

Skempton, a. W., 1961. Effective Stress in Soils, Concrete and Rocks. Pore Pressure And Suction In Soils, Butterworths, pp. 4–16.

Soni, A., 2017. Modified permeability modeling of coal incorporating sorption-induced matrix shrinkage. Southern Illinois University.ProQuest Number: 10196471.

Souley, M., Homand, F., Pepa, S., Hoxha, D., 2001. Damage-induced permeability changes in granite: a case example at the URL in Canada. Int. J. Rock Mech. Min. Sci. 38, 297–310. http://dx.doi.org/10.1016/S1365-1609(01)00002-8

Suklje, L., 1969. Theories of failure in soil mechanics. Rheol. Asp. soil Mech. John Wiley Sons 62.

Terzaghi, K., 1943. Theoretical soil mechanics. Géotechnique 510. https://doi.org/10.1016/0167-1987(88)90005-0

Teufel, L.W., Rhett, D. W., Farrell, H. E., 1991. Effect of reservoir depletion and pore pressure drawdown on in situ stress and deformation in the Ekofisk field, North Sea. In Proceedings of The 32nd U.S. Symposium on Rock Mechanics (USRMS), 10-12 July,

Norman, Oklahoma, Roegiers (Ed.), Rock Mechanics as a Multidisciplinary Science, pp. 63–72

Thomsen, L., 1986. Weak elastic anisotropy. Geophysics 51, 1954. https://doi.org/10.1190/1.1442051

Todd, T., Simmons, G., 1972. Effect of pore pressure on the velocity of compressional waves in low-porosity rocks. J. Geophys. Res. 77, 3731–3743. https://doi.org/10.1029/JB077i020p03731

van Bergen, F., Hol, S., Spiers, C., 2011. Stress-strain response of pre-compacted granular coal samples exposed to CO2, CH4, He and Ar. Int. J. Coal Geol. 86, 241–253. https://doi.org/10.1016/j.coal.2011.02.007

Walsh, J.B., 1965. The effect of cracks on the compressibility of rock. J. Geophys. Res. 70, 381–389. https://doi.org/10.1029/JZ070i002p00381

Wang, G.X., Wei, X.R., Wang, K., Massarotto, P., Rudolph, V., 2010. Sorption-induced swelling/shrinkage and permeability of coal under stressed adsorption/desorption conditions. Int. J. Coal Geol. 83, 46–54. doi:10.1016/j.coal.2010.03.001

Warpinski, N.R., Teufel, L.W., 1992. Determination of the Effective-Stress Law for Permeability and Deformation in Low-Permeability Rocks. SPE Form. Eval. 7, 123–131. https://doi.org/10.2118/20572-PA

Weniger, P., Kalkreuth, W., Busch, A., Krooss, B.M., 2010. High-pressure methane and carbon dioxide sorption on coal and shale samples from the Paraná Basin, Brazil. Int. J. Coal Geol. https://doi.org/10.1016/j.coal.2010.08.003

Zhang, R., Liu, S., Bahadur, J., Elsworth, D., Melnichenko, Y., He, L., Wang, Y., 2015. Estimation and modeling of coal pore accessibility using small angle neutron scattering.

Fuel 161, 323–332. https://doi.org/10.1016/j.fuel.2015.08.067

Zoback, M.D., 2007. Reservoir Geomehanics, in: First Edition. pp. 1–507.

Zoback, M.D., Byerlee, J.D., 1975. The effect of microcrack dilatancy on the permeability of Westerly granite. J. Geophys. Res. 80, 752–755. http://dx.doi.org/10.1029/JB083iB09p04451

APPENDICES

APPENDIX A

DETERMINATION OF BIOT'S-LIKE COEFFICIENT FOR CHAPTER 2

To determine the Biot's-like coefficient, results of the unconstrained hydrostatic (flooding) experiment were used. The set of equations presented as Equation 4(a-f) is simplified, given that external stresses were equal to pore pressure, as:

$$\sigma_1 = \sigma_2 = -p = (C_{11} + C_{12})\varepsilon_{11} + C_{13}\varepsilon_{33} - s_m^{a1}(p) \quad \text{(i)}$$

$$\sigma_3 = -\mathrm{p} = 2(\mathrm{C}_{13}\varepsilon_{11}) + \mathrm{C}_{33}\varepsilon_{33} - \mathrm{s}_{\mathrm{m}}^{\mathrm{a3}}(\mathrm{p}) \quad \text{(ii)}$$

Inverting the above compliance matrix to stiffness matrix gives the following:

$$\begin{bmatrix}\varepsilon_{11}\\ \varepsilon_{33}\end{bmatrix} = \begin{bmatrix}\frac{1-\nu_1}{E_1} & \frac{-\nu_3}{E_3}\\ \frac{-2\nu_3}{E_3} & \frac{1}{E_3}\end{bmatrix}\begin{bmatrix}s_{\mathrm{m}}^{\mathrm{a1}}(\mathrm{p}) - \mathrm{p}\\ s_{\mathrm{m}}^{\mathrm{a3}}(\mathrm{p}) - \mathrm{p}\end{bmatrix} \quad \text{(iii)}$$

Taking the derivative of Equation iii with respect to pressure and inverting the stiffness matrix gives the following:

$$\begin{bmatrix}\frac{ds_{\mathrm{m}}^{\mathrm{a1}}(\mathrm{p})}{dp} & -1\\ \frac{ds_{\mathrm{m}}^{\mathrm{a3}}(\mathrm{p})}{dp} & -1\end{bmatrix} = \begin{bmatrix}\frac{1-\nu_1}{E_1} & \frac{-\nu_3}{E_3}\\ \frac{-2\nu_3}{E_3} & \frac{1}{E_3}\end{bmatrix}^{-1}\begin{bmatrix}\frac{d\varepsilon_1}{dp}\\ \frac{d\varepsilon_3}{dp}\end{bmatrix} \quad \text{(iv)}$$

The inverse matrix on the right-hand side of the equation can be determined using the results of the helium, unconstrained experiment (Figures 2.4a) and the column matrix can be obtained from the results of the unconstrained methane experiment. The column matrix on the right-hand side can be estimated using the data presented in Figures 2.4b or 2.4c, for methane and carbon dioxide respectively.

Since Biot's-like coefficient is a pressure-dependent quantity, it can be presented easily as a graph. Figures 2.10 presents the Biot's-like coefficient for the coal types as a function of pressure. The figure shows a non-linear fit for the variation of Biot's-like coefficient to demonstrate that it is expected to increase significantly at low pressures and is better represented as a non-linear fit

(Espinoza et al., 2013).

APPENDIX B

DETERMINATION OF MATRIX SHRINKAGE COMPRESSIBILITY (C_M) FOR CH. 3

The matrix shrinkage compressibility (C_m) is another important compressibility component that was discussed in Liu and Harpalani (2013). The model provided by the authors predicts the value of C_m as a function of pore pressure. In their model, the authors predict the value of C_m assuming a constant value of the molar volume (V_o) as follows:

$$C_m = \frac{3a\rho RT}{E_A V_o}\left(\frac{b}{1+bP}\right) \quad \text{(i)}$$

However, the molar volume is itself a function of pressure and can be found using an equation of state. This paper has presented the method of calculating Biot-like coefficient used in Espinoza et al. (2013) and this coefficient contains molar volume as a function of pore pressure using the Van der Waal equation of state. Hence, it is proposed that using the Biot-like coefficient, matrix shrinkage compressibility can be calculated. The constitutive equation for the unconstrained test using methane has been shown as Equation (3.7). Taking the derivative of Eq (3.7) with respect to pressure, with p = 0 substituted since we are only interested in matrix shrinkage, gives the following:

$$\begin{bmatrix} \frac{d\varepsilon_x}{dp} \\ \frac{d\varepsilon_z}{dp} \end{bmatrix} = \begin{bmatrix} \frac{1-\nu_x}{E_x} & \frac{-\nu_z}{E_z} \\ \frac{-2\nu_z}{E_z} & \frac{1}{E_z} \end{bmatrix} \begin{bmatrix} \frac{ds_x^a(p)}{dp} \\ \frac{ds_z^a(p)}{dp} \end{bmatrix} \quad \text{(ii)}$$

where, left column matrix gives the linear matrix shrinkage compressibilities in the x-/y- and z- directions. Also, Biot-like coefficient can be written as:

$$bi(P) = ds_i^a/dp = ci(P)no(P)Vb(P) \quad \text{(iii)}$$

The values of Biot-like coefficient obtained using Equation (iii) were used to calculate the value of C_m in both vertical and horizontal the direction.

VITA

Graduate School
Southern Illinois University

Suman Saurabh

sumanan047@gmail.com

Indian Institute of Technology (ISM), Dhanbad
Bachelor of Engineering, Mining Engineering, May 2013

Dissertation Paper Title:
Geomechanical State of Rocks with Depletion in Unconventional Coalbed Methane Reservoirs

Major Professor: Dr. Satya Harpalani

Publications:

1. Saurabh, S. & Harpalani, S. Anisotropy of coal at various scales and its variation with sorption. *International Journal of Coal Geology*, Volume 201, 2019, pp 14-25.
2. Saurabh S and Harpalani S. Modeling of microbial methane generation from coal and assessment of its impact on flow behavior, *Fuel*, Volume 216, 2018, pp 274-283, ISSN 0016-2361, https://doi.org/10.1016/j.fuel.2017.12.015.
3. Saurabh S and Harpalani S. The effective stress law for stress-sensitive transversely isotropic rocks, *International Journal of Rock Mechanics and Mining Sciences*, Volume 101, 2018, pp 69-77, ISSN 1365-1609, https://doi.org/10.1016/j.ijrmms.2017.11.015.
4. Saurabh S and Harpalani S. Stress path with depletion in coalbed methane reservoirs and stress based permeability modeling, *International Journal of Coal Geology*, Volume 185, 2018, pp 12-22, ISSN 0166-5162, https://doi.org/10.1016/j.coal.2017.11.005.Saurabh S, Harpalani S, Singh V. Implications of stress re-distribution and rock failure with continued gas depletion in coalbed methane reservoirs. *International Journal of Coal Geology*, Volume 162, 2016, pp 183-192.

5. Feng R, Harpalani S, Saurabh S. Experimental investigation of in situ stress relaxation on deformation behavior and permeability variation of coalbed methane reservoirs during primary depletion. *Journal of Natural Gas Science and Engineering*, Volume 53, 2018, pp 1-11, ISSN 1875-5100, https://doi.org/10.1016/j.jngse.2018.02.019.